PhD Thesis

School of Aerospace Engineering
University "Sapienza" of Rome

"TECHNOLOGIES AND METHODS EMPLOYED TO DESIGN A UNIVERSITY-CLASS MICROSATELLITE, ACCORDING TO ESA STANDARDS"

Supervisor:
Prof. Filippo Graziani

Co-supervisor:
Ing. Gabriele Mascetti

PhD candidate:
Fabrizio Paolillo

XXIII ciclo a.a. 2007-2008

A Stefania e alla mia famiglia.

CONTENTS

Acronyms

Acronym	Definition
ASI	Italian Space Agency
ADCS	Attitude Determination and Control System
BCR	Bus Control Regulator
CDF	Concurrent Design Facility
CEF	Concurrent Engineering Facility
CGS	Core Ground Segment
COTS	Commercially-off-the-shelf
DRN	Data Relay Network
DRS	Data Relay Satellite
ECSS	European Cooperation for Space Standardization
EIRP	Effective Isotropic Radiated Power
ESA	European Space Agency
GAUSS	Gruppo di Astrodinamica dell'Università degli Studi "Sapienza" di Roma
GEO	Geostationary Earth Orbit
G/T	Receiver antenna gain / receiver system noise temperature
HEO	High Earth Orbit
IOT	In Orbit Test
LEO	Low Earth Orbit
LEOP	Launch and Early Orbit Phase
MAPC	Mission and Acquisition Planning Center
MDD	Mission Description Document
MEO	Medium Earth Orbit
OBDH	On Board Data Handling
P/L	Payload
RF	Radio Frequencies
RTV	Room Temperature Vulcanizing

SCC	Satellite Control Center
UGS	User Ground Segment

Capitolo I
Introduction

The objective of this thesis is the study of the applicability of ESA (European Space Agency) standards to university-class microsatellites missions. At the same time the university microsatellite design technologies used to manufacture EduSAT spacecraft have been investigated in depth and ESA standards have been applied during the EduSAT mission phases. Afterwards a micro satellite optical payload for in-orbit space environment monitoring has been designed, exploiting useful instruments provided by ESA ECSS (European Cooperation for Space Standardization) standards.

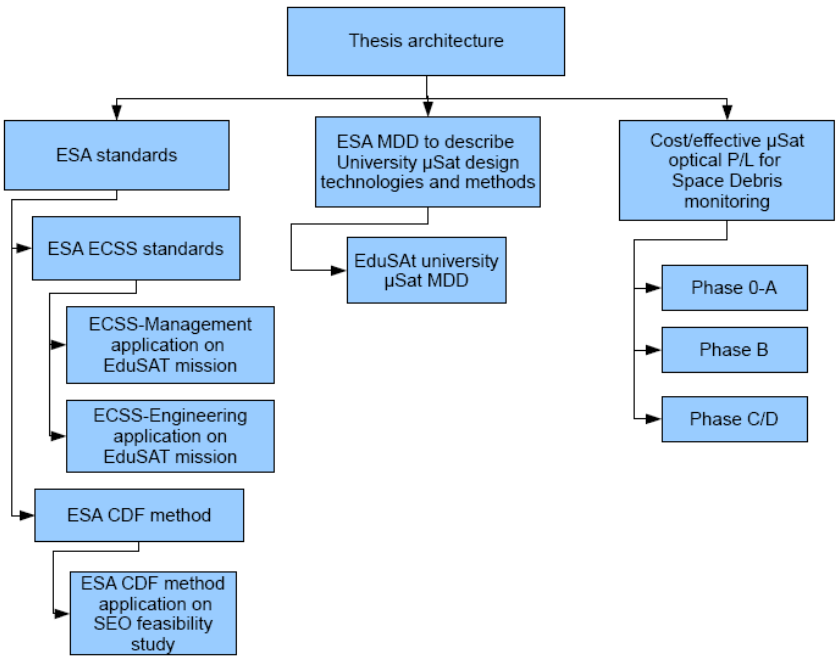

Fig. I-1. Thesis architecture.

The first part of this work is focused on the detailed study of ESA standards. They result from several years of experience in the field of space missions, summarizing technologies and methods employed in aerospace sector. For this reason they offer a valuable technical and scientific support and they are now considered as an international common language.

A lot of efforts have been carried out by ESA to produce technologies and design method standardization and now several European industrial projects adopt this system.

Do to the modern technologies the microsatellites class plays an important role in aerospace field. Microsatellites are cost/effective platforms and for this reason they have been largely enrolled in space industry.

University microsatellites are a branch of this class. The main characteristics are: the use of low cost Commercial Off The Shelf (COTS) components; the training of students in design, integration and operations of spacecrafts; to demonstrate the feasibility of using micro/nano COTS (Appendix I "University microsatellites classification").

Since 2007, as a member of GAUSS (Gruppo di Astrodinamica dell'Università degli Studi "Sapienza" di Roma) group, I have participated in the design, manufacturing and integration of EduSAT microsatellite, funded by the Italian Space Agency (ASI). EduSAT is an Educational SATellite (Ref. 1), entirely built and operated in orbit by students, researchers and professors of the School of Aerospace Engineering of University "Sapienza" of Rome.

The first part of Chapter II is devoted to the description of the ECSS standards. Afterwards, the ESA ECSS standards application on EduSAT mission is shown. As term of comparison will be shown the ESA ECSS standards application on a typical ESA mission (the BUGS experiment), in witch I have been involved. The second part of Chapter II is devoted to the description of the CDF (Concurrent Design Facility), a method adopted by ESA for space missions feasibility study. Finally the experience gained during the feasibility study of SEO (Space System for Earth Observation) mission exploiting CDF facility and method.

These standards, although not mandatory for university missions, would be usefully employed in university projects in order to adopt a valuable technical and

management support during all phases of a space mission, using design methodologies approved by the international industrial ad academic community.

In Chapter III the EduSAT design technologies are presented, through the use of an ECSS standard instrument: The Mission Description Document (MDD). The use of this document to describe the EduSAT mission demonstrates the applicability of this standard on a university project.

Although the university-class missions design guidelines (Appendix I) guide students to modestly-scoped missions, the recent trends are to attempt "real", relevant payloads, to tackle research problems that are not being addressed in industry. For this reason, after the analysis of the applicability of the ESA standard on a university project, and the study of technology of a university microsatellite, chapter IV is dedicated to design a microsatellite cost/effective optical payload. Moreover ESA ECSS standards have been adopted as support during the design process.

Capitolo II
ESA Standards application on university-class microsatellites

The first part of this chapter is devoted to the description of the ECSS. Then the ECSS standards applicability on EduSAT university microsatellite is described. Moreover as term of comparison will be shown the ESA ECSS standards application on BUGS experiment (a typical ESA student mission in witch I have been involved). The second part Chapter II is devoted to the description of the CDF (a method adopted by ESA for space missions feasibility study). Finally the experience gained during the feasibility study of SEO (Space System for Earth Observation) mission exploiting CDF facility and method.

II.1 ESA ECSS standards

Recently space systems developers have observed the growing potentiality of ESA ECSS standards. These standards are reference documents and tools that provide helpful instruments for both space mission management and engineering. ECSS documents may require "tailoring" when applied to specific projects. This means that they require a specific process before to be applied.

Space agencies and space companies, all around the word, widely use the ECSS standards. In this section the ECSS system description, implementation and general requirement will be shown in dept, according to ECSS-S-ST-00C(31July2008) document (Ref.1)

The ECSS standard are available free on the following website: http://www.ecss.nl/.

II.1.1ECSS system architecture

The ECSS standards are divided in three main branches: the management, the engineering and the quality branches. Moreover ECSS standards could directly refer to external standards (like ISO 14644-1 adopted for cleanroom classification).

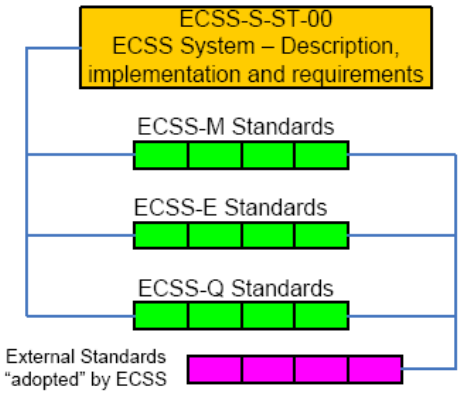

Fig. II-1. ECSS User Standards structured as Branches (ECSS-S-ST-00C, Ref. 2).

Each branch contains several documents belonged to different mission subsystem and disciplines.

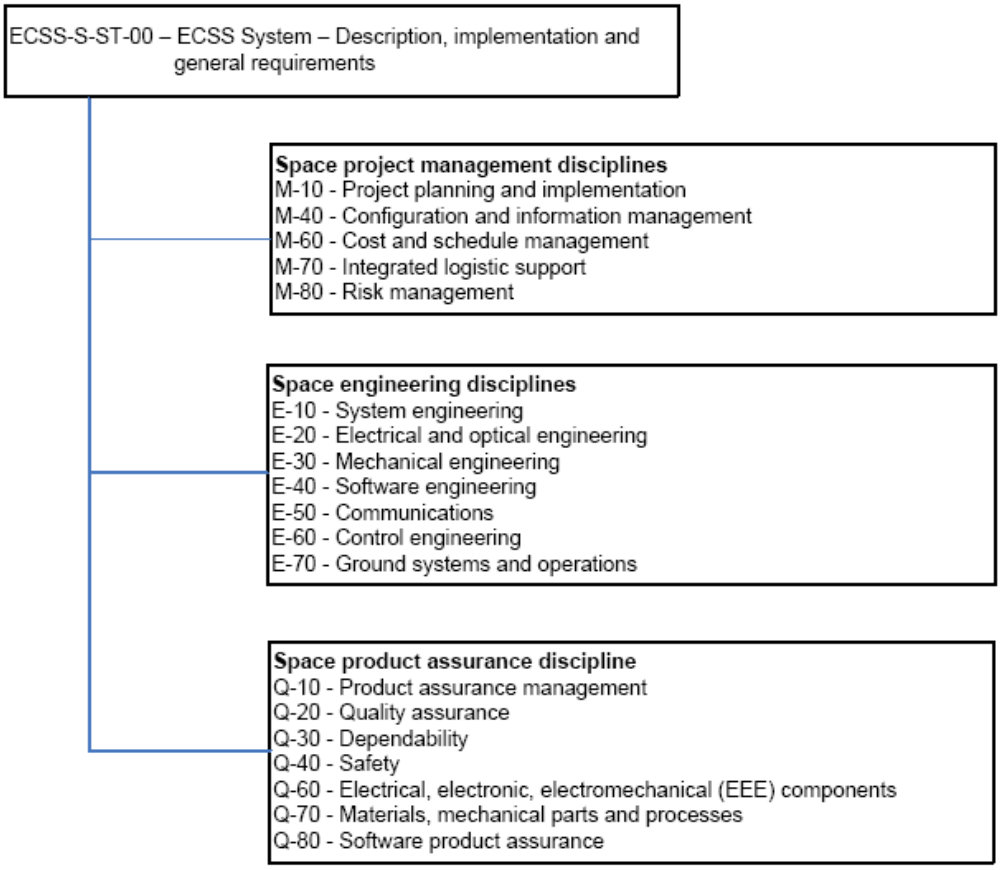

Fig. II-2. Disciplines of the ECSS Standards system (ECSS-S-ST-00C).

II.1.2 ECSS customer-supplier model and the applicability of ECSS standards

The production of space systems calls for the cooperation of several organizations that share the common objective of providing a product that satisfies the customer's needs (performance within cost and schedule constraints). All space project actors are either a customer or a supplier, or both. In its simplest form, a project can involve one customer with just one supplier; however, most space projects comprise a number of hierarchical levels, where the actor at the top level of the hierarchy is the top level customer, the actors at intermediate levels are both supplier and customer, the actors at the lowest level are suppliers only.

The ECSS standards provide useful documents to regulate relationships among all the project actors. These documents do not have legal standing and they do not constitute business agreements: they are only mentioned in business agreements and contracts.

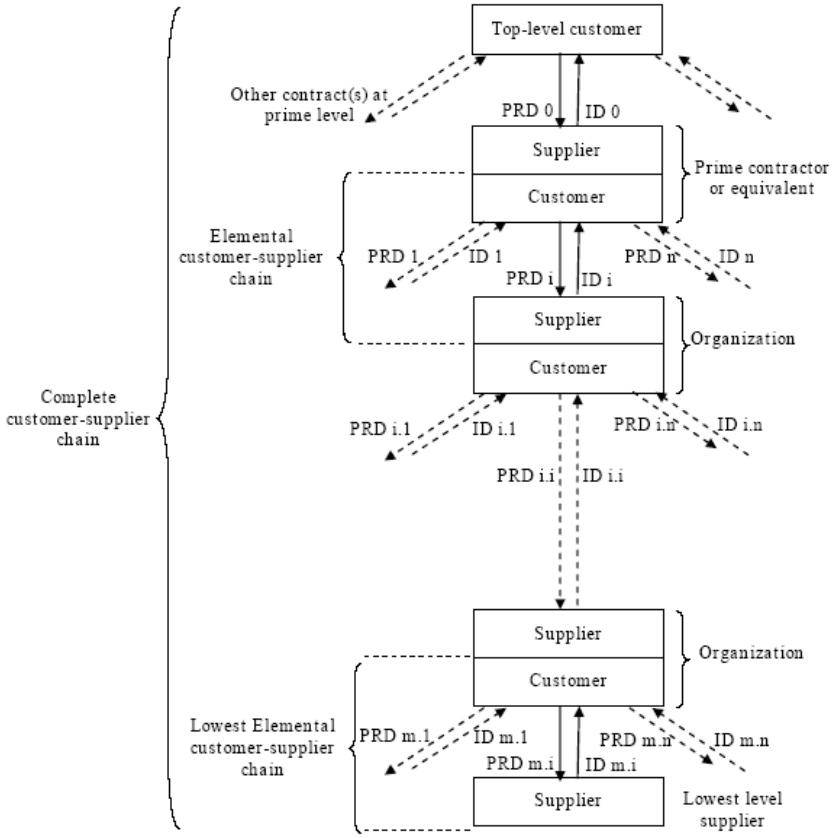

Fig. II-3. Customer–supplier network concept (ECSS-S-ST-00C).

The project requirements documents (PRDs) are used by the customer to specify the project requirements and ECSS standard applicability to the supplier.

This procedure have to be used in all the hierarchical level of the customer-supplier chain.

A supplier, at any level, is responsible for demonstrating compliance with the project requirements contained in his customer's PRD. The compliance to the PRD is presented in an Implementation Documents (IDs).

II.1.3 Application of ECSS Standards and the "tailoring" process

The ECSS Standards and requirements to be made applicable at each level of the customer–supplier chain are influenced by the type and phase of the project involved, and by the type of business agreement to be used for managing the project.

The ECSS System provides a comprehensive set of coherent standards covering the requirements for the procurement of a generic space product. This

system can be adapted to a wide range of project types. The process of adapting the requirements to the project specificities is called "tailoring".

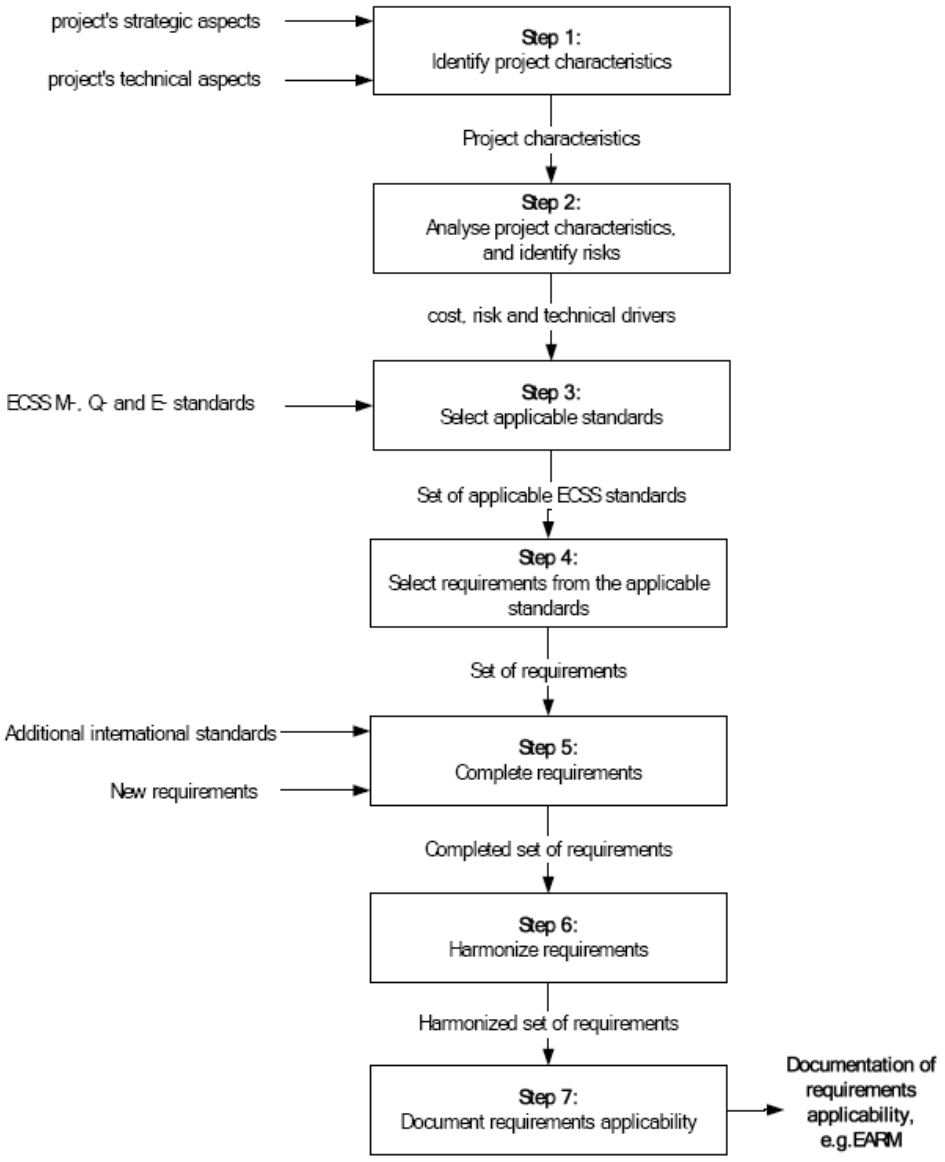

Fig. II-4. Tailoring process recommended steps (ECSS-S-ST-00C).

Fig. II-4 describes a recommended 7 step process for project preparatory activities and for application of tailoring to establish applicability of ECSS Standards and their requirements to a project and to apply tailoring as necessary:

- *Step 1 - Identification of project characteristics*

Overall project characteristics are derived taking into account experience gained and lessons learned from comparable projects, and are used for establishing the project

context, scope, scale, orientation and other elements key to the successful achievement of the project objectives.

- *Step 2 - Analysis of project characteristics and identification of risks*

Once identified the characteristics, the project is analysed to identify significant cost, schedule, technical drivers, as well as critical issues and specific constraints. These are used to identify and evaluate inherent and induced risks. Main strategic, organisational, economical or technical characteristics considered for a project are as follows:

- Objective of the mission (e.g. scientific, commercial, institutional);
- Product type (e.g. space segment, space transportation segment, ground segment and operations, equipment, instrument);
- Mission characteristics (e.g. type of orbit, expected life duration, availability);
- Constraints with the environment (e.g. external interfaces, external regulations, procurement constraints) the project belongs to;
- Expected cost to completion;
- Schedule drivers;
- Level of commitment (e.g. partnership, supplier) or type of business agreement (e.g. fixed price, cost reimbursement);
- Maturity of design or technology (e.g. recurrent development, readiness level);
- Technical product complexity;
- Organisational or contractual complexity;
- Supplier maturity.

The resulting project risk factors are documented and the causes and consequences of the identified risks are determined. This is the first step in the risk management process, which is continued to monitor and manage risk mitigation actions throughout the life of the project.

- *Step 3 - Selection of applicable ECSS Standards*

Using the results of the preparatory activities as primary input, the complete set of ECSS Standards is evaluated for relevance to the overall project needs. Those standards found to be relevant are identified as applicable standards for the

implementation of the project. In making this determination, it is important to recognise that at this level, due to the integrated structure of the ECSS System, identifying a standard as directly applicable also makes other standards called by it explicitly applicable.

- *Step 4 - Selection of requirements from applicable* standards

Each requirement within the applicable standards is assessed and classified as:

(Y) Applicable without change,

(M) Applicable with modification

(N) Not applicable (deleted).

- *Step 5 - Completion of requirements*

When a lack, which is not project specific, is identified in the requirements of an ECSS standard, a new requirement is generated or adopted preferably from a standard of SDO (standard development organization). Such requirements are classified as: (A) Additional requirement. For each requirement classified as (A), the complete new text is recorded and justified.

- *Step 6 - Harmonization of requirements*

The project is reviewed to eliminate the risk of conflict, duplication, or lack of necessary requirements.

- *Step 7 - Documenting of requirements applicability*

The method of recording the applicability of ECSS Standards and requirements for a project in an efficient and structured manner is to consolidate it into an "ECSS Applicability Requirements Matrix" (EARM) or equivalent document, which will be part of the PDR.

II.1.4 ECSS-M standards

The overall objective of project management is to implement a process to achieve successful completion of the project in terms of cost, schedule and technical performance. Project management is performed following a structured approach throughout all stages of its life cycle and at all levels of the customer-supplier chain.

II.1.4.1Project planning and implementation (ECSS-M-ST-10C Rev. 1 - 6 March 2009)

Project planning and implementation encompasses all of the processes carried out in order to plan and execute a space project from initiation to the completion at all levels in the customer-supplier chain in a coordinated, efficient and structured manner. This standard (Ref. 3) provides organizational structure (*Project breakdown structures*), a very useful instrument to obtain a clear and unambiguous definition and allocation of individual roles and responsibilities:

- *Funcion tree*

  The function tree is the breakdown of the system performances into functions.

- *Specification tree*

  The specification tree defines the hierarchical relationship of all technical requirements specifications for the different elements of a system or product.

- *Product tree*

  The product tree is the breakdown of the project into successive levels of hardware and software products or elements, articulated to perform the functions identified in the function tree.

Moreover the product tree forms the basis for the elaboration of the project work breakdown structure.

Work breakdown structure (WBS)

The WBS is the principal structure used in managing a project and provides a framework for managing cost, schedule and technical content. It divides the project into manageable work packages, organized according to the nature of the work by breaking down the total work to be performed into increasing levels of detail.

The successful of a space mission is due to cooperation between different groups. For this reason the use of Work package (WP) permits to explicitly identify the work of each supplier in the work breakdown structure.

Project phasing

"ECSS-M-ST-10C Rev. 1 - 6 March 2009" standard provides also the typical 7 mission phases and the typical project life cycle (Fig. II-5):

- Phase 0 - Mission analysis/needs identification
- Phase A – Feasibility
- Phase B - Preliminary Definition
- Phase C - Detailed Definition
- Phase D - Qualification and Production
- Phase E -Utilization
- Phase F - Disposal

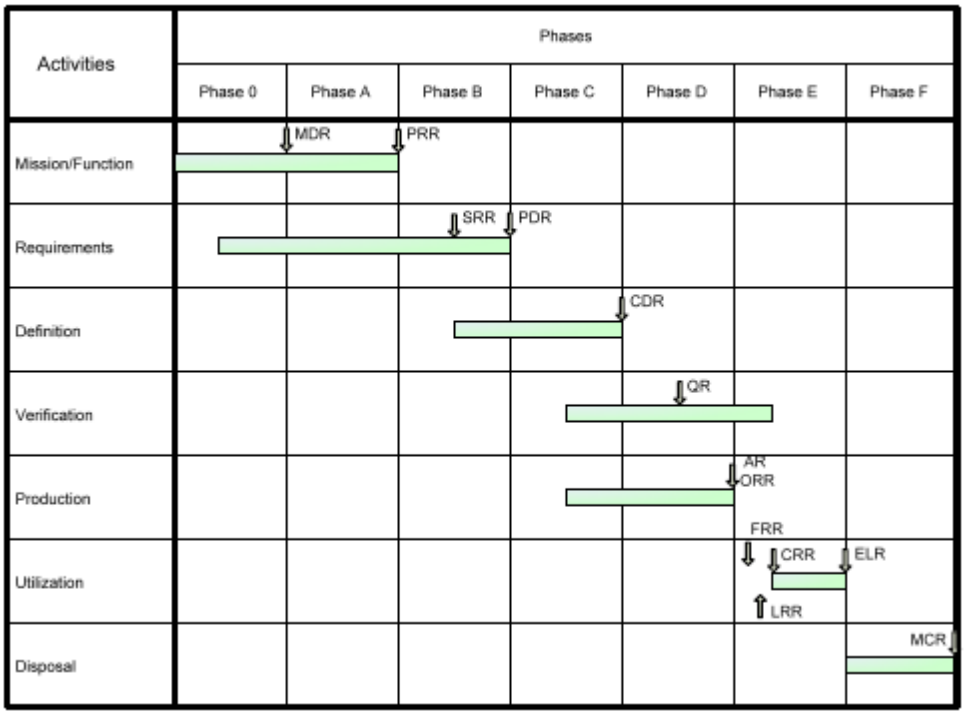

Fig. II-5. Typical project life cycle.

A typical space mission need more than five years from the phase 0 to the phase F. As will be described in depth in paragraph II.2.2.1, in a university project the main purpose is to reduce the cost and to minimize the time needed in order to allow students to participate in all the mission phases.

II.1.4.2Cost and schedule management (ECSS-M-ST-60C (31 July 2008))

Cost and schedule management standard (Ref. 4) provides a common working baseline for the mission planning. These instruments allow to plan

accurately the phasing of procurements, expenses and resources for the project, and to complete the project within the given time and financial constraints.

The Gantt chart

The commonly used project schedule presentation is the Gantt chart (or Bar chart). In a Gantt chart each activity is represented by a bar, the length of which corresponds to the duration of the activity. The links between the bars are shown with arrows (as illustrated in the application on EduSAT program in II.2.2.2 paragraph). The critical path is typically highlighted exploiting milestones. The activities can be grouped in conformance with the Work Breakdown Structure.

II.1.4.3 Risk management (ECSS-M-00-03A)

This standard (Ref. 5) provides simple method to risk management and assessment. This method is based on four main steps, as shown in Fig. II-6:

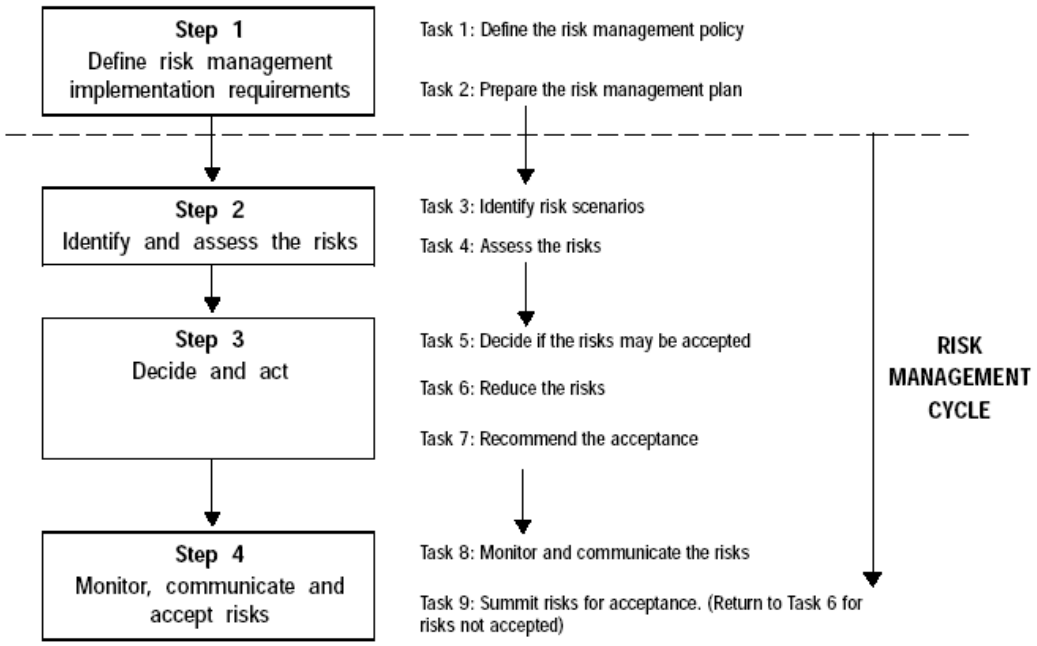

Fig. II-6. The tasks associated with the steps of the risk management process within the risk management cycle (ECSS-M-00-03A).

At the beginning of a project (Step1) the risk management policy (Task 1) and risk management plan (Task 2) have to be performed. Then the implementation of the risk management process consists of a number of "risk management "cycles" over the project duration comprising the Steps 2 to 4, subdivided into the 7 Tasks from 3 to 9.

In Tab. II-1 the ECSS standard structure example for risk assessment and remediation is shown. This procedure is useful because can reassume the 3 steps of the risk management cycle. Starting with the risk scenario identification, through the determination of the severity and the likelihood of each risk scenario, to arrive at the identification of acceptable risks and the determination of mitigation measures for each unacceptable risk.

ID	I - 01 (I - Implementation, M – Mission))
Name	Destruction of a critical component
Description	Critical component is destroyed during implementation of the experiment.
Consequences	Objectives can not be achieved
Severity	5
Probability	2
Total Risk	10
Prevention	Have 2 spare parts in store
Reaction	Exchange of critical component
Recovery	Full recovery after test

Tab. II-1. ECSS standard structure for risk management.

"ECSS-M-00-03A" standard provides also the typical risk trend belonged to different mission phases (Fig. II-7). Moreover it proposes the actions to be adopted according to different risk level calculated (Fig. II-8).

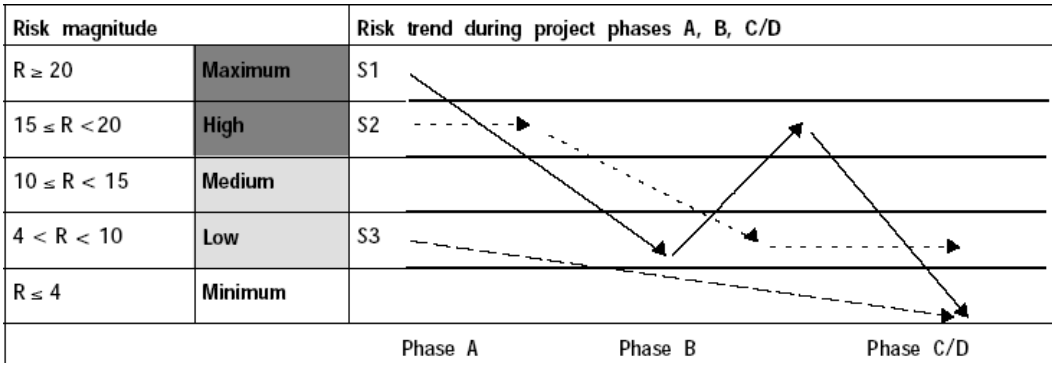

Fig. II-7. Example of a risk trend during the project phases (ECSS-M-00-03A).

Fig. II-7 gives an example of risk trend during the project phases. An extensive test campaign is needed to evaluate and to reduce risk occurrence and magnitude for devices with high and medium risk.

Risk index	Risk magnitude	Proposed actions
R ≥ 20	Maximum risk	Unacceptable risk: implement new team process or change baseline – seek project management attention at appropriate high management level as defined in the risk management plan.
15 ≤ R < 20	High risk	Unacceptable risk: see above.
10 ≤ R < 15	Medium risk	Unacceptable risk: aggressively manage, consider alternative team process or baseline – seek attention at appropriate management level as defined in the risk management plan.
4 < R < 10	Low risk	Acceptable risk: control, monitor – seek responsible work package management attention.
R ≤ 4	Minimum risk	Acceptable risk: see above.

Fig. II-8. Example of proposed actions during the project phases (ECSS-M-00-03A).

II.1.5 Standard ECSS-E

Engineering branch of ECSS system (ECSS-E) is divided in disciplines, covering the engineering aspects of space systems and products, including:

- *E-10.* System Engineering
- *E-20.* Electrical and Optical Engineering
- *E-30.* Mechanical Engineering
- *E-40.* Software Engineering
- *E-50.* Communications
- *E-60.* Control Engineering
- *E-70.* Ground Systems and Operations

This standards provide engineering process as applied to space systems and their elements or functions, and technical aspects of products used to accomplish, or associated with, space missions.

Several ECSS-E standards has been studied during the EduSAT design process. In the following paragraphs two example of ECSS-E standards belonged "System Engineering" (E-10) and "Electrical and Optical Engineering" (E-20) disciplines will be described.

II.1.5.1 Photovoltaic assemblies and components (ECSS-E-ST-20-08C (31July2008))

This standard (Ref. 6) is part of a branch that defines the technical requirements from solar array specification down to component level, in order to

guarantee that lower level components and sub-assemblies are qualified according to specifications. This branch defines also the set of requirements from component level up to photovoltaic assemblies (PVA) to enable a generic qualification for each level of assembly for about 90 % of the solar array applications within a certain range; for example, deployable solar arrays for GEO orbit or LEO orbit.

In particular this standard outlines the requirements for the qualification, procurement, storage and delivery of the main assemblies and components of the space solar array electrical layout: photovoltaic assemblies, solar cell assemblies, bare solar cells, coverglass and protection diodes.

As an example of technical specifications to be considered during a space system design phase, the test environment requirements needed for photovoltaic assemblies are here shown:

Test environment requirements

The atmospheric conditions during photovoltaic test operations and storage is suggested in this standard:

- Pressure: (1 013,25 ± 33) hPa. (1 atm = 1 013,25 hPa = 760 mmHg)
- Temperature: (23 ± 5) °C.
- Average relative humidity: 40 % - 60 %.
- Semiconductor devices (i.e. planar diodes) can short-circuit if no special precautions are taken during long storage periods under certain atmospheric conditions. This is because chlorine content, in combination with illumination, can produce metal contact migrations on these semiconductor devices
- The room cleanliness level should be airborne particle count: Class 8 ISO 14644-1.

It is important to emphasize that the last requirement is an example of how ECSS standards could recall external standards if existing.

ISO classification number (*N*)	Maximum concentration limits (particles/m³ of air) for particles equal to and larger than the considered sizes shown below (concentration limits are calculated in accordance with equation (1) in 3.2)					
	0,1 µm	0,2 µm	0,3 µm	0,5 µm	1 µm	5 µm
ISO Class 1	10	2				
ISO Class 2	100	24	10	4		
ISO Class 3	1 000	237	102	35	8	
ISO Class 4	10 000	2 370	1 020	352	83	
ISO Class 5	100 000	23 700	10 200	3 520	832	29
ISO Class 6	1 000 000	237 000	102 000	35 200	8 320	293
ISO Class 7				352 000	83 200	2 930
ISO Class 8				3 520 000	832 000	29 300
ISO Class 9				35 200 000	8 320 000	293 000
NOTE Uncertainties related to the measurement process require that concentration data with no more than three significant figures be used in determining the classification level						

Tab. II-1. ISO Standard 14644-1 Class Limits (ECSS-Q-70-01B Draft 1 -16 April 2008)

The maximum permitted concentration of particles, Cn, for each considered particle size, D, is determined from the equation:

$$Cn = 10N \cdot \frac{0.1}{D} \cdot 2.08,$$

where Cn is the maximum permitted concentration (in particles per cubic metre of air) of airborne particles that are equal to or larger than the considered particle size. Cn is rounded to the nearest whole number, using no more than three significant figures. N is the ISO classification number, which does not exceed a value of 9. Intermediate ISO classification numbers can be specified, with 0,1 the smallest permitted increment of N. D is the considered particle size, in micrometres. 0,1 is a constant, with a dimension of micrometres (ECSS-Q-70-01B Draft 1 -16 April 2008, Ref. 7).

In particular for particles up to 0.5 µm:

$$Cn\_ISO8 = 3.5 \times 10^6 \ \text{particles}/\text{m}^3$$

II.1.5.2Space environment (ECSS-E-ST-10-04C)

Even if the most of ECSS-E standards are devoted to the space systems design method and technique, the document objective of this paragraph (Ref. 8) is an important reference for space environment physical models. In particular this standard deal with the standardization of mathematical model in different scientific fields:

- Gravity
- Geomagnetic field
- Natural electromagnetic radiation and indices
- Neutral atmosphere
- Plasmas
- Energetic particle radiation
- Space debris and meteoroids
- Contaminationnts

In paragraph II.2.3.2 the space debris and meteoroids model will be adopted in order to calculate Edusat impact risk assessment.

Space debris and meteoroid impact risk assessment

Space debris are a concern for human spaceflight activities. The total population of objects larger than 1 cm is on the order of 500 000 to 700 000 and could be catalogued as follows (Ref. 8and Ref. 9):

- *Expl. Fragments.* The major source of space debris, fragmentations of space objects, originates from spare fuel that mostly remains inside pressurized tanks once the rocket stage is discarded into Earth orbit. Over time, and in the harsh environment of space, the mechanical integrity of the boosters internal components breaks down and tanks start to leak. The resulting sudden releases of pressure or even high energetic explosions expel numerous fragments into orbit.
- *Coll. Fragment.* Fragmentation objects result of three in-orbit impact event.
- *LMRO*. Spent payloads and upper stages called launch/mission related objects (LMRO)

- *SRM Slag and Dust*. The most important non-fragmentation source is solid rocket motor (SRM) firings during which aluminium oxide (Al2O3) in the form μm sized dust and mm to cm sized slag particles is exhausted.
- *NaK Droplets.* A second important source was the ejection of reactor cores during the end of operation of the Russian RORSATs (Radar Ocean Reconnaissance Satellites) in the 1980's, which released droplets of the reactor coolant (sodium potassium alloy (NaK)) into space.
- *Ejecta*
- *Paint Flakes*. Finally, under the influence of the harsh space environment (extreme ultra violet radiation, impinging atomic oxygen and micro particle impacts), surfaces of space objects start to erode. This leads to mass losses of surface coatings and to the detachment of flakes of the surface paint, both with μm and mm sizes.

Moreover meteoroids are particles of natural origin and originate from asteroids or comets:

- *Meteoroid.* The natural meteoroid flux represents, at any instant, a total of about 200 kg of mass within 2 000 km of the Earth surface. Meteoroid streams are accumulations of meteoroids with nearly identical heliocentric orbits. Relative to Earth all particles of a given meteoroid stream have nearly identical impact directions and velocities. Encounters with meteoroid streams typically last from a few hours to several days. Meteoroids which do not form part of identified streams are called sporadics. Their flux is fairly constant over the year and they do not follow any apparent pattern with respect to incident direction or velocity. The annual integrated flux of meteoroid streams amounts to about 10% of the sporadic meteoroid flux.

ESA MASTER-2005 tool

ESA ECSS provides a useful tool, the ESA MASTER-2005 (Ref. 9), to perform space debris and meteoroids impact risk assessments. ESA MASER 2005 is a free software provided by ESA to calculate debris and meteoroids flux for Earth altitudes below 36 786,0 km.

In particular it is possible to evaluate the impact risk probability, tailoring the deterministic method and the statistical flux models (specified in clause 10.2.2, 10.2.3 and 10.2.4 of ECSS-E-ST-10-04C) with the specific mission parameters.

Space debris semi-deterministic model

The space debris impact risk assessment is calculated with a semi-deterministic approach, using both a deterministic method and a statistical method:

- *Deterministic contribute* – Orbit propagation of trackable oblects (10 cm to 100 m size), whose orbital elements are known, allow to access collision between debris and satellites. The DISCOS database (Ref.10) provides the orbiting object population catalogue. The object main feature is the diameter. For conversion between mass and diameter an average density of 2,8 g/cm^3 (that is the average density of space debris objects > 1mm) and a spherical shape are considered.
- *Statistical contribute* – Cumulative meteoroid and space debris statistical fluxes (particles size from 1 μm to 100m) can be obtained directly from the flux models shown in next session.

Space debris model uncertainties is mainly due to sub-mm size objects in orbits below 1000 km. These objects have short lifetimes of weeks or months and a long period estimation of this small objects population can vary by an order of magnitude.

In Fig. II-9 the space debris percentage trend with respect to the semi-major axis classification is shown.

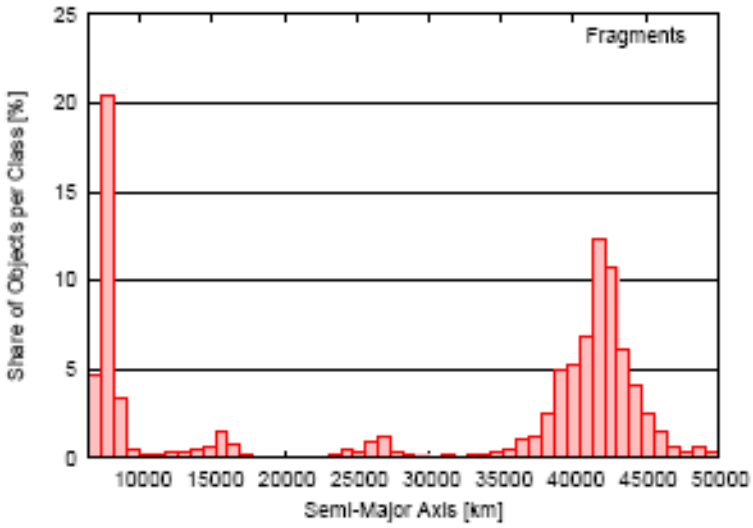

Fig. II-9. Space debris % vs. Semi-Major Axis.

Meteoroid statistical model

The meteoroid sporadic flux model is calculated taking into account:

- Isotropic flux with respect to the Earth surface.
- Flux enhancement from gravitational attraction
- Earth shielding
- Spacecraft motion

Both Earth shielding and spacecraft motion introduce a directional dependence that is responsible for changing in flux value.

The reference meteoroid mass density is 2,5 g/cm^3. Moreover peak activity stream fluxes can exceed the sporadic one by a factor five or more. Meteoroid storm exceed sporadic one by a factor 10 000. They happen occasionally (like Leonid streams in 1998, 1999 and 2001) and can be encountered for short periods (1-2 hours).

Uncertainties in the meteoroid models mainly result from uncertainties in particle densities and masses.

II.2 ESA ECSS standards application on EduSAT mission

EduSAT (Educational SATellite) is an university microsatellite coordinated and funded by the Italian Space Agency and commissioned to GAUSS group (as prime contractor), in collaboration with an Italian company (IMTsrl) which is active in the field of space systems.

The satellite is entirely built and operated in orbit by students, researchers and professors of the GAUSS group. EduSAT primary payload is an analog sun sensor developed by IMTsrl in collaboration with several high schools.

The main project goal is to promote space education among high school students and to support scientific careers of PhD and university students.

As a PhD student involved in EduSAT program my years of research have been focused on the microsatellite design and on the study of applicability of ESA standards on EduSAT mission.

In paragraph II.1 we have presented the ECSS system. Now the applicability study of ECSS standards at university-class microsatellites is shown. In particular the ECSS application on EduSAT program will be described.

II.2.1 ECSS System (ECSS-S) standard application on EduSAT mission

According with ECSS-S-ST-00C(31July2008) document, described in paragraph II.1, the EduSAT project has been organized following the standard customer-supplier chain shown in Fig. II-3. In particular EduSAT program is funded by ASI, the top level customer. IMT acts as suppliers only. GAUSS group acts at an intermediate level of the hierarchy, and is both supplier and customer.

The hierarchical structure in Fig. II-10 constitutes the customer–supplier chain within Edusat project.

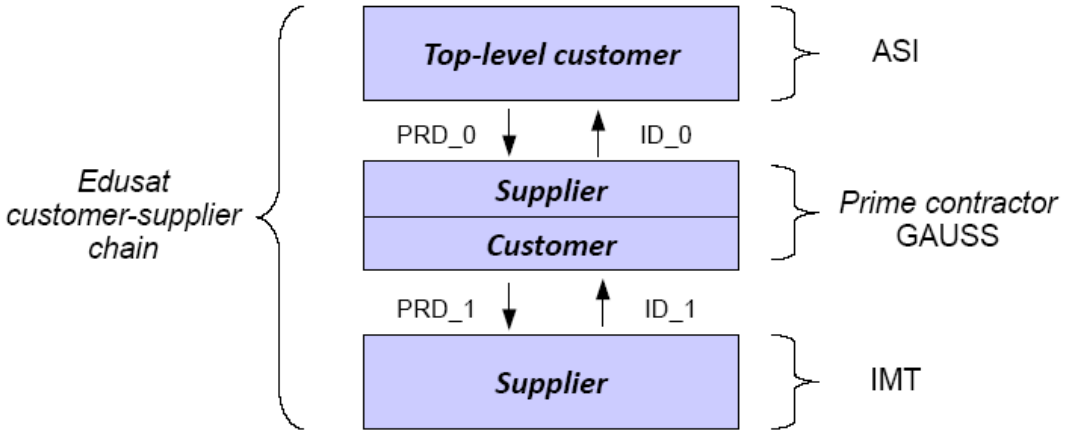

Fig. II-10. EduSAT customer-supplier chain.

The applicability of standards and requirements is specified in the project requirements documents (PRDs), which are included in business agreements, which are agreed by the parties.

A supplier, at any level, is responsible for demonstrating compliance with the project requirements contained in his customer's PRD, through, for example, the elaboration of a compliance matrix, and ultimately for supplying a conforming product. The compliance to the PRD is presented in an Implementation Documents (IDs).

This method has been used during the IMT payload delivery in July 2010. They provided the compliance matrix and the product conforming to the GAUSS-IMT contract requirements.

II.2.2 Management ECSS (ECSS-M) standards application on EduSAT mission

In the following pages the main ECSS standards belonged to the Management branches (ECSS-M) will be presented, investigating the applicability of these standards in EduSAT university microsatellite project.

II.2.2.1Project planning and implementation (ECSS-M-ST-10C Rev. 1 - 6 March 2009) standard application on EduSAT mission

The application of "Project planning and implementation" standard to EduSAT mission is presented in the following section.

Work Breakdown Structure (WBS)

Management instruments ensure an effective and efficient management approach. However, university projects do not use management methods. In EduSAT project the WBS structure has been implemented.

The successful of a space mission is due to cooperation between different groups. For this reason dedicated organization and planning methods play a key role, especially if the founds are limited and the objectives of the mission have to be satisfied minimizing cost and time needed (as in the case of EduSAT program). With this aim, the use of Work package (WP) permits to explicitly identify the work of each supplier in the work breakdown structure.

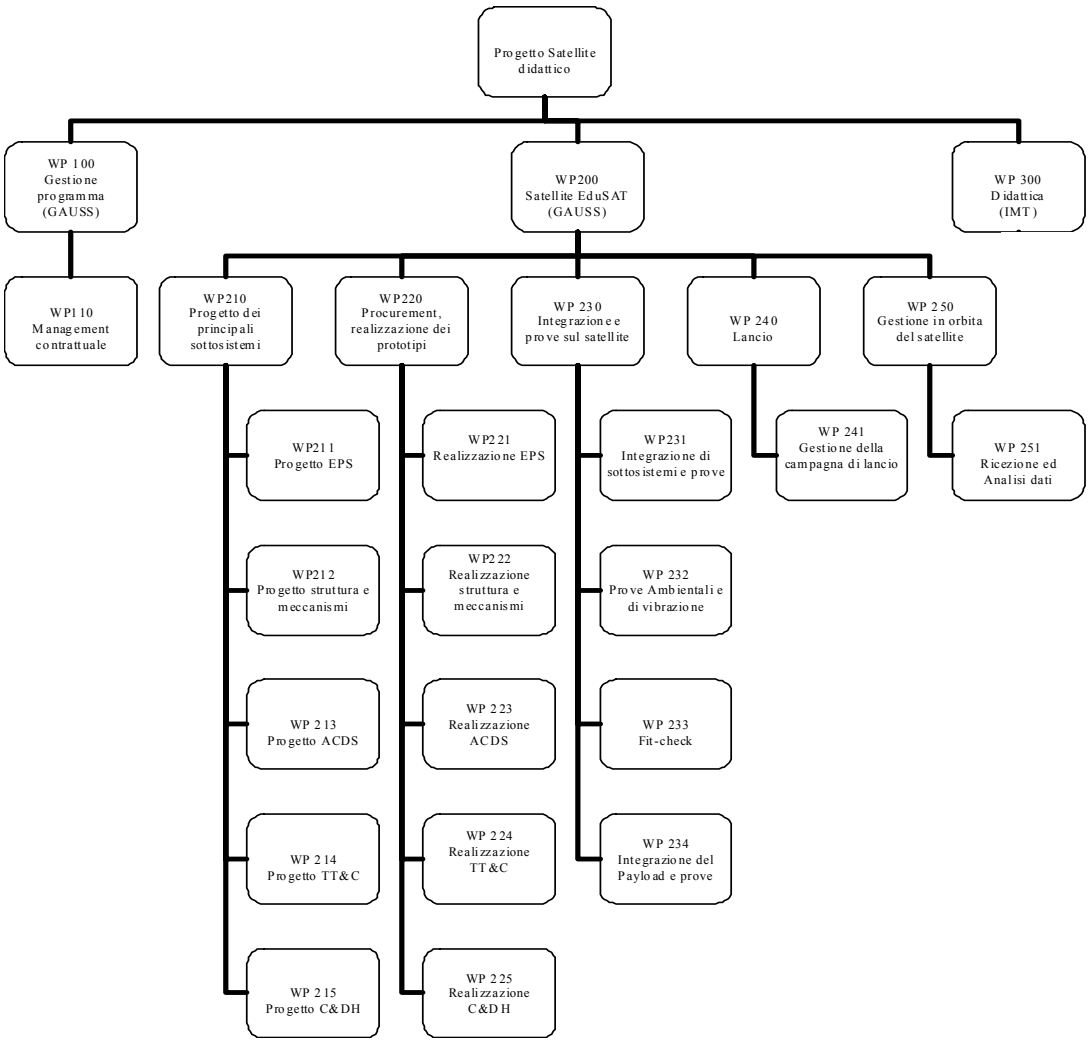

Fig. II-11. EduSAT WBS (Ref. 1).

The WP100 belongs to the program management activities. The WP 200 groups all the design, manufacturing, integration, launch campaign and in orbit

operations activities. Finally WP300 belongs to the students training in several high schools.

Project phasing

From 2000 to 2006 GAUSS group have launched 4 UNISAT microsatellites, with the main intent to give to masters students the opportunity to follow all the mission phases, from the concept design to the launch and in orbit operations. In the EduSAT program several milestones have been fixed, to allow GAUSS group to provide the project status to the top-level customer ASI. In particular have been chosen tree project reviews:

- *First progress meeting.* Equivalent to the Critical Design Review (CDR), is used to judge the readiness of the project to move into phase D.
- *Second progress meeting.* Equivalent to the Qualification Review (QR), used to confirm that the verification process has demonstrated that the design, including margins, meets the applicable requirements.
- *Final Review.* Equivalent to the Acceptance Review (AR), used to verify that all deliverable products are available for the approved deliverable items list.

II.2.2.2Cost and schedule management (ECSS-M-ST-60C (31 July 2008)) standard application on EduSAT mission

The Gantt chart

In order to produce a precise and useful project schedule, I grouped the activities in conformance with the Work Breakdown Structure. In Fig. II-12 there is the Edusat Gantt chart.

It's important to emphasize that project phases are closely linked to activities on system and product level but depending on the specific circumstances of a project and the acceptance of involved risk, activities can overlap project phases.

This management instrument is more powerful if work packages are scheduled with detail, allowing critical mission phases detection.

Moreover in university project low cost constraint is the primary design driver and the milestones have to be more flexible as possible. For example, EduSAT microsatellite will be launched in Piggy-Back mode to reduce launch costs. This launch mode weakness is the uncertainty of the launch date. In particular EduSAT first launch date was fixed on November 2009. Afterwards it has been changed in

April 2010 and now is confirmed on March 2011. EduSAT program kick-off meeting was on 11 December 2007. As shown in the EduSAT Gantt chart, the satellite design and construction phase was originally 2 years, in order to allows students to participate the program. Each Work Packages duration have been planned according to the design experience of UNISAT3 satellite (launched by GAUSS group in 2006).

It's important to emphasize that WP200 activities are grouped according to the different phases of the project: the design phase, the manufacturing phase, the integration phase, the launch campaign and the in orbit operations activities.

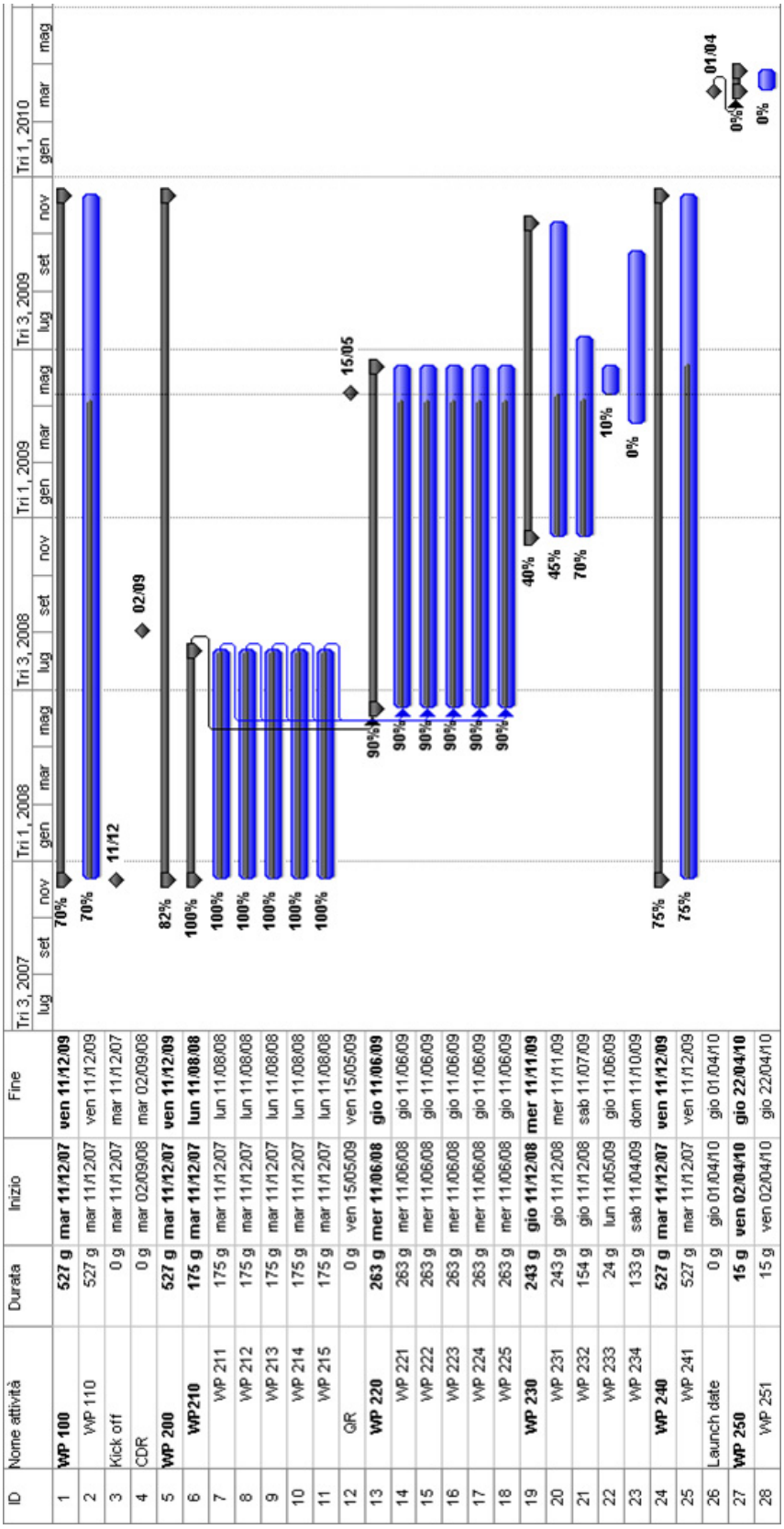

ID	Nome attività	Durata	Inizio	Fine
1	**WP 100**	**527 g**	**mar 11/12/07**	**ven 11/12/09**
2	WP 110	527 g	mar 11/12/07	ven 11/12/09
3	Kick off	0 g	mar 11/12/07	mar 11/12/07
4	CDR	0 g	mar 02/09/08	mar 02/09/08
5	**WP 200**	**527 g**	**mar 11/12/07**	**ven 11/12/09**
6	**WP210**	**175 g**	**mar 11/12/07**	**lun 11/08/08**
7	WP 211	175 g	mar 11/12/07	lun 11/08/08
8	WP 212	175 g	mar 11/12/07	lun 11/08/08
9	WP 213	175 g	mar 11/12/07	lun 11/08/08
10	WP 214	175 g	mar 11/12/07	lun 11/08/08
11	WP 215	175 g	mar 11/12/07	lun 11/08/08
12	QR	0 g	ven 15/05/09	ven 15/05/09
13	**WP 220**	**263 g**	**mer 11/06/08**	**gio 11/06/09**
14	WP 221	263 g	mer 11/06/08	gio 11/06/09
15	WP 222	263 g	mer 11/06/08	gio 11/06/09
16	WP 223	263 g	mer 11/06/08	gio 11/06/09
17	WP 224	263 g	mer 11/06/08	gio 11/06/09
18	WP 225	263 g	mer 11/06/08	gio 11/06/09
19	**WP 230**	**243 g**	**gio 11/12/08**	**mer 11/11/09**
20	WP 231	243 g	gio 11/12/08	mer 11/11/09
21	WP 232	154 g	gio 11/12/08	sab 11/07/09
22	WP 233	24 g	lun 11/05/09	gio 11/06/09
23	WP 234	133 g	sab 11/04/09	dom 11/10/09
24	**WP 240**	**527 g**	**mar 11/12/07**	**ven 11/12/09**
25	WP 241	527 g	mar 11/12/07	ven 11/12/09
26	Launch date	0 g	gio 01/04/10	gio 01/04/10
27	**WP 250**	**15 g**	**ven 02/04/10**	**gio 22/04/10**
28	WP 251	15 g	ven 02/04/10	gio 22/04/10

Fig. II-12. EduSAT Gantt chart.

II.2.2.3 Risk management (ECSS-M-00-03A) standard application on EduSAT mission

Since the beginning of the program, EduSAT risk assessment and management process has been carried out identifying the risks according to the ECSS standards. In the following pages only the high severity risks will be investigated and the methods to reduce the associated risk values will be presented.

ID	Edusat Risk -01
Name	IMT payload electrical discharge
Description	Accidental platform damage due to payload electrical block lightning or electrostatic discharge.
Consequences	Satellite subsystems failure. Communication system don't receive ground station command or it is not able to send telemetry data.
Severity	5
Probability	1 = A
Total Risk	5 = Low Risk
Prevention	Dedicated platform electrical interface have been designed. Dedicated payload safety system for the electrical link with the satellite has been imposed by satellite developers as payload requirements.

Tab. II-2. Edusat Risk -01= low risk.

The Edusat Risk -01 severity is high. However dedicated electrical interface between platform and payloads has been developed to obtain risk probability 1. This low risk has to be monitored and controlled during the payload integration phase and flight model functional test, and is under the Edusat C&DH (Commands and Data Handling) system responsible (with the contribute of the risk responsible).

ID	Edusat Risk -02
Name	MRFOD ejection mechanism
Description	Not correct hatch opening during the MRFOD ejection phase
Consequences	Collision or mechanical interference between MRFOD and VHF antenna or between MRFOD and the sun sensor
Severity	4
Probability	2 = B
Total Risk	6 = Low Risk
Prevention	Dedicated devises has been manufactured to allow a safety MRFOD hatch deployment. Dedicated upper panel structural configuration has been designed to obtain a safe distance between IMT sun sensor, VHF antenna and MRFOD launcher

Tab. II-3. Edusat Risk -02

The MRFOD (Morehead-Roma Femptosat Orbital Deployment) is the femptosatellite deployment system invented by Professor Robert Twiggs and boarded on EduSAT. MRFOD characteristics will be described in detail in the following chapter. Now we will investigate the risks related to MRFOD use. MRFOD hatch has been designed to avoid interference during the femptosatellite ejection with the VHF antenna and the IMT sun sensor.

ID	Edusat Risk -03
Name	MRFOD ejection system - electrical interface
Description	MRFOD hatch cannot be opened due to Edusat C&DH failure.
Consequences	Femptosatellites are not ejected
Severity	5
Probability	1 = A
Total Risk	5 = Low Risk
Prevention	Safe electrical circuit developed, based on the MRFOD periodic test of the Edusat C&DH correct operations.
Reaction	-
Recovery	-

Tab. II-4. Edusat Risk -03

In the case of Edusat C&DH (Command and Data Handling) or Communication systems failures, the MRFOD hatch cannot be opened and the femptosatellites cannot be ejected. The first solution for the femptosatellites ejection was the activation of 2 thermal cut (for redundancy reason), once Edusat is switched on (trough the mechanical switch activated during the spacecraft separation from the launch vehicle). However in this critical phase the satellite is not safely positioned in its final orbit.

With this solution, the risk probability of a MRFOD failure was 4, leading to an unacceptable maximum risk value (Tolal Risk = 20). During the EduSAT early orbit phase, the satellites have not yet reached the attitude stability and the spin rate is not controlled. Edusat Power system cannot provide the nominal power (solar panels orientation with respect to the sun light direction). For this reason during this phase only Edusat C&DH and communication system are switched on allowing only critical operations (such us communication test with the ground station) and avoiding any other secondary functions (such as MRFOD ejecting).

To solve this problem, MRFOD electronic device has been designed to eject femptosatellites only after the in orbit test phase. After a dedicated threshold time (representative of the in orbit test phase), MRFOD start to periodically test EduSAT performances. If EduSAT C&DH system don't replies the periodic MRFOD interrogation signal, MRFOD autonomously ejects the femptosatellites.

ID	Edusat Risk -04
Name	Ground-satellite communication link failure
Description	Failure in the downlink or uplink communication systems.
Consequences	UHF or VHF or S-Band communication link is interrupted.
Severity	3
Probability	3 = B
Total Risk	9 = Low Risk
Prevention	With a dedicated SCC command the frequencies failed can be excluded, and the survived frequencies could be switched on emergency mode
Reaction	-
Recovery	-

Tab. II-5. Edusat Risk -04

EduSAT allows VHF, UHF and S-Band communications in both uplink and downlink. However, if one of these frequencies don't work, the survived frequencies cold be switched on emergency mode, in which both uplink and downlink communication are satisfied.

II.2.3 Engineering ECSS (ECSS-E) standards application on EduSAT mission

In the following pages some example of ECSS E standards applied on EduSAT project will be shown.

II.2.3.1Photovoltaic assemblies and components (ECSS-E-ST-20-08C (31July2008)) standard application on EduSAT mission

According to the cleanroom characteristics suggested by ECSS-E-ST-20-08 and ISO 14644-1 standards (described in paragraph II.1.5.1), during the assembly and test of photovoltaic system, the maximum permitted concentration of particles "Cn" (for particles up to 0.5 μm) is :

$$Cn\_ISO8 = 3.5 \times 10^6 \ \text{particles}/\text{m}^3$$

Now I will describe the process adopted to demonstrate the GAUSS cleanroom conformance with ECSS standards.

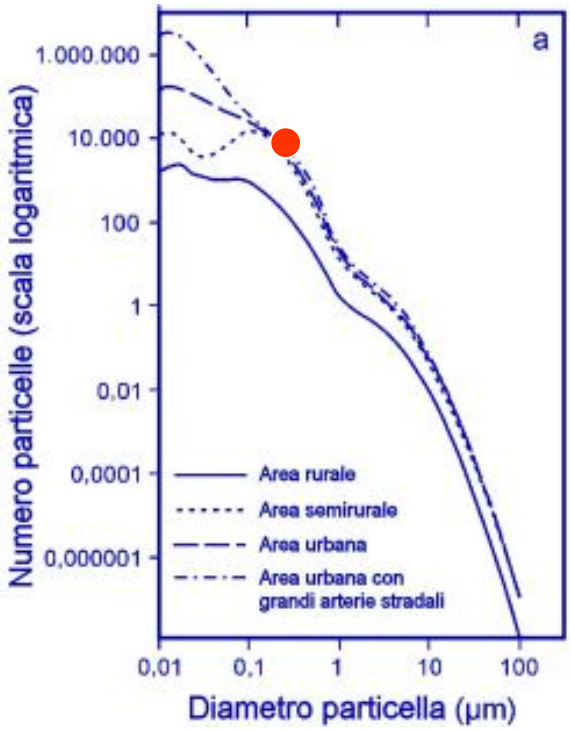

Fig. II-13. Concentration of airborne particles in different urban areas (in particles per cubic centimetre of air) (Ref. 11).

In Fig. II-13 is shown the concentration of airborne particles in different urban areas (in particles per cubic centimetre of air). The concentration Cn of particles up to 0.5 μm diameter is about 10^10 particles/m^3.

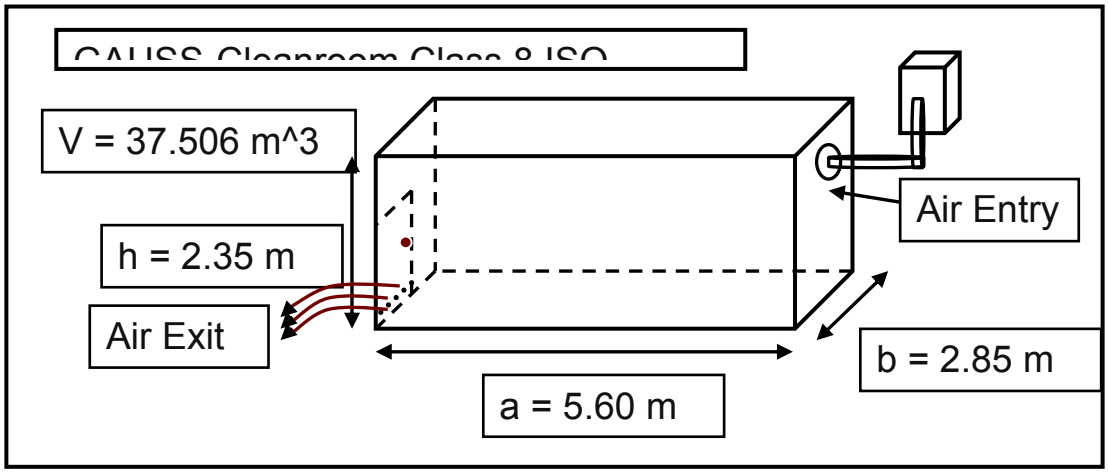

Fig. II-14. GAUSS clean room architecture.

In Fig. II-14 the GAUSS clean room architecture and features are shown. In particular the room volume is V = 37.506 m^3.

The clean room air pump have two different modes:

Mode 1

P_air1 = 480 m^3/h @ 230 V, 50 Hz

Eff1 = 99 % @ 0,3 μm;

Mode 2

P_air2 = 400 m^3/h @ 230 V, 50 Hz,

Eff2 = 99,97 % @ 0,3 μm.

Where P_air is the pump capacity and Eff is the pump efficiency. For these reasons the clean room need different time to obtain regime condition:

$$\Delta t\_regime = \frac{P\_air}{V},$$

Obtaining:

Δt_regime1 = 4,68825 [’] and Δt_regime2 = 5,6259 [’].

However if in the mode 2 only the 0.03% of the airborne concentration remain in the clean room (Eff2 = 99,97 %), in the mode 1 the 1% will remain (Eff1 = 99 %). It means that only the mode 2 satisfy the ECSS photovoltaic assemblies and test environment standard:

$$Cn1 = 1\% \cdot Cn = 10^8 \ \text{particles}/\text{m}^3 > Cn\_ISO8;$$

$$Cn2 = 0.03\% \cdot Cn = 10^6 \ \text{particles}/\text{m}^3 < Cn\_ISO8$$

The application of this standard is just un example of the ECSS-E possible technical support. Several suggestions in this standard has been considered during the photovoltaic assemblies and test phase, as the measurement tolerance to be adopted during the solar cell characterization and procedure to avoid Electrostatic discharge.

II.2.3.2 Space environment (ECSS-E-ST-10-04C) standards application on EduSAT mission

In the following pages the space debris and meteoroids model (described in paragraph II.1.5.2) will be applied to estimate EduSAT satellite impact risk assessment.

EduSAT impact risk assessment exploiting ESA MASTER-2005 tool

EduSAT impact risk assessments has been performed exploiting ESA MASTER-2005 tool, tailoring the deterministic method and the statistical flux models specified in ECSS-E-ST-10-04C standard with the specific EduSAT mission parameters. MASER 2005 is the free software provided by ESA to calculate debris and meteoroids flux for Earth altitudes below 36 786,0 km.

EduSAT structure shape and EduSAT LEO orbit characteristics have been taken into account to estimate the impact risk value. As shown in Fig. II-9, LEO orbits are very crowded of space debris, and a preliminary impact risk assessment is needed. EduSAT features have been used as MASTER-2005 input data, as shown in Fig. II-15.

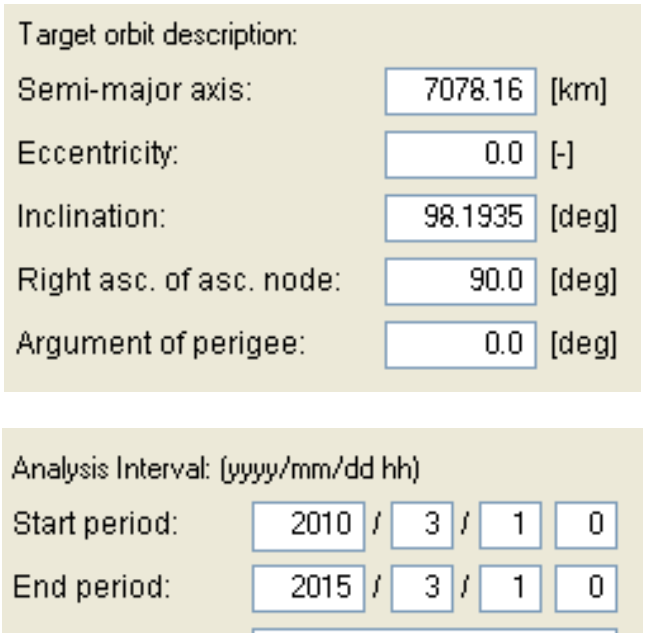

Fig. II-15. EduSAT impact risk assessment. MASTER 2005 input values.

Running a five year simulation it is possible to obtain the object flux [1/m^2/year] belonged to different kind of orbiting objects. In particular the result trend is depicted in Fig. II-16 and Fig. II-17 for both mass and diameter variation.

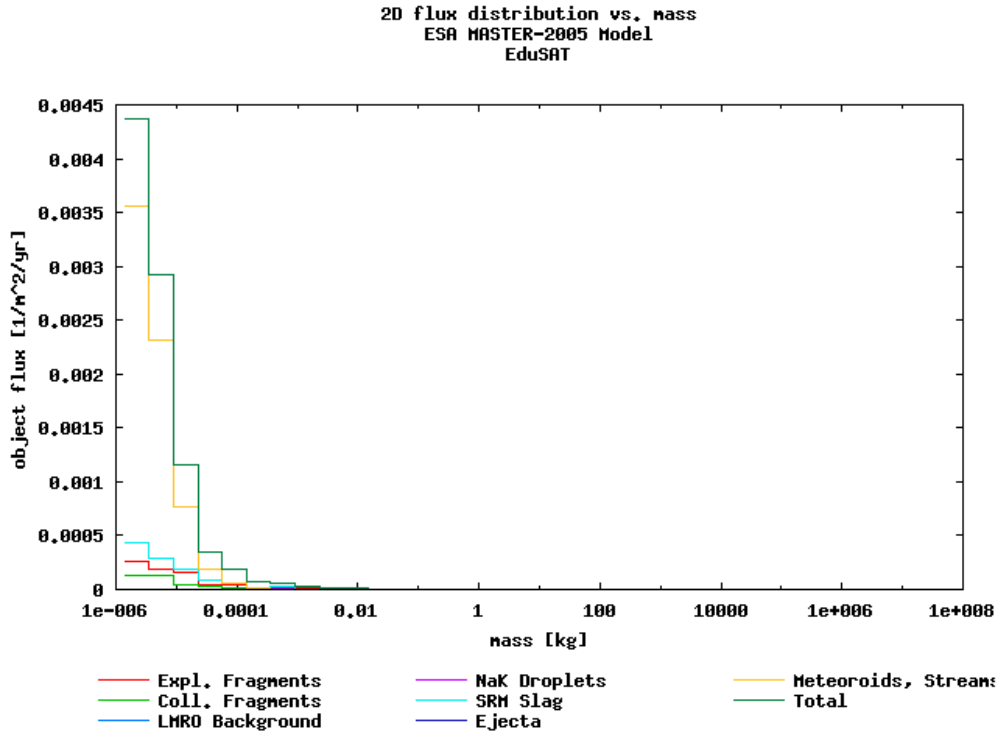

Fig. II-16. MASTER 2005 five year simulation on EduSAT mission. Object flux for different kind of orbiting objects and belonged to object mass.

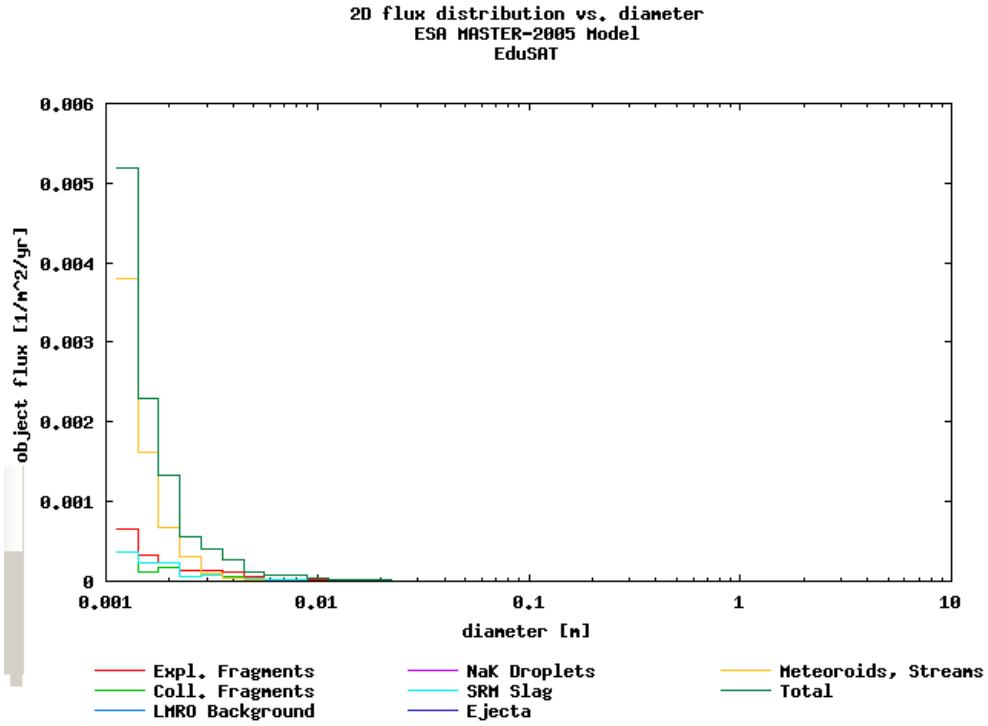

Fig. II-17. MASTER 2005 five year simulation on EduSAT mission. Object flux for different kind of orbiting objects and belonged to object diameter.

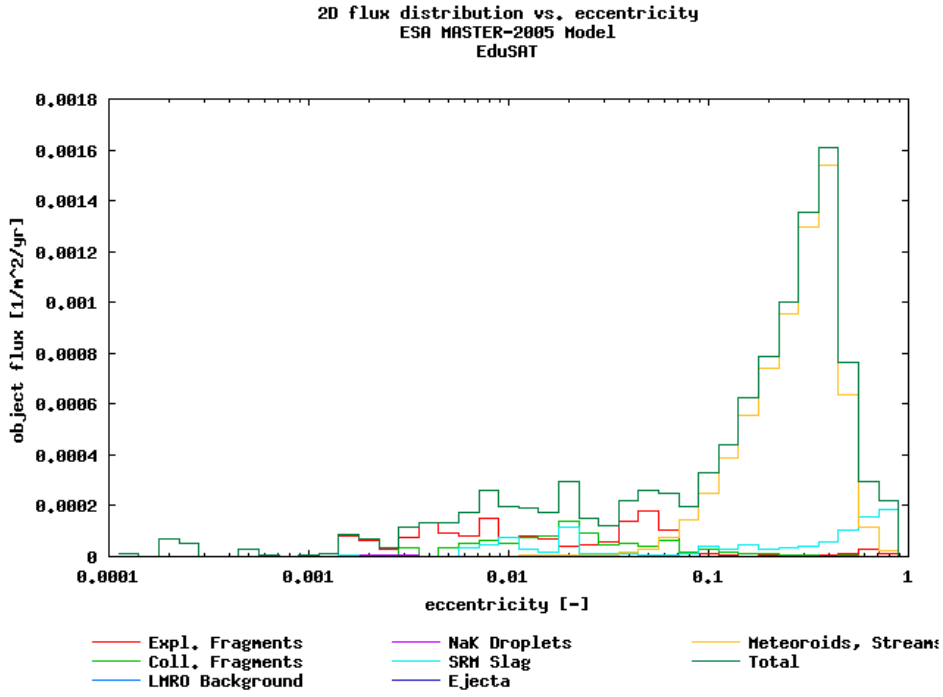

Fig. II-18. MASTER 2005 five year simulation on EduSAT mission. Object flux for different kind of orbiting objects and belonged to object eccentricity.

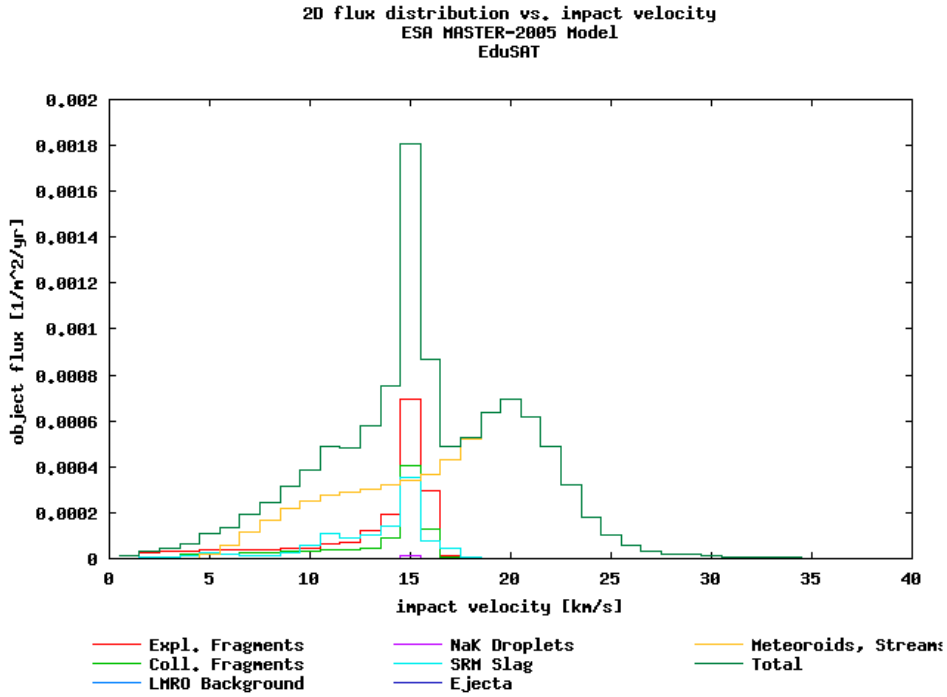

Fig. II-19. MASTER 2005 five year simulation on EduSAT mission. Object flux for different kind of orbiting objects and belonged to object impact velocity.

The higher contribute to the flux is due to small size and high eccentricity meteoroids (see also Fig. II-18). Then an important contribute is given by explosion fragments, LMRO and collision fragments. It is also important to emphasize that in-orbit impact velocities can range from 0 to about 25 km/s with two different peak values at an average velocity of 15 km/s and 20 km/s.

Once the flux F has been estimated, the number of impact N per years (T = 1 year) can be calculated as follow:

$$N = F \cdot A \cdot T \quad ,$$

where Edusat exposed area is A = 0,0832 m^2.

Finally the probability of exactly n impacts occurring in the corresponding time interval shall be determined according to the expression:

$$P_n = \left(\frac{N^n}{n!} \right) e^{-N} .$$

With this method the Edusat impact probability has been calculated and the results are shown in the following table:

Object diameter [m]	Flux [1/m^2/year]	P [n=1, T=1]
0,01	3 x 10^ -5	2.4959 x 10 ^ -6
0,001	5,2 x 10^ -3	4.3245 x 10^ -4

Tab. II-6. Edusat impact probability per year and for different object diameter.

As underlined in the FAA AC431-35-1 standard (Ref. 12), the safety probability for flying spacecraft is P <= 10 ^ -5. The catastrophic impact events occur when a spacecraft collides with an orbiting object with diameter >= 0.01 m. Orbiting objects smaller than this size are considered dangerous for the sub system impacted, but statistically cannot cause the mission loss. For this reason EduSAT catastrophic impact probability is lower than the limit value seen above, and it means that EduSAT do not need collision avoidance capability.

II.3 ESA ECSS standards application on BUGS experiment

In this paragraph the ESA BUGS experiment will be shown. In this project I have participated as responsible of boom vibration analysis (through dedicated imaging sensors) and ECSS standards application. This experience gave me the opportunity to compare a typical ESA student mission with EduSAT university-class design methods. Firstly the BUGS experiment will be introduced. Afterwards the application of ECSS standard belonged to the management branch on BUGS experiment will be analysed.

II.3.1 The BUGS experiment overview and objectives

BUGS experiment, Boom for University Gravity-Gradient stabilized Satellites, has the main goal to perform test in spaceflight conditions of a boom prototype which could be used on board UNISAT-5 satellite (a future GAUSS mission) for gravity gradient attitude stabilization system.

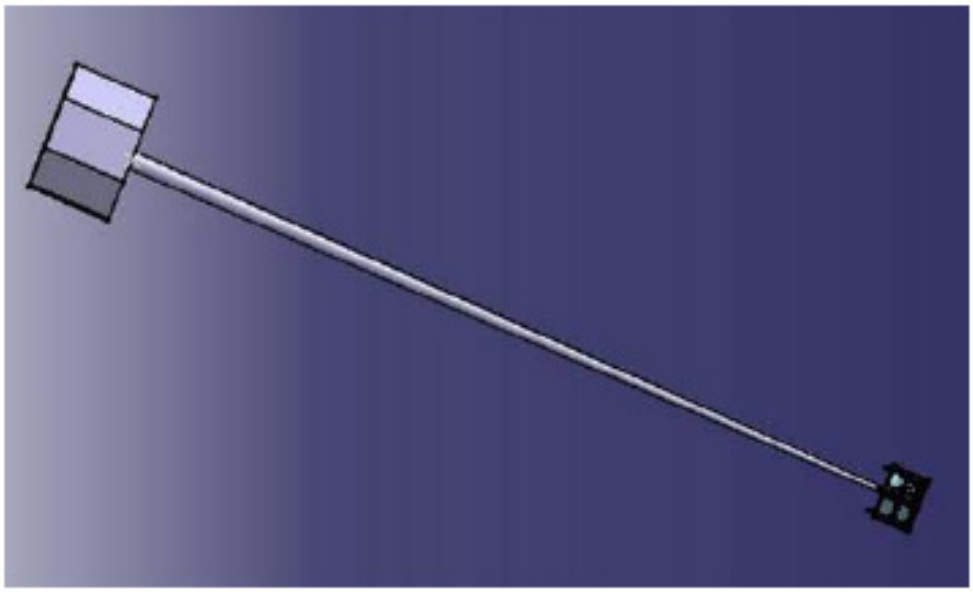

Fig. II-20. UNISAT-5 with boom and active tip mass

The proposed boom for BUGS experiment (Ref. 13) is based on an innovative, low cost concept, which uses the principle of the tape coil spring (Fig.

II-20); it can be deployed once and it maintains its rigidity since every coil is blocked inside the following one.

Even if the boom has been undergone to an extensive ground test campaign, the students and researchers involved in this project had not idea about the effective deployment in spaceflight conditions. The presence of gravity does not permit to test real boom aperture due to the friction effect among coils during deployment phase.

The ESA REXUS rocket's trajectory gave us the required spaceflight conditions to test the boom deployment. As matter of fact, thanks to this experiment it will be possible to evaluate the boom dynamic behaviour during the deployment phase in spaceflight conditions.

The idea of this experiment is to perform a deployment test in microgravity conditions in order to study the effective boom behaviour in spaceflight conditions. The boom deployment will be recorded by a couple of video cameras. The idea is to compare flight tests with system modal shapes analysis obtained from finite elements simulations of the boom. These simulations are not trivial due to imprecision in friction modelling. In flight test results have been employed to improve simulations of the boom dynamics. Moreover, collected data have been used to model real perturbation introduced by the boom deployment giving an accurate idea of the satellite attitude motion in orbit.

Fig. II-21. Tape coil spring employed for boom prototype development

This experiment overview is presented with the aim to introduce this ESA students mission experience. In the following paragraph the ESA management methods adopted in this project (following ECSS-M branch standards) will be shown in dept as term of comparison with the EduSAT program management method.

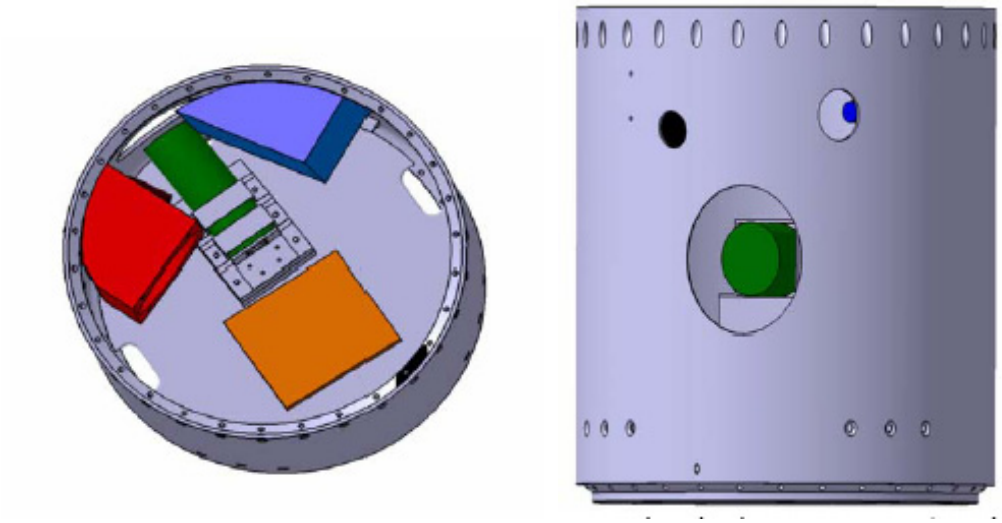

Fig. II-22. BUGS preliminary mechanical arrangement on board REXUS module.

II.3.1 Management ECSS (ECSS-M) standards application on BUGS experiment

In the following pages the applicability of standards belonged to the Management branches on BUGS experiment will be shown.

II.3.1.1Project planning and implementation (ECSS-M-ST-10C Rev. 1 - 6 March 2009) standard application on BUGS experiment

The application of this standard to BUGS missions is presented in the following section.

Work Breakdown Structure (WBS)

The BUGS experience has been useful to understand the ESA method to manage and develop a university space project. During this project the WBS has been requested by ESA support specialists at the beginning of the mission.

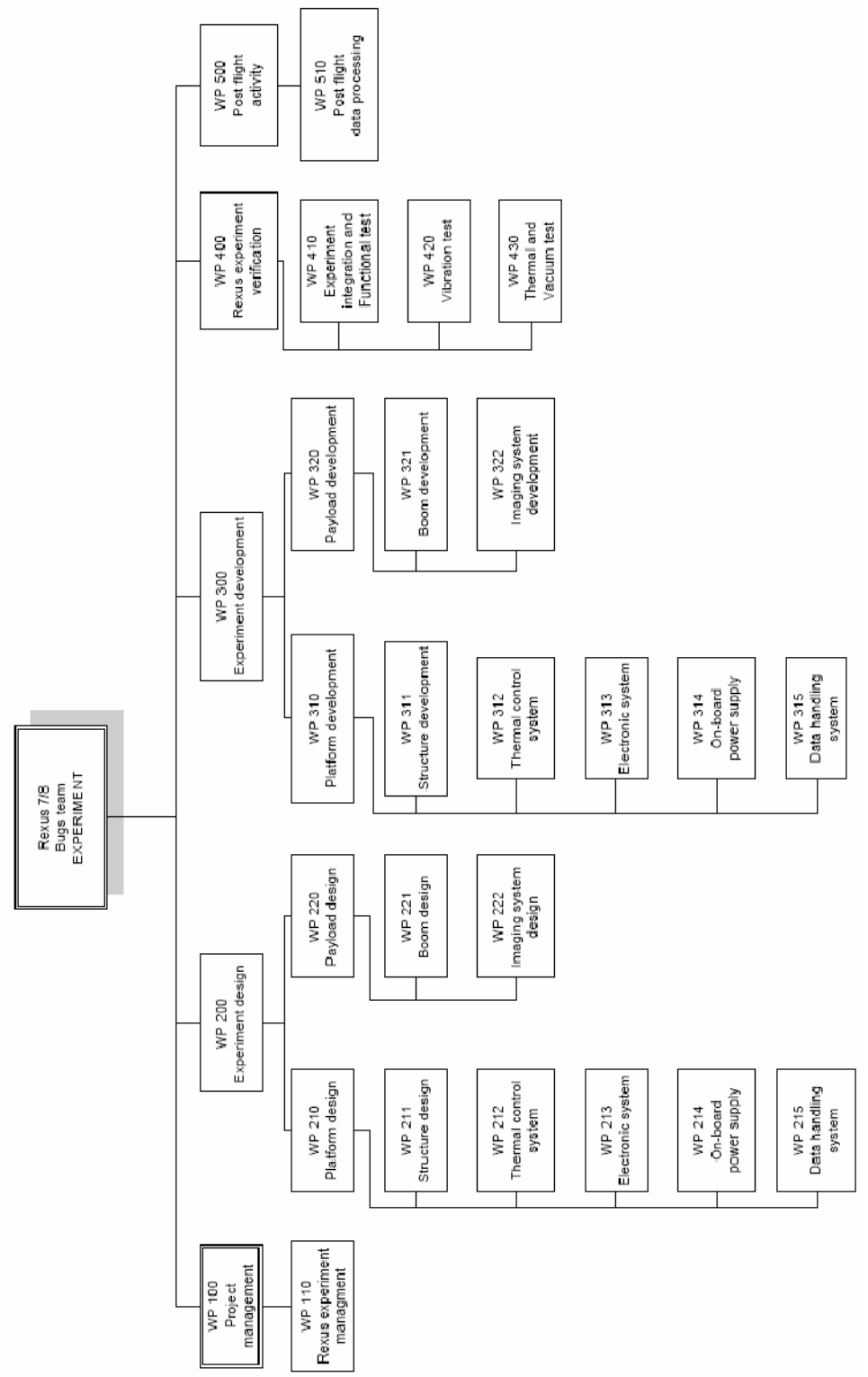

Fig. II-23. Bugs experiment WBS.

The WP100 belongs to the program management activities. The WP 200 groups all the design work packages while the WP300 describes the manufacturing

activities. The WP400 is representative of the integration and tests work packages and finally WP500 belongs to post flight activity.

This experience gave me the opportunity to understand how the WBS management instrument is usually adopted in ESA missions.

Project phasing

The BUGS project, funded and supervised by ESA, has a really short schedule:

- 1 Sep 2008 Announcement of opportunity for REXUS 7/8 experiments
- 17 Nov 2008 Deadline for applications
- 19 Dec 2008 Announcement of shortlisted proposals and invitations to Selection Workshop
- 4 Feb 2009 Selection Workshop at ESA-ESTEC in Noordwijk, The Netherlands
- 13 Feb 2009 Announcement of final selection of experiments for REXUS 7/8
- 23 Mar 2009 Student Training Week and Preliminary Design Review (PDR) at Oberpfaffenhofen, Germany
- Jun 2009 Critical Design Review (CDR)
- Dec 2009 Delivery of experiments to Esrange for Experiment Acceptance Review (EAR)
- Mar 2010 REXUS 7/8 Launch Campaign at Esrange
- Jun 2010 Submission of Experiment Reports to ESA

This schedule highlights how a typical ESA students mission is developed in a very short time to allow student to participate in the project.

II.3.1.2Cost and schedule management (ECSS-M-ST-60C (31 July 2008)) standard application on BUGS experiment

The Gantt chart

The Gantt time schedule applied to the BUGS experiment is important to emphasize that project phases are closely linked to activities on system and product level but depending on the specific circumstances of a project and the acceptance of involved risk, activities can overlap project phases.

In BUGS experiment work packages have been scheduled with detail, allowing critical mission phases detection.

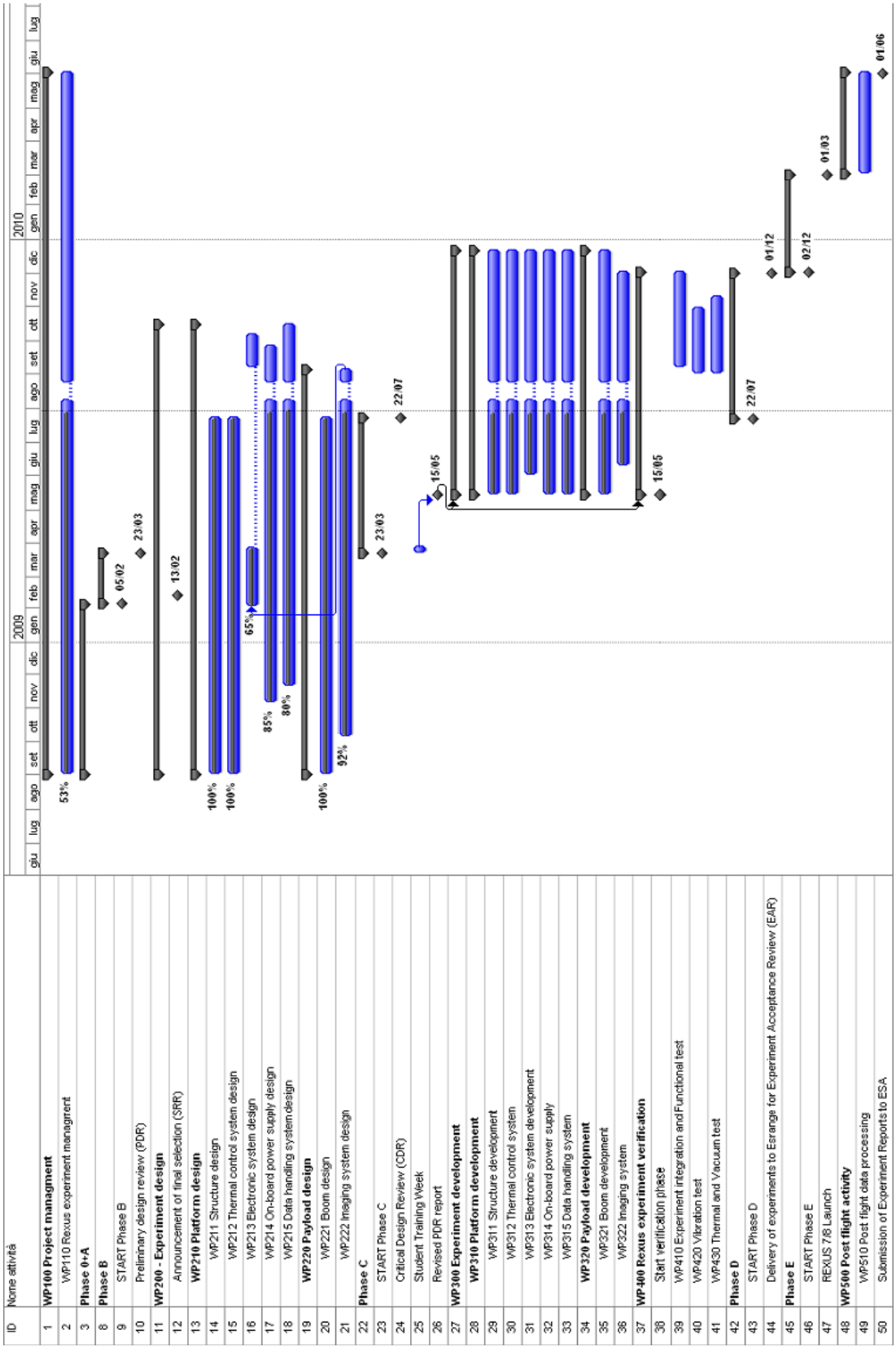

Fig. II-24. Gantt time schedule of the BUGS experiment preparation.

II.3.1.3 Risk management (ECSS-M-00-03A) standard application on BUGS experiment

The ESA Bugs experiment has been a valid training to understand in dept the importance of the risk management and assessment process. As shown in Fig. II-24, the 22nd of July 2009 BUGS team has presented the status of the experiment at the CDR (Critical Design Review) meeting. During CDR meeting BUGS risk assessment and management have been presented but ESA committee evaluation was: "CDR not passed". In particular the ESA committee was asking for:

- Assess risk of accidental boom deployment due to lightning or electrostatic discharge.
- Assess risk associated with all other possible triggers of boom deployment.
- Assess risk of accidental boom deployment during the early part of the flight.

After ESA committee evaluation, a more detailed risk analysis has been carried out in order to be accepted for the Phase D. These risks are here presented, highlighting the solutions adopted in order to mitigate high risks..

ID	BUGS Risk -01
Name	Boom deployment
Description	Difficulty in the boom deployment during flight
Consequences	Experiment can not be performed
Severity	5
Probability	3 = C
Total Risk	15
Prevention	Mechanical interface in order to reduce this risk occurrence. This is a cylinder able to guide the boom in the right direction for deployment.

Tab. II-7. BUGS Risk -01: High risk.

In order to mitigate the risk a mechanical interface has been manufactured. This is a cylinder able to guide the boom in the right direction during the deployment.

ID	BUGS Risk -02
Name	Camera resistance - TV cannel
Description	Camera Crash due to launch accelerations- Camera Malfunction
Consequences	Data can not be achieved
Severity	3
Probability	2 = B
Total Risk	6

Prevention	Two different kinds of cameras have been selected in order to reduce this risk occurrence. Both the cameras will be used to record vibration data of the boom.

Tab. II-8. BUGS Risk -01: Low risk.

Risk is low because it has been selected a camera already tested on the REXUS launcher.

ID	BUGS Risk -03
Name	Ejection system
Description	Thermal cut malfunction
Consequences	Thermal cut does not work: boom is not ejected before parachute opening
Severity	4
Probability	3 = C
Total Risk	12
Prevention	Two thermal cut systems in parallel will be used for redundancy

Tab. II-9. BUGS Risk -03: Medium risk.

Two thermal cut systems in parallel will be used for redundancy in order to avoid this risk (4 blades). For high and medium risk devices, the risk magnitude has been reduced by mean of an extensive test campaigns.

ID	BUGS Risk -04
Name	Injury for people during integration phase due to accidental boom deployment.
Description	Accidental deployment due to lightning or electrostatic discharge.
Consequences	Boom could hits people
Severity	4
Probability	3 = C
Total Risk	4
Prevention	People never have to work in front of the boom deployment direction. People could wear special glasses to protect eyes. A blocking system to be removed before flight is under design.

Tab. II-10. BUGS Risk -04: Medium risk.

An accidental boom opening due to vibrations has a low probability to occur because a similar device has already passed the vibration test for the DNEPR launch vehicle.

ID	BUGS Risk -05
Name	Rocket damage during integration phase or flight phase due to accidental boom deployment.
Description	Accidental deployment due to lightning or electrostatic discharge.
Consequences	Boom could damage Rexus module
Severity	2
Probability	3 = c
Total Risk	6
Prevention	A blocking system to be removed before flight is under design.

Tab. II-11. BUGS Risk -05: Low risk.

The severity is low because the force of the spring is not so high to produce damage . An accidental boom opening due to vibrations has a low probability to occur because a similar device has already passed the vibration test for the DNEPR launch vehicle.

ID	BUGS Risk -06
Name	Experiment lost during integration phase or flight phase due to accidental boom deployment.
Description	Accidental deployment due to lightning or electrostatic discharge.
Consequences	Could cause experiment lost
Severity	2
Probability	1 = A
Total Risk	2
Prevention	A blocking system to be removed before flight has been designed.

Tab. II-12 BUGS Risk -05: Minimum risk.

The severity is low because in the flight phase when the hatch is opened the boom can be anyway deployed. During the integration phase we only need to re-close the boom. An accidental boom opening due to vibrations has a low probability to occur because a similar device has already passed the vibration test for the DNEPR launch vehicle.

II.4 ESA CDF method

ESA Concurrent Design Facilities (CDF) is a state-of-the-art facility equipped with a network of computers, multimedia devices and software tools, which allows a team of experts from several disciplines to apply the concurrent engineering method to the design of future space missions. As described in Ref. 14, this facility and method facilitates a fast and effective interaction of all disciplines involved, ensuring consistent and high-quality results in a much shorter time.

Fig. II-25. ESA CDF panoramic view.

University-class mission is very short duration mission, from the conceptual design to the manufacturing and in-orbit operations. For this reason it could drastically take advantage of the new capabilities offered by the CDF, reducing the pre-Phase A (preliminary design) study duration from several months to a few weeks while increasing design quality.

The spacecraft design is based on mathematical models, which make use of custom software and linked spreadsheets. By this means, a consistent set of design parameters can be defined and exchanged throughout the study, and any changes which may have an impact on other disciplines can immediately be identified and collectively assessed. In this way, a number of design iterations can be performed, and different design options can easily be analysed and compared.

CDF activities are conducted in sessions: plenary meetings in which representatives of all space engineering domains participate, from the early phases

(requirement analysis) to the end of the design (costing). Even those disciplines that were traditionally involved at a later stage of the process are given the opportunity to participate from the beginning and to identify trends that might later invalidate the design.

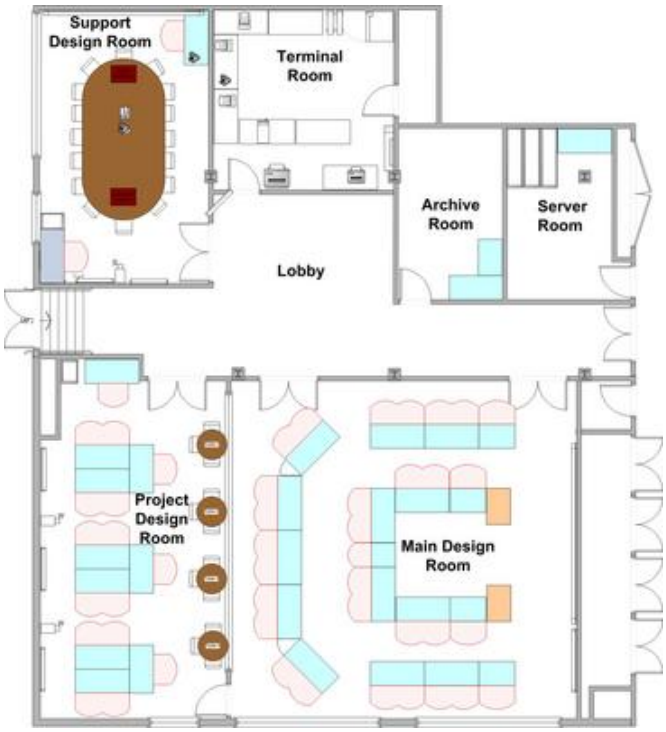

Fig. II-26. ESA CDF facility.

The ESA Integrated Design Model (IDM) is the tool, installed in the CDF computers, that allows the data sharing among the missions actors during the study sessions.

Due to the growing interest of ESA partners, Industry and Academic in the ESA CDF IDM, now the Open Concurrent Design Server (OCDS) is the next generation of the CDF design model. It make use of a Service Oriented Architecture (SOA) using web services, a centralised database and many client tools such as the OCDS Study Manager (OSM) and OCDS enabled spreadsheets. For this purpose an ECSS Working Group (ECSS-TM-10-25 "System Engineering - Engineering Design Model Data Exchange") was formed responsible for creating a Technical Memorandum (TM) which defines the recommendations for model based data exchange for the early phases of engineering and design.

II.5 ESA CDF method application on SEO study

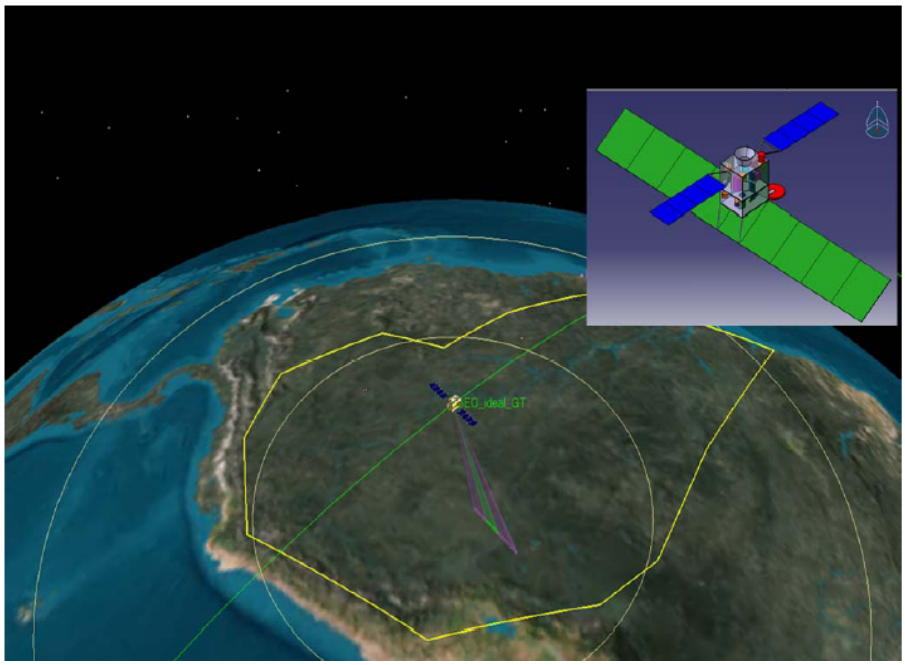

Fig. II-27. SEO mission scenario

SEO (Space system for Earth Observation) study (Ref.15 and 16) was performed in the ESTEC Concurrent Design Facility (CDF), under the responsibility of Claudio Portelli (Study Manager), by the following interdisciplinary ASI Team:

TEAM LEADER	Massimo Bandecchi (ESA- ESTEC)		
AOCS	Giovanni Valentini	MECHANISM	Claudio Portelli
COMMUNICATIONS	Gianni Casonato	POWER	Carlo Del Vecchio Blanco
CONFIGURATION	Simone Pirrotta	PROGRAMMATICS/AIV	Silvana Rabbia
COST	Giampiero Belvedere	PROPULSION	Rocco Carmine Pellegrini
DATA HANDLING	Marino Crisconio	RISK	Silvana Rabbia
GS & OPS	Fabrizio Paolillo	STRUCTURES	Simone Pirrotta
INSTRUMENTS	Maria Libera Battagliere	SYSTEMS	Claudia Facchinetti
MISSION ANALYSIS	Manfredi Porfilio	THERMAL	Mario Salatti

Fig. II-28. ASI team in SEO study.

As shown in Fig. II-28, I have been involved as Ground Segment and Operations discipline responsible (Ref.15 and 16).

The team leader was Mr. Massimo Bandecchi, ESTEC head of Concurrent Engineering (CE) section and the team was supported by a group of ESTEC experts.

ASI has its own Concurrent Engineering Facility (CEF). The study was performed to train the ASI team on the concurrent design approach applied to a complex study.

The team held 8 sessions in the CDF, supported by 8 half-day off-line preparation work, splinter meetings and discussions. The study was done between May and June 2010.

The main objectives of the CEF Team were the following:

- Give a set of coherent requirements and mission constraints.
- Generate a certain number of trade off to offer at ASI management different choice at high level.

The study subject is a Space system for Earth Observation (SEO).

The study was aimed to develop:

- the Mission Concept, with a high level description of the SEO mission
- SEO project feasibility assessment and preliminary system and subsystems configuration
- mission programmatic elements (summary bar chart), as well as application and technological aspects
- risk evaluation
- Cost estimation, detailed per products and activities (Management, Development, etc.).

The study outputs can be used to put together the requirements and constraints for a potential Phase A/B industrial contract definition.

II.5.1 SEO mission objective and architecture

The Primary Objective of the SEO satellite is to acquire SAR (Synthetic Aperture Radar) images of the amazonian region in stripmap mode, covering in one month the total area .The satellite/mission is required to meet revisit time, response time and information age requirements with an operative life of 5 years and to download the acquired data with a rate of at least 155 Mbit/sec.

From a programmatic standpoint, the development is required to be completed in five years and to be compatible with a medium-class launcher. There is a constraint on the mission overall cost.

As an option, aiming at dramatically improving the information age requirement, the system could make use of a GEO Data Relay Satellites(s) System in order to collect and forward towards the earth all the scientific raw data.

The complete set of requirements has been collected in the "Space system for Earth Observation (SEO) - Mission Needs & User Objectives" document.

During the study, two options were developped:

- Option1: S-band link for TM/TC and X-band link for SAR data download
- Option2: S-band link for TM/TC and Ka-band link to DRS for SAR data download

The best orbit was identified to be a low inclination at 18° and 575 km circular orbit. The VEGA launcher was discarded, due to the satellite dimensions exceeding the fairing envelope. The selected launcher was a PLSV indian launcher, wich offers, however a mass capability much higher than needed. The launch costs therefore, should be shared with a copassenger.

In Option 1, two ground stations were identified, Kourou and Malindi, for the TC/TM link communications (S band) and for the scientific data download (X band).

In Option 2, one DRS and the Malindi station alone, for the TC/TM link communications (S band) and for the scientific data download (X band), were found adequate. This last option would allow a reduced information age.

II.5.2 SEO subsystems overview

The system mass budget amounts to 1392 kg in Option 1 and 1371 kg in Option 2, both including a 20% margin.

The power budget (worst case, in Earth acquisition mode) amounts to 1730 W.

Structure, Thermal, Propulsion and AOCS (Attitude and Orbit Control System) subsystems (s/s) have been assessed to be feasible using well established/high TRL (Technologies Readiness Level) technologies.

The satellite configuration includes, as far as the communication s/s, 2 S-Band antennas , which typically provide a wide field of view and a link capability without steering capability and one fixed X-band antenna. In Option 2, one Ka-band antenna with steering capability is added.

The Power s/s and the Communication s/s are anticipated to require development activities and adequate hw modeling.

The radar payload, in L-band, working at a central frequency of 1275 MHz, is a passive deployable planar array SAR antenna. The electronic is in a dedicated box located on the spacecraft body. Total antenna length is 16,94 m, composed by 9 panels, 88 kg mass. It operates in stripmap mode in full polarisation. There are not very significant changes in the payload configuration when the option 2 (DRS) is considered.

The interferometry based on one spacecraft is acceptable as for deforestation, forest biomass changes and reforestation a time interval of weeks or months, one spacecraft is sufficient. The SAR antenna, most of all, has low TRL, thus requiring an extensive breadboarding/engineering modeling and qualification activities.

At System level, a Protoflight approach has been selected, but an Avionic Test Bench has been foreseen as well, for an extensive pre-integration test campaign of the interfaces between Payload, Data Handling, Cmmunications and Power subsystems. This test campaign, to be performed through the integration of EQM (Engineering Qualification Model) models, should allow to proceed into the PFM (Proto-Flight Model) with less risk of malfunction/anomalies detection during integration and functional performance test.

The GS&Ops (Ground System and Operations) system, based on the Ground Stations, the Satellite Control Center, the Mission Planning Center and the User Ground Segment units, requires an extensive set of tests, to reduce the risks and the duration of the commissioning phase.

To comply with the DRS use (Option 2), the Ground Segment level, requires an additional connection in its network to interface with the tipical terrestrial DRS P/L data distribution from the receiving ground network of the DRS geostationary satellite.

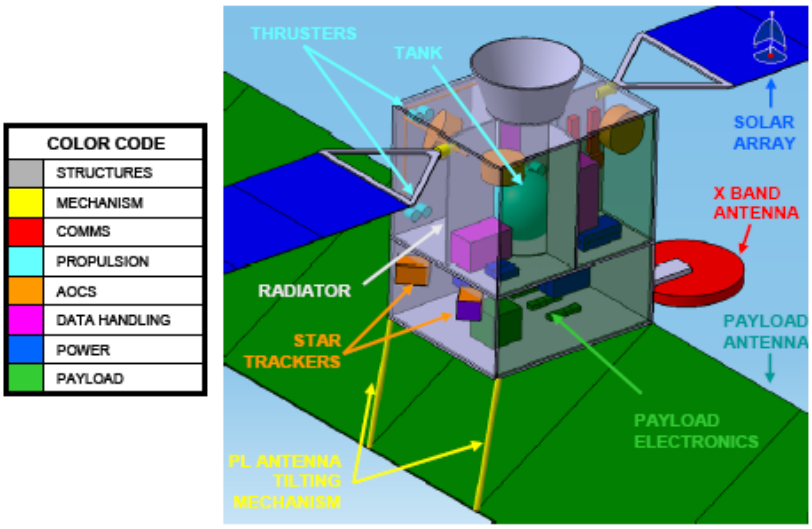

Fig. II-29. SEO main elements

II.5.3 SEO results

From the schedule point of view, the study resulted in identifying that the system development cannot meet the 5 years requirement. One additional year is needed, maily to accommodate adequate development activities for the most critical parts: the payload and its interfaces. The payload is the design driver for the overall satellite design and planning. Risk wise, the schedule and, from a technical standpoint, the interfaces among payload, communication system, data handling system and power system are introducing the most relevant risks, to be mitigated by moving the delivery date and executing an extensive test campaign at avionic test bench level. The target costs was met with both Options, being the Option 2 the less espensive one.

II.5.4 SEO GS&Ops

As aforementioned, in SEO study I have been involved as GS&Ops responsible. The detailed results of my contribute is shown in the following pages, through the use of a report form (that is a specific standard form used at the end of a CDF study to describe final results of each discipline).

II.5.4.1 SEO GS&Ops Requirements and Design Drivers

Requirements

The GS & Ops requirements have been identified at the beginning of the SEO mission study, and are summarized as follow:

- *GS & Ops general requirements, mainly focused on the following tasks:*
  - To provide and maintain the ground segment to space segment communication links.
  - To provide and maintain the ground to ground link, that is the link among the different ground segment elements.
  - To provide the User interface.
- *Mission and System requirements:*
  - The low inclination orbit lead to the choice of low latitude ground antennas.
  - The ground antennas have to be located about 90 degree apart in longitude in order to minimize blind orbits.
  - The operational phase has to be at least 5 years.
- *Communication and Data Handling requirements:*

  The communication link features (radio frequencies used in uplink and downlink, and the relative data rates) and the satellite data storing capabilities determine:
  - The ground antennas characteristics.
  - The number of ground stations to be used.

Design Drivers

The longest is the operational phase, the highest are the ground segment costs. In order to minimize the costs two design drivers have been adopted:

- To identify pre-existing facilities in order to avoid the development of new one.
- To identify ASI internal facilities in order to avoid the rent of external one.

II.5.4.2 SEO GS&Ops Assumptions and Trade-Offs

The additional use of a data relay satellite (Option2 in the Option1 vs. Option2 trade-off) has been take into account in order to estimate the differences in

the GS & Ops architecture, costs and in the ground stations modes. More details are shown in the following paragraphs.

II.5.4.3 SEO GS&Ops Baseline Design

GS & Ops Architecture

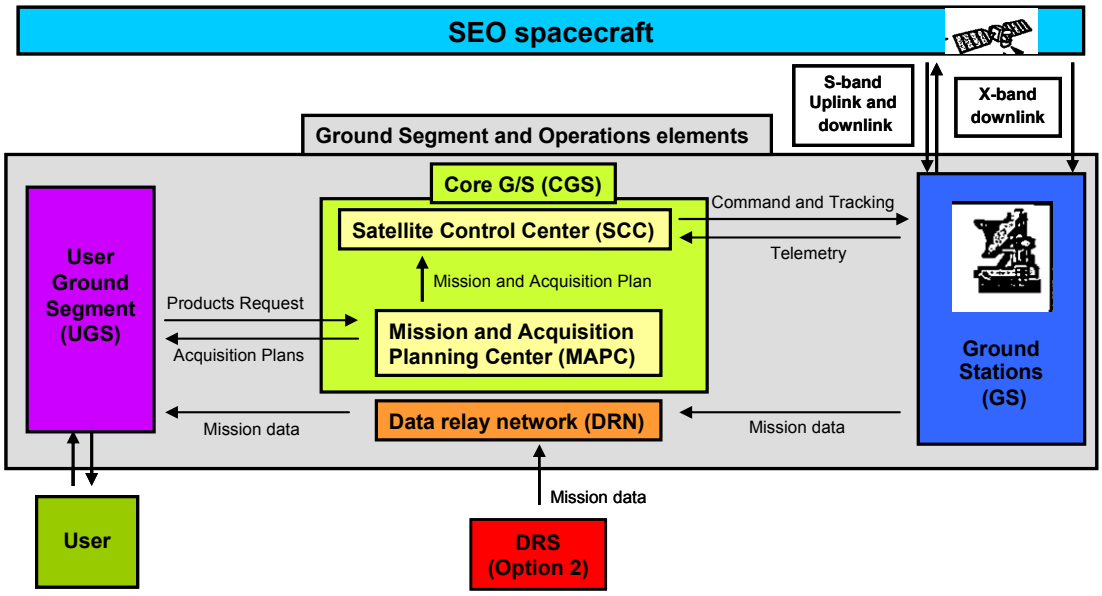

Fig. II-30. SEO GS & Ops Architecture.

GS & Ops subsystem has been divided in four elements (as suggested in Ref. 17). Each element has been customized to match SEO mission requirements and the overall architecture is shown in Fig. II-30:

- *Ground Stations (GS)*: this element is responsible for the Space segment to Ground segment communication links.
- *User Ground Segment (UGS)*: it provides the interface with the user community. It allows users to browse the image product catalogue, submit requests, track request status, and receive the requested products. Moreover it provides the infrastructure for data processing and archiving. These processing instruments are able to generate standard or added-value image products. In particular the geocoded product (obtained projecting the data onto a regular grid in a earth ellipsoid surface, chosen as cartographic reference system) needs one hour processing time.
- *Core Gruond Segment (CGS)*: it includes two subsystems. The Mission and Acquisition Planning Center (MAPC) and the Satellite Control Center (SCC).

MAPC pre-processes the Products Requests received from UGS, sorting the requests taking into account the relative priority, and forwarding the selected requests to the SCC. The SCC is responsible for the SEO satellite Command and Tracking (through the S-Band uplink) and for the SEO satellite Telemetry data acquisition (through the S-Band downlink).

- *Data Relay Network (DRN)*: the elements of SEO Ground Segment are sited on different geographical places, thus necessitate of Data Relay Network (DRN) to interact each other. In particular the ground stations send the mission data, obtained through the X-Band downlink, to the UGS using the DRN communication system (ftp server, DVD etc.). In the Option2 study case, the UGS obtains the mission data also through the Data Relay Satellite (DRS). In this case the DRN provides a dedicates ftp server to allow DRS ground segment to send the SEO mission data to the UGS.

Ground stations features

In order to satisfy the GS & Ops requirements and design drivers, Malindi and Kourou ground stations have been selected. The main features (see Ref. 18) are shown in Tab. II-13.

STATION	LOCATION	ANTENNA DIAMETER [m]	ELEVATION ANGLE [deg]	RF BAND	EIRP [dBW]	G/T [dB/K]	TRACKING MODE	Antenna Speed [deg/s]	Azimuth Range [deg]	Elevation Range [deg]
MALINDI	2.996°S 40.196°E	10	5 (worst case)	S / S X	68.7 (S)	21.3 (S) 31.8 (X)	Auto (S X) / Program	Az: 21.0 El: 7.0	+/- 420	- 4 to 90
KOUROU	5.251°N 52.805°W	15	5 (worst case)	S X / S X	81.2 (S) 82.8 (X)	29.1 (S) 37.5 (X)	Auto (S X) / Program	Az: 15 El: 5	0 to 720	-1 to 181

Tab. II-13. Malindi and Kourou antennas main features.

The Malindi site (Fig. II-31) is made available to Italy based on an international agreement between the governments of Italy and Kenya. The exploitation of the site is carried out by ASI and the Centro di Ricerca Progetto San Marco (CRPSM) of the University of Rome. Malindi is also part of the ESA Estrack Augmenteted Network Stations.

The Kourou site (Fig. II-32) is made available to ESA, based on an international agreement between ESA and the Government of France and is part of the ESA Estrack Core Network Stations.

The sites have a low latitude and are located about 90 degree apart in longitude (second column in Tab. II-13). Fig. II-31 and Fig. II-32 show also the antenna horizon masks (the fourth column of Tab. II-13 shows the horizon worst case values). Both antennas (Malindi with a 10 meter diameter antenna and Kourou with a 15 meter diameter antenna) provide S-Band uplink and downlink commnications plus X-Band downlink communication (Kourou provides also X-Band uplink communications, not used in SEO mission). Columns 6 and 7 show the main antenna features used for the ground segment to space segment communications link design: the Effective Isotropic Radiated Power (EIRP) and the ratio between the receiver antenna gain and the receiver system noise temperature (G/T). Finally, the antennas mechanical characteristics are shown in columns 8, 9,10 and 11: both antennas are able to track orbiting objects following a Program (based on the knowledge of the orbiting object coordinates) or automatically (using the received radio frequency informazion to calculate the object movement). Moreover it is important to emphasize that both antennas have high tracking speed (about 0,3 degrees per secons are need to track low Earth orbit objects) in all elevation and azimuth ranges.

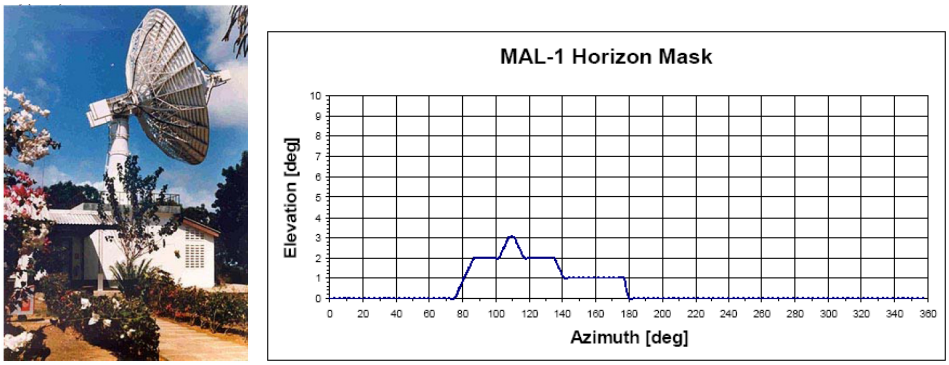

Fig. II-31. Malindi-1 (MAL-1) Antenna and Horizon Mask (Ref. 18)

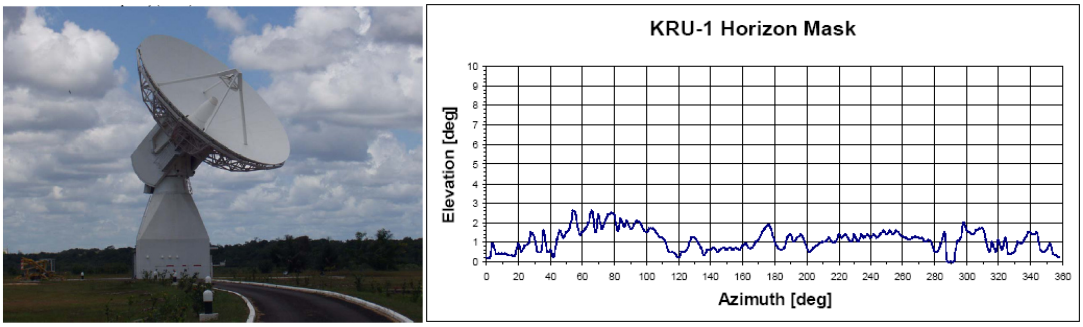

Fig. II-32. Kourou-1 (KRU-1) Antenna and Horizon Mask (17Ref. 18)

Five additional low latitude stations (belonged to the U.S.A DoD PrioraNET ground stations network) satisfy the SEO GS & Ops requirements, and have been selected to be considered as back up stations:

- Guam (Western Pacific Ocean)
- DGS – Diego Garcia Station (Indian Ocean Station)
- Bangalore Station
- Singapore Station
- Hawaii Station

In particular the first one (Guam station) is located about 100 degree apart in longitude (eastward) with respect to the Malindi station, minimizing the number of blind orbits.

GS and Ops phases and modes

	Duration	Option 1		Option 2	
		Malindi	Kourou	Malindi	Kourou
LEOP	0,5 months	S / S	S / S	S / S	S / S
IOT	4 months	S / S X	S / S X	S / S X	Not used
Operative Qualification	2 months	S / S X	S / S X	S / S X	Not used
Operational	5 years	S / S X	S / S X	S / S X	Not used

Fig. II-33. Operations phases and Ground Stations modes

The GS and Ops phases duration and ground stations operative modes (both in Option 1 and Option2 study cases) are shown in Fig. II-33. Due to the long payload calibration phase estimated by the payload specialist (L band SAR needs several in-orbit calibration procedures), the In Orbit Test (IOT) phase will take a lot of time with respect to the others commissioning phases. In particular, because of the low complexity of the others SEO subsystems, Operative Qualification phase will not need more than 2 months.

ID	Nome attività	Inizio	Fine
1	**SEO**	**mer 15/06/16**	**gio 30/12/21**
2	SEO Launch date	mer 15/06/16	mer 15/06/16
3	LEOP	gio 16/06/16	gio 30/06/16
4	IOT	ven 01/07/16	lun 31/10/16
5	Operative Qualification	mar 01/11/16	sab 31/12/16
6	Operational	dom 01/01/17	gio 30/12/21

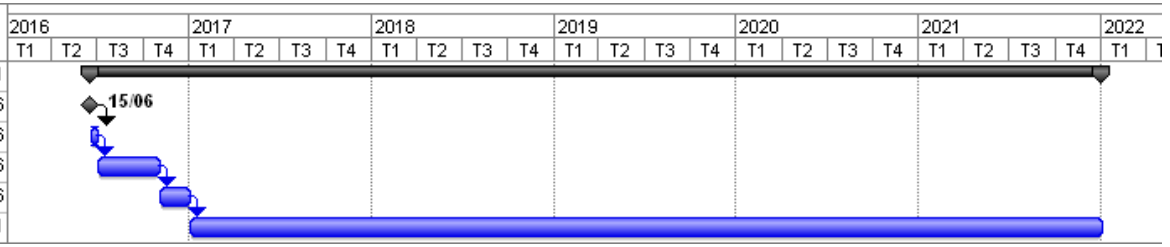

Fig. II-34. SEO Operations Gantt

During the Launch and Early Orbit Phase(LEOP) the SAR antenna do not acquires images. For this reason both Malindi and Kourou ground stations are fully dedicated to the S-Band communications uplink and downlink (S/S), that are the links devoted to Telemetry, Tracking and Command (TT&C) activities.

For Option 1 and in IOT, Operative Qualification and Operational phases, both Malindi and Kourou ground stations provide S-Band communication uplink and S plus X-Band communications downlink (S / S X). In these mission phases but in Option2, Malindi station and the DRS provide the S / S X link, Kourou station is not used.

In Fig. II-34 the Gantt chart shows the GS and Ops phases, highlighting the SEO Launch date milestone (15th of June 2016).

GS & Ops budgets evaluation method

In the ESA CDF approach, the GS & Ops specialist have to evaluate the costs belonged to the ground segment hardware and software, and to the personnel involved in the satellite operations.

Otherwise, in the ASI CEF approach, also the GS & Ops cost evaluation is carried out by the Cost specialist. However in the SEO study the GS & Ops cost evaluation has been obtained as a result of a joint cooperation between GS & Ops and Cost specialists. The following figures show the method used to evaluate the personnel and facilities that the GS & Ops subsystem need. This information have been forwarded to the Cost specialist to perform the cost estimation.

GS & Ops Elements / Personnel / Mission Phases	CGS						UGS	
	SCC				MAPC			
	FDSs	*Sys. Eng.*	*OPSs*	*Maint.*	Mission Planning Specialists	Maint.	Data storing and processing Specialists	Maint.
LEOP	2	8	5	0	0	0	0	0
In Orbit Test (IOT)	2	4	5	-	4	0	6	0
Operative Qualification	1	0	4	1	2	1	3	1
Operational	1	0	4	1	2	1	3	1

Fig. II-35.Personnel evaluation method.

Fig. II-35 shows the personnel evaluation method (each person is calculated 24 hours per day and 7 days per week) adopted in different SEO phases and for

different GS & Ops Elements. The GS and DRN personnel is included in the GS and DRN facilities cost and so are not shown in Fig. II-35.

In the SCC element different specialists are involved in different phases. In particular in LEOP and IOT phases 2 Flight Dynamic Specialists (FDSs) are involved to manage the SEO satellite maneuvers and 8 Satellite Sub-Systems Engineers (Sys. Eng.) are involved to monitor the right operation of the SEO satellite sub-systems (more Sys.Eng. in LEOP phase because of the important of this critical phase). The Mission Operation Specialists (OPSs) are responsible for the satellite operation management and monitoring during all the phases. Mission Planning Specialist are involved in the MAPC element and Data Storing and Processing Specialists are involved in the UGS element. They are not needed in LEOP phase but they have to be involved in IOT and Operative Qualification phases (twice in IOT phase), when the link between SCC and UGS has to be tested, and in the Operational phase when they have to carry out the SCC-UGS link management and maintenance. Except for the LEOP and IOT phases, hardware and software maintenance team (Maint.) are involved in all the GS & Ops elements shown in Fig. II-35.

The GS & Ops elements geographical site are shown in Fig. II-36 with the aim to provide the GS & Ops facilities costs estimation method to the Cost specialist. It is important to emphasize that only pre-existing facilities has been selected in order to satisfy the GS & Ops design drivers. In particular the Malindi ground stations and the Matera data storing and processing center are ASI internal facilities (Int.). However Kourou ground station (only used in Option1) and the CGS are external facilities (Ext.).

GS & Ops elements / SITE	GS		CGS		UGS
	S-Band	X-Band	SCC	MAPC	
Malindi	Int.	Int.	-	-	-
Matera	-	-	-	-	Int.
Telespazio facilities	-	-	Ext.	Ext.	-
Kourou	Ext.	Ext.	-	-	-

Fig. II-36. GS & Ops elements geographical site

Capitolo III ESA ECSS MDD to describe EduSAT design technologies and methods

In the last twenty years a large impulse to the production of micro and nanosatellites has been recorded overall the world. A number of space university programs have started in different Countries with the aim to provide students with an hands-on training in the field of space technologies. In this field the GAUSS group, performs its activity since more than 15 years with the UNISAT program. GAUSS is a team of master students, PhD students, researchers and professors, involved in the design, manufacturing, launch and operation in orbit of small UNIversity SATellites: the UNISAT program. In the framework of this program four satellites have been launched: UNISAT (September 2000), UNISAT-2 (December 2002), UNISAT-3 (June 2004), and UNISAT-4 (July 2006) (Ref 19 and 20). UNISAT-3 is still operative and telemetry data are received by the "San Pietro in Vincoli" (SPIV) Ground Station, located at School of Aerospace Engineering of Roma (Ref. 21 and 22). Unisat-4 did not reach the orbital phase, because of the launch vehicle failure in 2006. Currently, three new educational projects are under development: UNISAT-5, EduSAT and UNICubeSAT (Fig. III-1 and Ref. 23).

In particular in the following pages the EduSAT mission will be shown, following the ECSS-E-ST-10C (6 March 2009) document suggestion (Ref. 24) for MDD (mission description document) preparation, and underlining the main features of both space and ground segments.

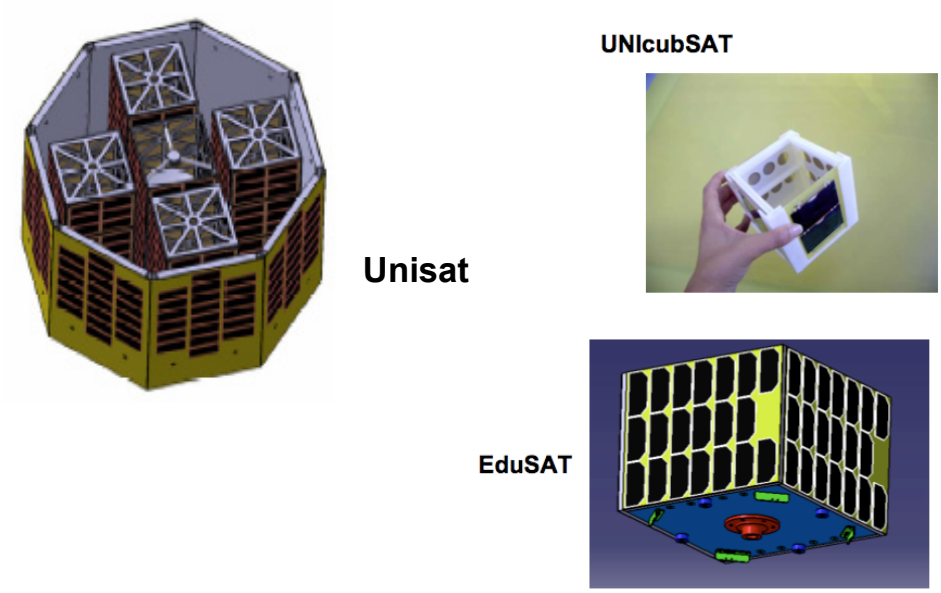

Fig. III-1. GAUSS on-going activities

III.1 The ECSS Mission Description Document

The MDD defines a concept that aims at satisfying the preliminary technical requirements specification, and presents how the objectives, operation profile, major system events and capabilities, contingencies and performance standards are expected to be achieved. It is prepared in Phase 0 and Phase A.

The MDD shall provide:

- Overview of the concept
- Mission analysis
- System description, element by element

For example, for a spacecraft, its ground control segment, and its user segment, MDD could be developed trough the description of the following discipline:

- Payload
- Mission Analysis
- Platform and configuration
- Power
- Attitude Determination and Control System (ADCS)
- On Board Data Handling (OBDH)
- Telecommunication
- Programmatics

- Risk analysis
- Ground Segment and Operations (GS&Ops)

III.2 EduSAT MDD

In 2005, the Italian Space Agency (ASI) proposed a program to launch in orbit an educational satellite named EduSAT (Educational SATellite), with the main goal to promote space education among high school students and to support scientific careers of PhD and university students. In the following paragraphs the EduSAT mission will be described according to the MDD (ECSS-E-ST-10C (6 March 2009)) form.

Ref. 25, 26, 27, 28, 29, 30, 31, 32, 33, 34 and 35 have been adopted as reference documents.

As member of GAUSS group I have actively participated in the design and development of Mission Analysis, Power, Programmatics, Risk Analysis, and GS&Ops subsystems and disciplines. Finally I have spent a lot of efforts in order to produce the EduSAT MDD.

III.2.1 EduSAT mission introduction and objective

EduSAT kick-off meeting was on 11 December 2007 and EduSAT launch is planned on March 2011. The project is coordinated and funded by the Italian Space Agency and commissioned to GAUSS group, in collaboration with an Italian company (IMTsrl) which is active in the field of space systems. This project is organized in two main activities:

- Design, manufacturing and launching in to orbit the university-class microsatellite
- laboratory activity with high school students

Satellite design, building and in-orbit operations are performed by GAUSS group, as project prime contractor and on the basis of its previous experience in this field. The IMTsrl is responsible for building of the primary payload and for the high school teaching activities in the field of space systems.

III.2.2 Edusat payloads

EduSAT primary payload is the analog sun sensor developed by IMTsrl in collaboration with several high schools.

EduSAT will be launched by DNEPR LV. The first launch date was planned on November 2009. Due to launcher problems, the launch has been delayed several times and now is fixed on March 2011 (fit check completed in September 2010).

Due to the additional year available for satellite design and manufacturing, a secondary payload have been developed.

III.2.2.1Payloads requirements and design drivers

In the case of satellite for commercial use, both mission objectives and payload characteristics impose the baseline satellite design requirements and drivers. For this reason in the MDD document usually the payload is the subsystem that drastically affect the other spacecraft subsystems design.

In the case of a university-class microsatellite one of the main purpose is the student training and to do this the time needed for the entire project have to be reduced to fit with academic cycle of studies. Moreover to assure the success of the mission, a complex satellite design is not suggested.

For this reason small size and simple design became the main requirements and design drivers. In EduSAT project this fact results in the chose of simple payload that fits standard university microsatellite dimension, power and communication capabilities.

In this background, the payload has to respect the following requirements:

- *Programmatics requirements:* the entire satellite and payload design, manufacturing and test time is two years, to fit the university students master degree period.
- *Mission requirements*: the primary payload is a solar sensor to detect the position of the satellite with respect to the Sun position. Orbit and satellite attitude control system have to be considered in the selection of the payload shape and line of sight.
- *satellite requirements*: dimension, weight, power supply, electrical and mechanics interfaces.

The main design drivers are here shown:

- low cost materials and manufacturing methods
- standard space process and materials when low cost constraint is respected.
- COTS component to reduce costs.

III.2.2.2 Analog sun sensor

The analog sun sensor is the EduSAT primary payload. The sensor features are given in the following table:

Dimension	10x10x10cm
Power peak (max 2 min)	5 W
Mean power	0.5 W
Input voltage	8 V
P/L – satellite electrical interface	2 analog channel (0-5 V)
EduSAT ADCS	Passive magnetic
Attitude accuracy	10°

Tab. III-1. Sensor requirements from satellite constraints.

Four solar cells made of monocrystalline silicon, closed on a resistive load, provide the sun light direction identification (see Ref. 29).

Fig. III-2. Technique of solar cell assembly on the sun sensor.

Different solar radiation angles (with respect to the cell surface) result in the variation of the output voltages of the cells, and these values can be used to set the different inclination angles of the satellite with respect to the Sun. The IMTsrl sun sensor has a very simple and efficient configuration, to fit the EduSAT university microsatellite constraints. It is made by four solar cells mounted on the four sides of a metallic frustum of pyramid (Fig. III-3).

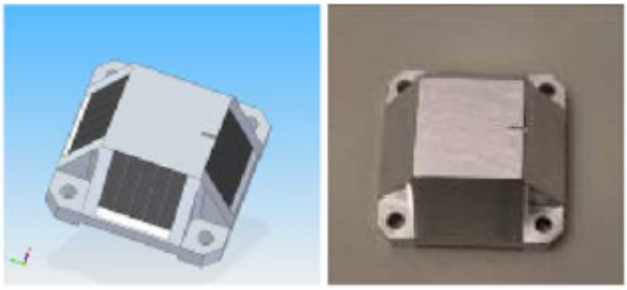

Fig. III-3. Metallic frustum of pyramid where the cells are mounted.

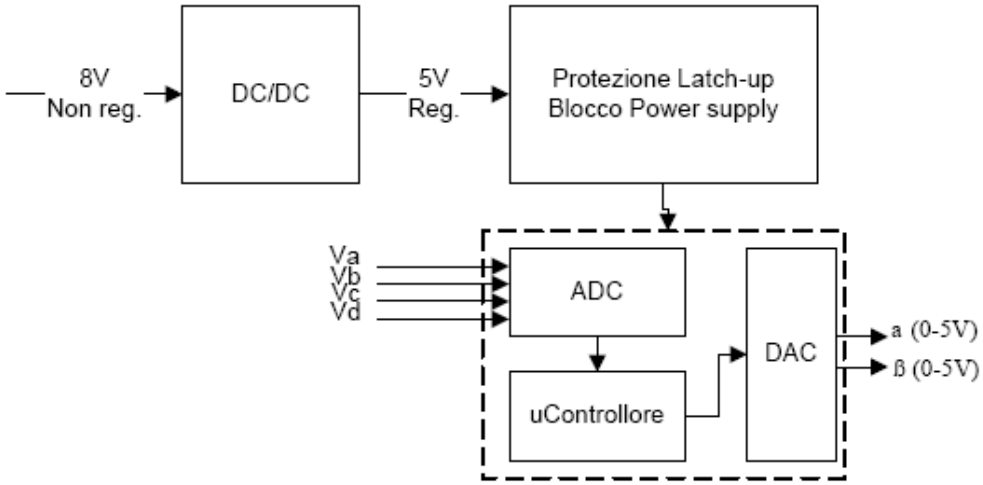

Fig. III-4. Sun sensor architecture

The payload box has been developed with standard space process and materials and with respect to the time schedule constraint. Moreover it has an own electronic circuit, responsible for the detection of the voltage level at the terminal of each resistor. Each cell can provides two analog outputs (0-5 voltage range). Further a cylindrical shield protects the sun sensor from solar radiation coming from undesirable directions (Fig. III-5).

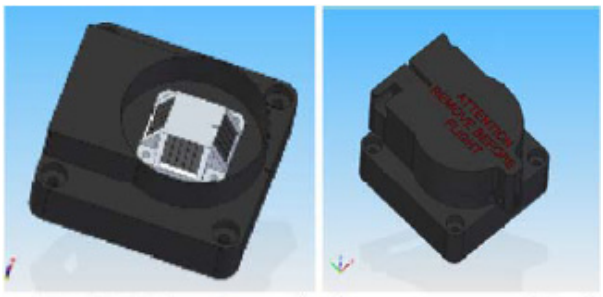

Fig. III-5. CAD drawing of solar sensor assembly (left side) and the solar sensor with the cover (right side).

III.2.2.3 MRFOD

EduSat will contain 8 PocketQubs (femtosatellites invented by Professor Robert Twiggs of Morehead State University) which will be ejected from the "mothership" at apogee, using MRFOD (Morehead-Roma Femptosatellites Orbital Deployment system) device. These femtosatellites will be the smallest satellites ever launched. Each one will have earth and space monitoring sensors, testing micro/nano technology for space applications.

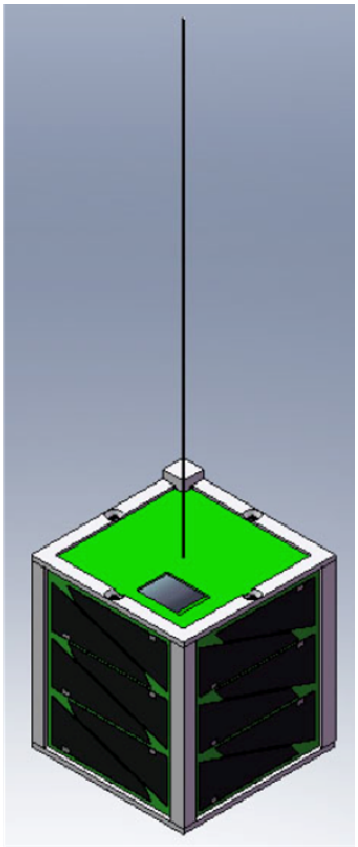

Fig. III-6. PocketQub

The PocketQub main features are given in the following table:

Weight	125 g
Dimension	5 x 5 x 5 cm
Capabilities	Autonomous OBDH and Communications system
Sensors	Earth and Space monitoring sensors
Objective	Test micro/nano technology for space applications
Deorbiting System	Tethered or deployable

Tab. III-2. PocketQub main characteristics.

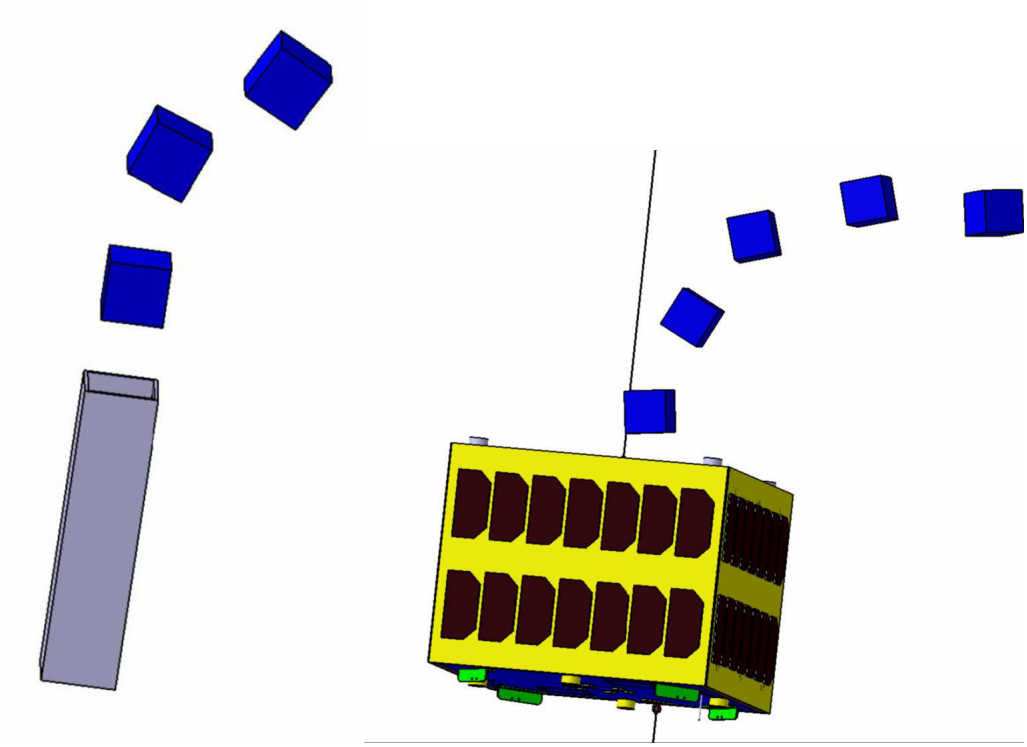

Fig. III-7. PocketQub launches from EduSat: MRFOD

EduSAT will board four MRFOD, and each MRFOD will launch in orbit 2 PocketQub. Each MRFOD is a 6.9cm by 7 cm by 25 cm box.

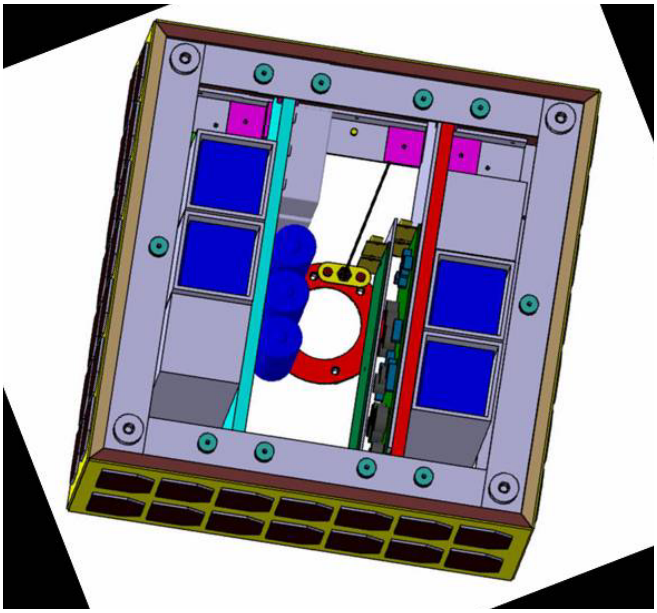

Fig. III-8. EduSAT boarding four MRFOD

III.2.3 Edusat mission analysis

III.2.3.1Mission analysis requirements and design drivers

EduSAT main purpose is educational: it means that the following requirements have to be considered during the mission design:

- *Programmatics requirement*: developing times have to be compatible with academic lifetime of the students (university students, high school students and PhD students). Due to this constraint, the mission full developing has been fixed in about two years, starting from the preliminary mission design until the satellite launch and commissioning in orbit.
- *Piggy-back launch:* As piggy-back by DNEPR LV, thus it is designed to fit different orbits in the range 500-900 km. As nominal design orbit has been selected a polar orbit with 700 km altitude.

III.2.3.2 MIssion analysis baseline design

EduSAT will be launched in a LEO Sun Synchronous Orbit by DNEPR-1 LV from Yasny launch base. This is a cluster launch and the list of the spacecrafts (SC) and their purpose are given in the following figure:

SC Name, Launch Services Customer	SC Purpose
Sich-2 NSAU, Yuzhnoye SDO, Ukraine	Optical–electronic Earth observation space system Sich-2 with MC-2-8 SC (hereafter Sich-2 SC) is intended for imaging the specified Earth areas in visible and infra-red electromagnetic wavelength ranges, for storage and transmission of images to the ground information complex, and to obtain scientific measurement data under POTENTIAL Project.
NigeriaSat-2, NigeriaSat-X, SSTL (Great Britain) for National Agency of Space Research and Development (NASRD), (Nigeria)	The main purpose of NigeriaSat-2 SC is quick presentation of high-resolution images for map-making, food security, observation of catastrophes, etc. NigeriaSat-X SC – ERS, observation of quick-changing phenomena of natural and anthropogenic nature in the interests of agriculture and environment protection.
RASAT Scientific Technological Council of Turkey Research Institute of Space Technologies TÜBİTAK UZAY, Turkey	RASAT SC is a civil scientific ERS satellite whose main purpose is testing of equipment created by TÜBİTAK UZAY in space conditions and try-out of systems technologies to use them in future national projects.
EDUSAT Aerodynamics Team of La Sapienza University, Италия	EDUSAT SC in a student's satellite created to solve educational and scientific problems.
APRIZESAT-5, APRIZESAT-6 SpaceQuest, USA	Minor low-orbit spacecraft links. Destination – transmittal and reception of small data bursts from stationary and mobile stations

Fig. III-9. Dnepr-1 LV launch from Yasny launch base (ref. 30).

The EduSAT launcher flight schematics in the following figure depicts the three stages separation (highlighting the propulsion systems PS ignition periods) and satellites separation. The first stage will impact to the dedicated ground area, while second stage will impact a dedicated area in the Indian Ocean.

After the II stage/Upper Stage (US) separation, the upper stage turn 180degrees in 7 second, and once reached the orbit, allows the satellites in-orbit injection without using springs.

Then there are 2 seconds interval among AprizeSat-5, AprizeSat-6, EDUSAT, NigeriaSat-X separations. 1,5 seconds interval for the RASAT separation. 3 sec for the separation of the Sich-2. Later with interval of 2 sec separation Platform A with the Payload Fairing (PF) lower section and with interval in 1,5 sec separation

the NigeriaSat-2; after separation of the Sich-2, the upper stage continues its motion with the fixed program angles until propellant depletion.

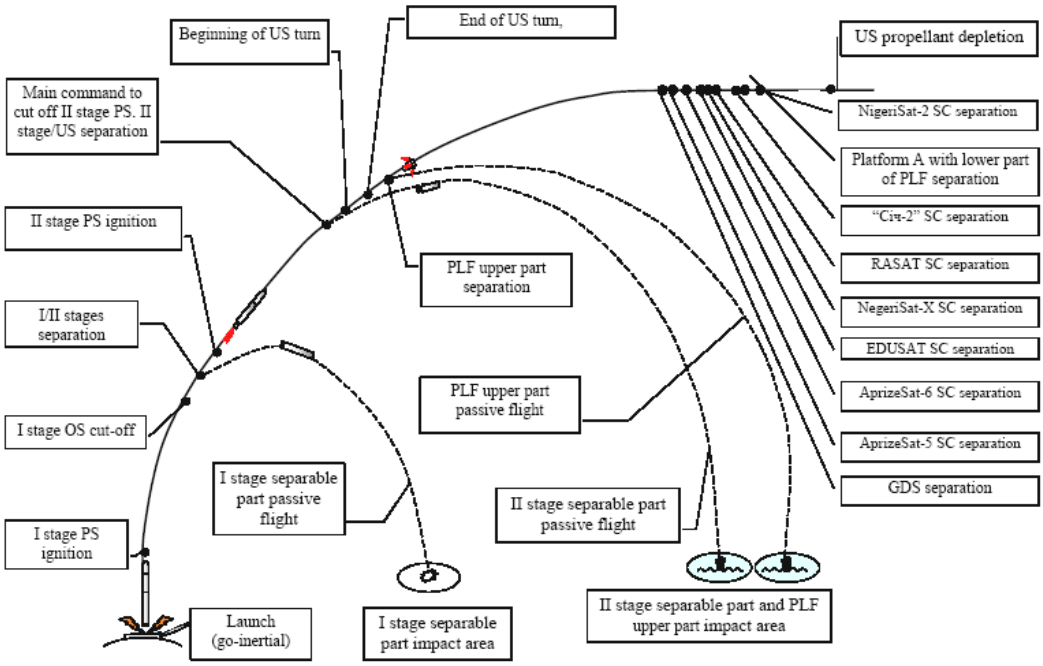

Fig. III-10. Insertion schematics of AprizeSat-5, AprizeSat-6, EDUSAT, NigeriaSat-X, RASAT, Sich-2 and NigeriaSat-2 by Dnepr LV.

The EduSAT osculating orbit parameters at the moment of the separation are provided in the ICD (Interface Control Document) (Ref. 30) and given in the following table, highlighting the maximum deviation (2,7 σ) allowed (for some orbit parameters the accuracy is not allowed (NA)).

	Value	**Accuracy**
Semi major axis [km]	7050,1	± 10
Perigee height [km]	643,8	NA
Apogee height [km]	700,2	NA
Orbit period [sec]	5891,3	NA
Eccentricity	0,004	NA
Inclination [deg]	98,25	± 0,03
LTAN	22 hours 30 min	± 20 sec

Tab. III-3. EduSAT osculating orbit parameters and injection accuracy.

The perigee and apogee heights were defined for the Earth equatorial radius RE =6378.13 km. Moreover EduSAT angular velocity after the separation will not exceed 22 deg/s around any axis.

The ICD document also provides relative distances among cluster launch satellites. In the following figures the relative distances between AprizeSat-6 and EDUSAT and between EDUSAT and NigeriaSat-X

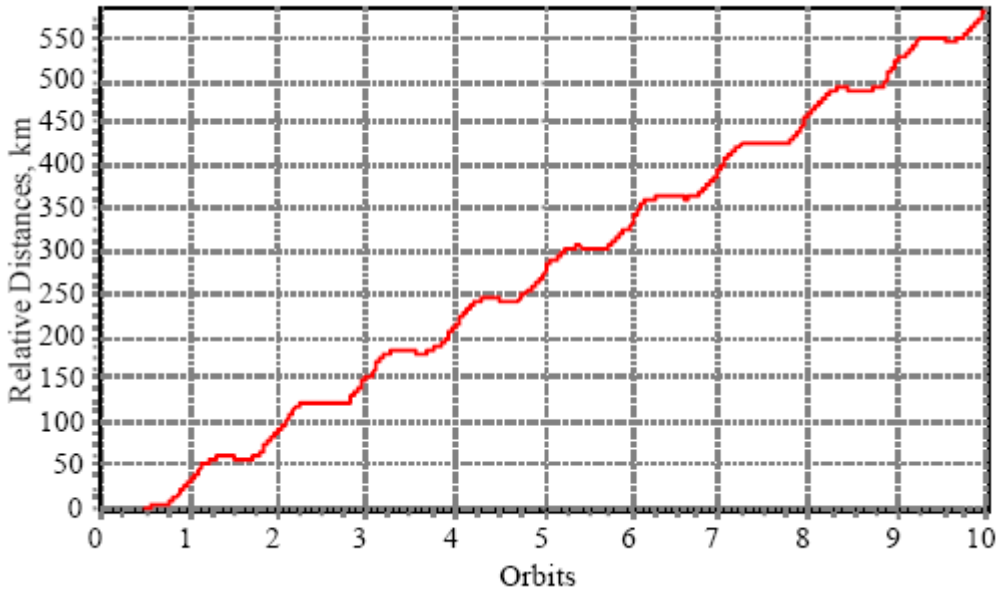

Fig. III-11. Relative Distances between AprizeSat-6 and EDUSAT.

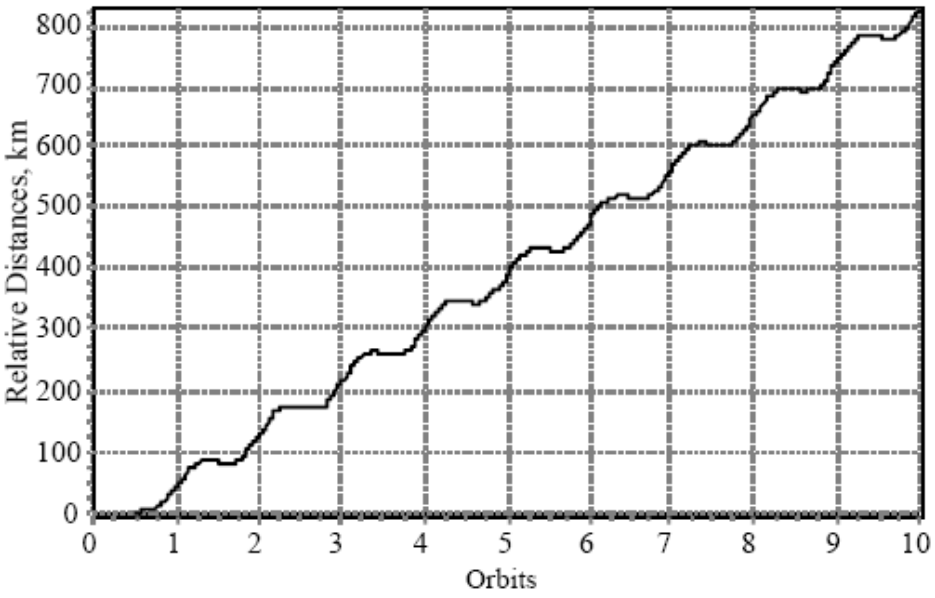

Fig. III-12. Relative Distances between EDUSAT and NigeriaSat-X.

III.2.3.3 EduSAT mission modes

Four EduSAT mission operational modes have been identified. This modes are representative of the satellite in-orbit operations. In Tab. III-4 each line describes the specific mode, highlighting subsystems features.

In mode 1, the IDLE mode, the satellite reaches the orbit and is switched on. In this phase, if the satellite is in eclipse, its survival depends entirely on the batteries. When the satellite is not in eclipse the ground station sends a the command to initialize the START UP mode. In this phase all the subsystems are fully operative while the sun sensor and the MRFOD devise electronics are switched off. After the in orbit test phase, two nominal modes are described. Mode 4 is representative of the satellite operations in eclipse condition.

N	MODE	Definition	Subsystem	Requirements
1	IDLE	Spacecraft ON, waiting for commands Its survival depends entirely on the batteries (if in eclipse)	ADCS	Restoring torque and Oscillation de-damping
			OBDH	Commands reception from VHF Transponder and command distribution. Acquisition of telemetry from subsystems. Telemetry sending to UHF Transponder
			COMMS	UHF and VHF antenna on. Other functions switched off.
			POWER	Power available to support essential functions.
			SUN SENSOR	All functions - OFF
			MRFOD	All functions – OFF
2	START UP	Solar array on power supply. Batteries as power accumulation system. Not in eclipse condition	ADCS	Restoring torque and Oscillation de-damping
			OBDH	Cmd reception from VHF, UHF, S-Band Transponders and cmd distribution Acquisition of telemetry from S/S, Telemetry sending to VHF, UHF, S-Band Transponders
			COMMS	UHF, VHF and S-Band antenna on.
			POWER	Switch from batteries to

				solar array
			SUN SENSOR	Functional test
			MRFOD	OBDH test the MRFOD electronic MRFOD autonomous electronic switch on and test the OBDH
3	NOMINAL	Not in eclipse condition	ADCS	Restoring torque and Oscillation de-damping
			OBDH	Cmd reception from VHF, UHF, S-Band Transponders and cmd distribution Acquisition of telemetry from S/S, Telemetry sending to VHF, UHF, S-Band Transponders
			COMMS	UHF, VHF and S-Band antenna on.
			POWER	Operational power to service module and instruments.
			SUN SENSOR	100% operational
			MRFOD	100% operational
4	NOMINAL ECLIPSE	Eclipse condition Battery ON	ADCS	Restoring torque and Oscillation de-damping
			OBDH	OFF
			COMMS	UHF, VHF and S-Band antenna OFF.
			POWER	Supply to essential functions if needed
			SUN SENSOR	All functions - OFF
			MRFOD	All functions – OFF

Tab. III-4. EduSAT operative modes.

III.2.3.4 End of Life

In order to overestimate the satellite de-orbiting calculation, an orbit altitude of 750 km has been used. Considering 0,11m^2 of wetted area, EduSAT satellite at the end of life re-enters in 95,5 years and there is need of a passive de-orbiting system to comply with the disposal requirements of the Inter-Agency Space Debris Coordination Committee or to the European Code of Conduct on Space Debris (which prescribe to reduce the residual orbital lifetime below 25 years). For this

reason a de-orbiting system based upon deployable technology will be boarded on EduSAT, increasing the wetted area to 0,33m^2 (Life Time = 24 years).

III.2.4 EduSAT configuration

III.2.4.1 Configuration requirements and design drivers

The general requirements adopted for EduSAT configuration are:

- fit the fairing of DNEPR-LV launcher;
- interface with LV by the EduSAT adaptor;
- accommodate all subsystems and the required solar panels;
- accommodate the payloads, accordingly with the sun sensor field of view and the femptosatellites launcher system (MRFOD);
- allow to access individual components for testing or replacement
- allow to build satellite in two years

As main design driver, EduSAT have to reduce as much as possible deployable devices, in order to avoid the use of mechanism and complex configuration.

III.2.4.2 Configuration assumptions and trade-off

The following assumptions have been adopted:

- The sun sensor is placed so that its field of views is unobstructed by antennas and MRFOD hatch (during femptosatellites launch).
- The SSO orbit, the magnetic passive attitude stabilization system and the minimization of the number of mechanisms impose the solar arrays to be fitted on the satellite lateral panels.
- Fairing of DNEPR-LV launcher and the launcher adaptor characteristics have been taken into account in the configuration design.
- The permanent magnet and permeable rods have been positioned to provide an optimal restoring torque and oscillation damping.

A shape trade-off has been considered during the feasibility study phase: the classical UNISAT-class shape or a new box shape. New box shape provides more space to board more devices and payloads. Moreover it provide optimal access during assembling and test phases.

III.2.4.3 Configuration baseline design

EduSAT's structure is a square prism with height size 26 cm and base size 31.5 cm (Fig. III-13). Satellite expected weight during the design phase was about 10 Kg. The short times required for the mission developing and realization need of a design philosophy based on the parallel developing of all subsystems. This is a highly interactive process which requires the flexibility of the main subsystems and a modular architecture able to be quickly adapted to different missions.

The inner space is divided by two vertical panels (Fig. III-14), which host subsystems hardware and electronic boards, and payload. On the bottom plate are arranged mechanical interface with the launcher, antennas for S band transmission and for down link data transmission in UHF band (436 MHz), switches to turn on the satellite during the separation phase from the launcher. On the upper plate are arranged antennas for uplink data transmission in VHF band (145 MHz) and the sun sensor developed by IMTsrl. Between the two inner vertical panels have been boarded all the satellite subsystems (Fig. III-15). The two external spaces host the MRFOD devices. Solar arrays are fixed on the lateral panels.

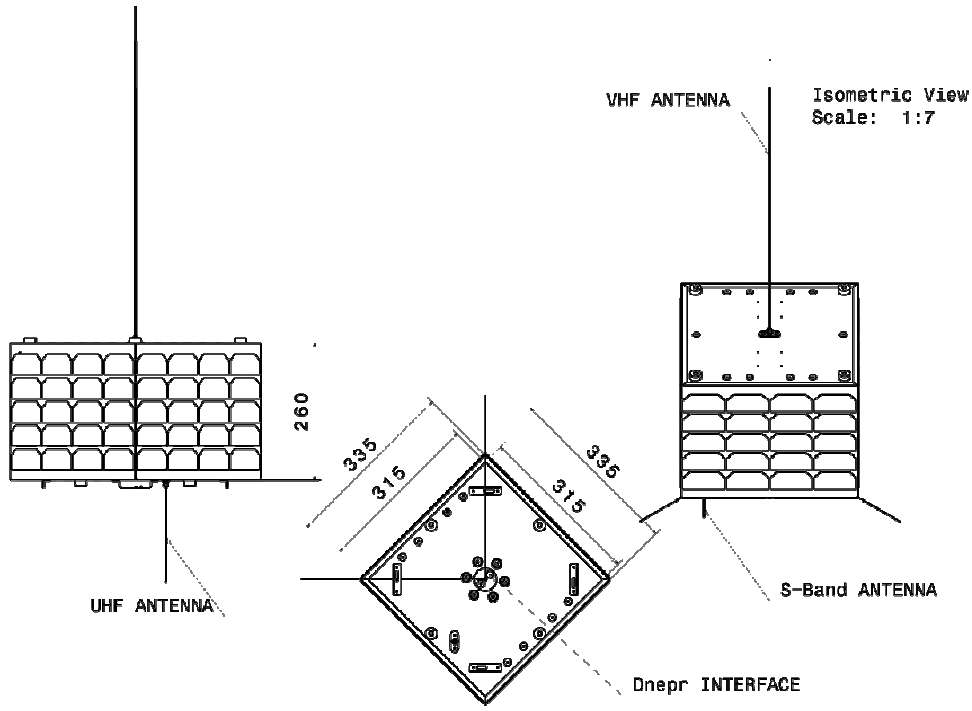

Fig. III-13. EduSAT external configuration

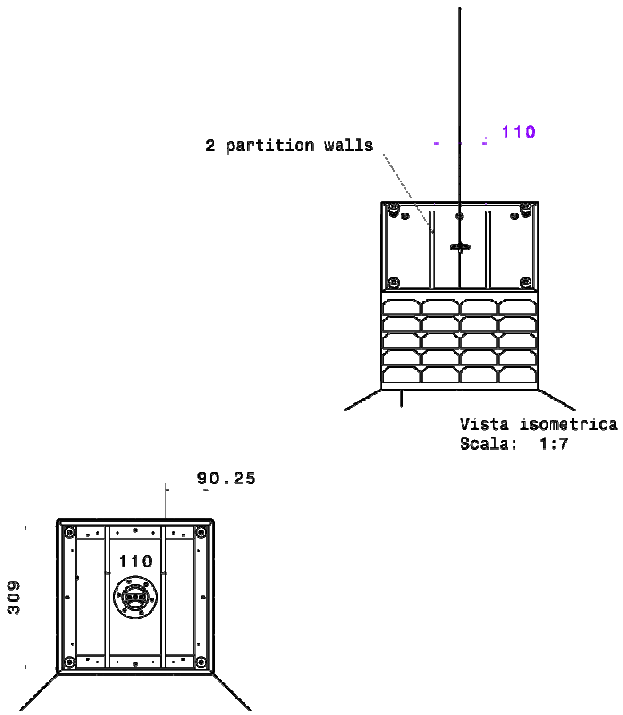

Fig. III-14. EduSAT internal configuration

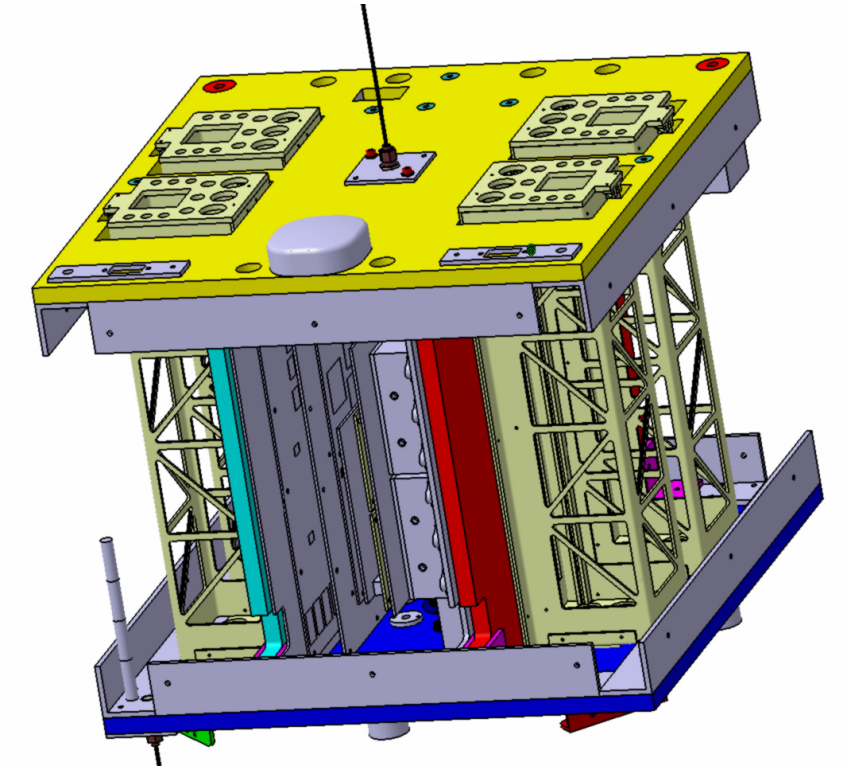

Fig. III-15. EduSAT LAY-OUT

III.2.5 EduSAT structure

III.2.5.1Structure requirements and design drivers

The following structure requirements have been taken into account:

- Weigh about 10 kg
- Provide support and containment for the units of subsystem and instruments.
- *DNEPR ICD requirements*: Ensure sufficient stiffness to decouple spacecraft modes from the LV ones. In particular the satellite shall be designed with the same stiffness which would provide values of a structure natural frequency, when it is attached rigidly in a separation plane, no less than:
  - 20 Hz in longitudinal axis;
  - 10 Hz in transverse axis.

  Withstand the design limit loads without failing:
  - a Sinusoidal Vibration Amplitudes and duration threshold (in longitudinal direction) as shown in Tab. III-5
  - Shock Spectrum as in Tab. III-6.

Frequency Sub-Range, Hz	5-10	10-15	15-20
Amplitude, g	0.4	0.8	0.4
Duration, sec	10	30	60

Tab. III-5. Sinusoidal Vibration Amplitudes in longitudinal direction (Ref. 30).

Loading case	Frequency bands, Hz							Number of actions
	30-50	50-100	100-200	200-500	500-1000	1000-2000	2000-5000	
	Values of shock spectrum, g							
PLF jettison, Upper Stage separation, separation of other spacecraft	5-10	10-25	25-100	100-350	350-1000	1000	1000	5
SC separation	5-10	10-25	25-100	100-350	350-1000	1000	1000-3000	1

Tab. III-6. Shock Spectrum for EDUSAT interface (Ref. 30).

III.2.5.2 Structure assumptions and trade-off

Due to the launch and in-orbit test, UNISAT-class satellite materials have been used. Inner vertical panels replace the UNISAT four aluminium columns, to ensure the longitudinal stiffness.

III.2.5.3 Structure baseline design

Lateral panels, inner vertical panels, upper and bottom plates have been manufactured by using Aluminium honeycomb (Al 3003-3/8-0.0015, density 83 kg/m3) with face sheets in Aluminium Al 5251 H16 (thickness 0.5 mm). The vented Aluminium honeycomb has been selected to minimize weight (Fig. III-16 and Fig. III-17).

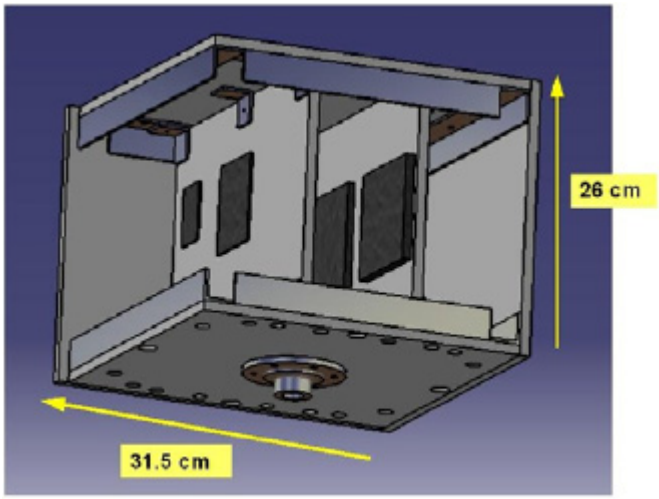

Fig. III-16. EduSAT structure digital mock-up.

Fig. III-17. EduSAT structure mock-up.

EduSAT mass budget	
Structur (laeral panels, inner vertical panels, adaptor, secondary structures, mechanism)	**3,3**
Electrical Power System (battery package, solar arrays)	**1**
Payloads	**3,4**
Electronics (PCB, magnetometer, antennas, radios, GPS)	**4,4**
Total mass	**12,1**

Fig. III-18. EduSAT mass budget

EduSAT moments of inertia have been calculated on satellite digital mock-up with respect to main axis of inertia (green axis=x, red axis=y, blue axis=z, Fig. III-19); they are Ix=0.094 kg·m2, Iy =0.11 kg·m2, Iz=0.12 kg·m2.

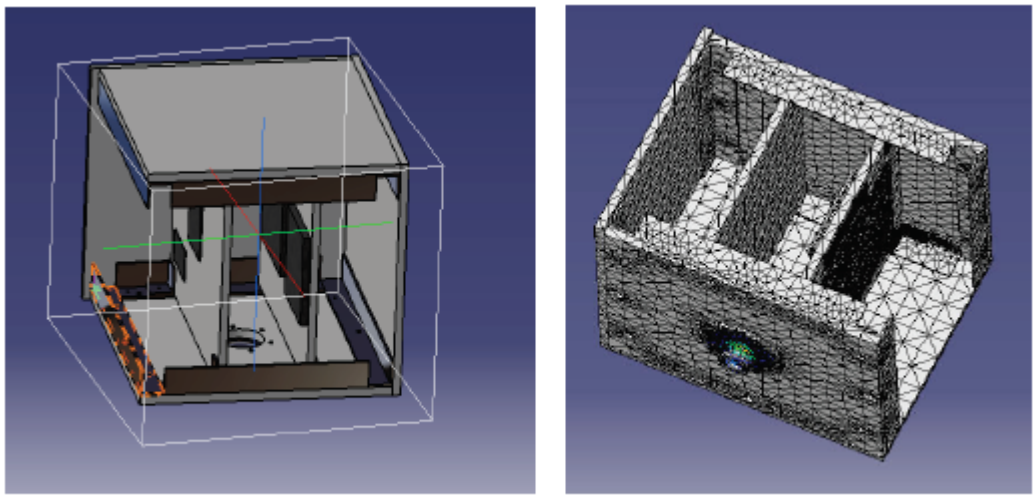

Fig. III-19. A) EduSAT digital mock-up employed for preliminary FEM analysis; B) model mesh

In order to satisfy structure vibration modes requirements, preliminary analysis FEM using specific software has been assessed in the design phase. A launch-vehicle structure has natural frequencies responding to forces from both internal (engine oscillations) and external (aerodynamic effects) sources. For DNEPR requirements are: natural frequencies larger then 10 Hz for lateral axis and larger then 20 Hz for longitudinal axis (see requirements). The results of the preliminary analysis shown the first ten satellite natural vibration frequencies (Tab. III-7). First natural vibration frequency is 97 Hz, greater than launcher requirements.

The first vibration frequency is related to satellite oscillations on pyrotechnic which works as cantilevered element.

Moreover the UNISAT-4 vibration test, exploited at OERLIKON CONTRAVES in 2005, also confirm these results (Fig. III-21).

Vibration Mode	Frequency (Hz)
1	97
2	100
3	264
4	493
5	829
6	1440
7	1802
8	2080
9	2393
10	2618

Tab. III-7. EduSAT structure natural vibration mode

Fig. III-20. UNISAT-4 vibration test.

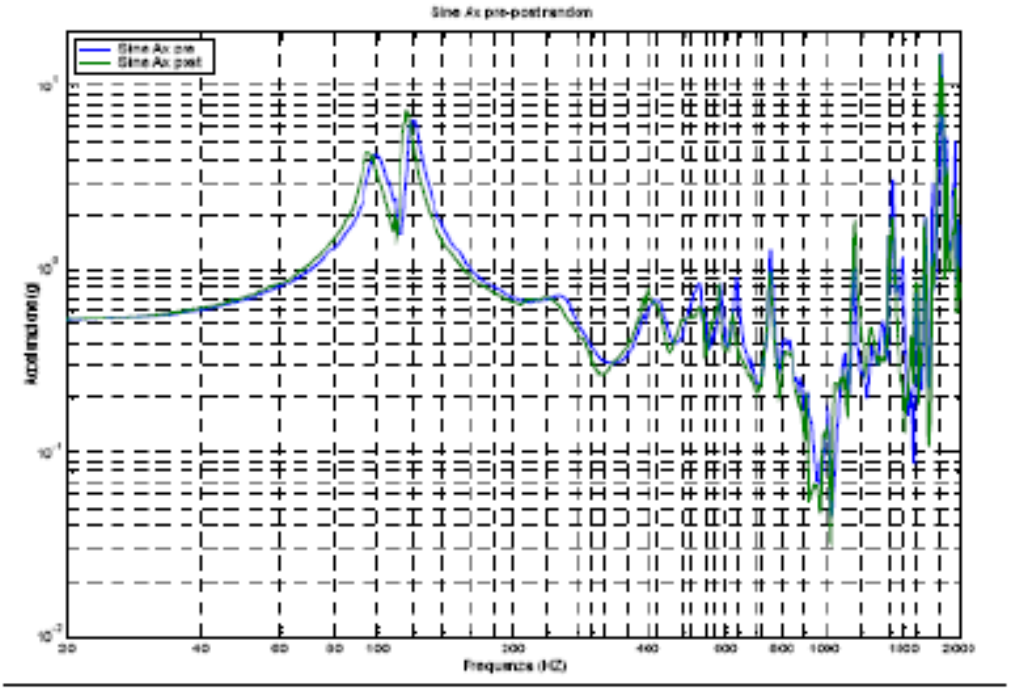

Fig. III-21. UNISAT-4 vibration test results.

III.2.6 Edusat Power

III.2.6.1 Power requirements and design drivers

- Low cost materials
- COTS components
- Low cost assembly method for solar arrays

III.2.6.2 Power assumptions and trade-off

Assuming the UNISAT -3 in orbit experience, a trade-off between cost and efficiency has been carried out during the design phase, selecting the terrestrial triple junction solar cells.

Results in orbit for the terrestrial solar cells demonstrated an efficiency loss of 20% per year (Fig. III-23 and Fig. III-24).

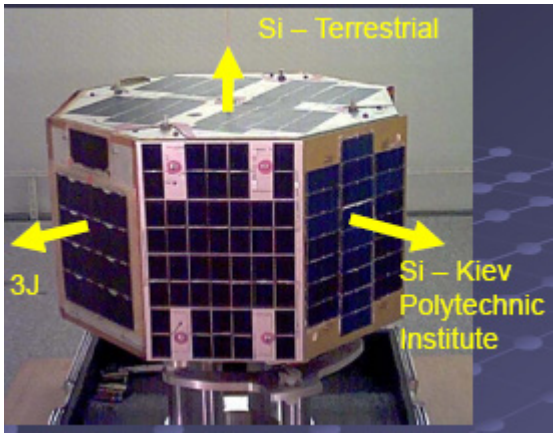

Fig. III-22. UNISAT-3 solar arrays (Ref. 32).

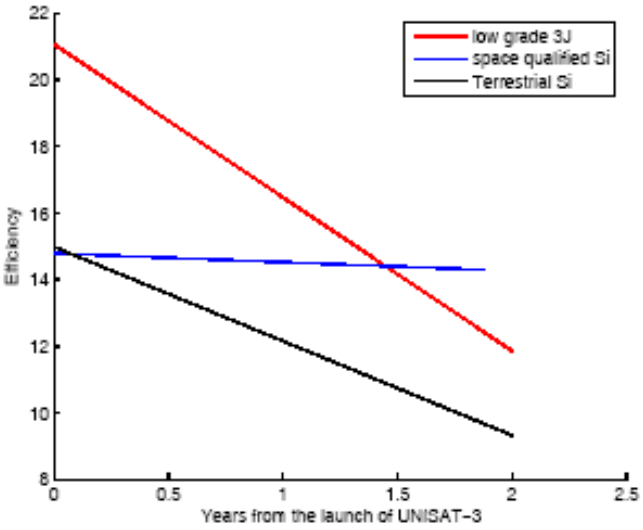

Fig. III-23. Unisat-3 solar arrays efficiency comparison (Ref. 32).

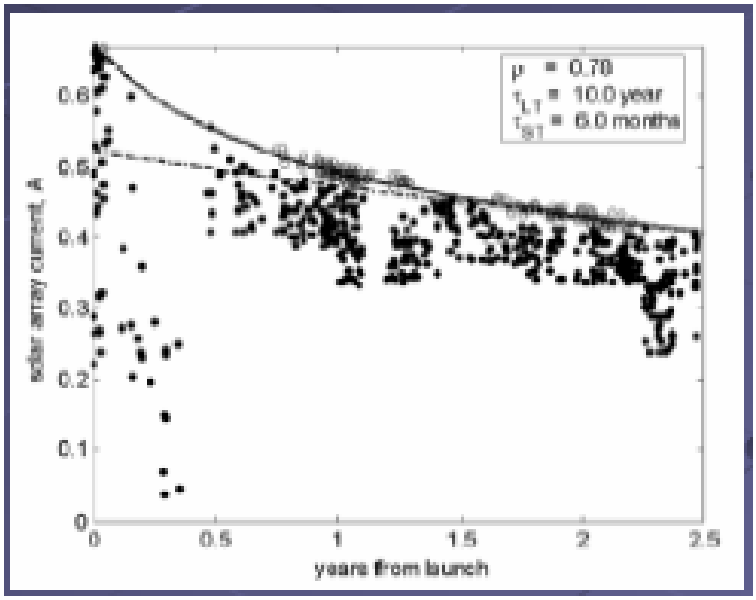

Fig. III-24. UNISAT3 in orbit results analysis (Ref. 32).

It has been assumed for the solar panels assembly the procedure used during UNISAT-3 and UNISAT-4 manufacturing, because it has been extensively tested in orbit.

III.2.6.3 Power baseline design

The photovoltaic system is based upon a new kind of terrestrial triple junction solar cells never used in UNISAT3 and UNISAT4 experience. These cells allow 28% efficiency. Four solar panels with 2 strings (7 cells each one) provide power required for the spacecraft. Each cell is 40mm by 80mm by 0.1mm (32 cm^2) and the total surface available for each panel is 448 cm^2.

The solar cells are glued to a non conductive support and than body mounted exploiting the RTV (Room Temperature Vulcanizing) silicone. This adhesive is qualified for wide temperature range. However it is not space qualified, but it is widely used in terrestrial severe application. To assure a homogeneous gluing phase, the vacuum bag technique (Fig. III-25) is used.

In order to select the better cells and avoid the use of not efficient cells, an intensive cells characterization campaign has been carried out (Fig. III-27).

Solar cells and epoxy support previously assembled are successively bonded onto the satellite Aluminium honeycomb lateral panels with the same RTV silicone and the same bonding technology.

The battery package for energy storage is made of 6 batteries Ni/Cd Sanyo (out production from 2007) that allow fast charge. A BCR (Bus Control Regulator) interface with the OBDH electronic, allowing battery overcharge and discharge protection, and voltage regulator.

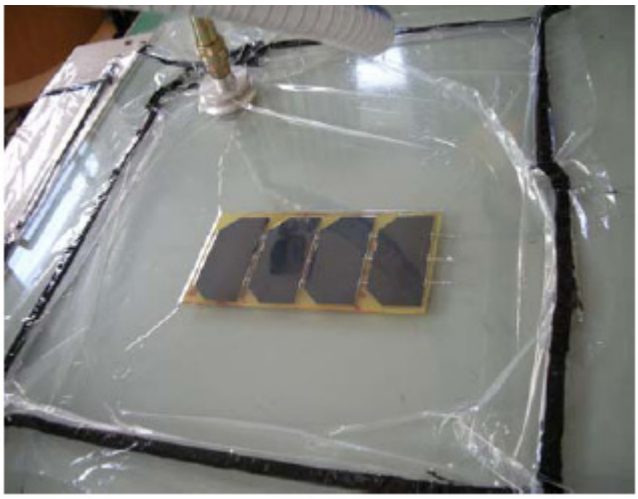

Fig. III-25. Vacuum bag and prototipe solar panel during the gluing phase.

In order to estimate the solar-array area it has been considered a low Earth orbit with 700 km of height and the worst illumination condition in the case of one solar-array facing to the Sun direction (EduSAT is stabilized using a passive magnetic system).

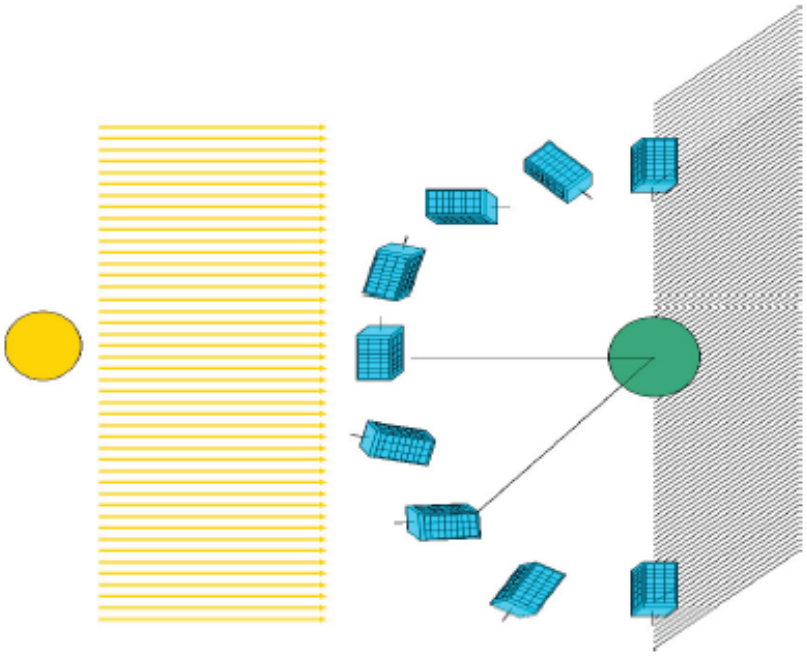

Fig. III-26. Sun exposition in orbit for EduSAT satellite (Ref. 32).

To evaluate the minimum solar array size it is necessary to compare the satellite power consumption during the whole orbit with the photovoltaic system power generation during daylight. Satellite power loads are sketched in the following table.

P (W)	t/T	Subsystem	Required mean power (W)
0,5	0,5	Attitude determination (sensors)	0,3
4,0	0,125	Data transmission (down link)	0,5
2,0	0,5	Payload	1,0
2,0	1,0	CPU (OBDH)	2,0
8,5	-	Total	3,75

Tab. III-8. Satellite power loads

P is the required power, t is the operation time and T is the orbital period. Minimum estimated area for each solar panel is 400 cm^2, considering triple junction solar cells not space qualified, with efficiency 28%.

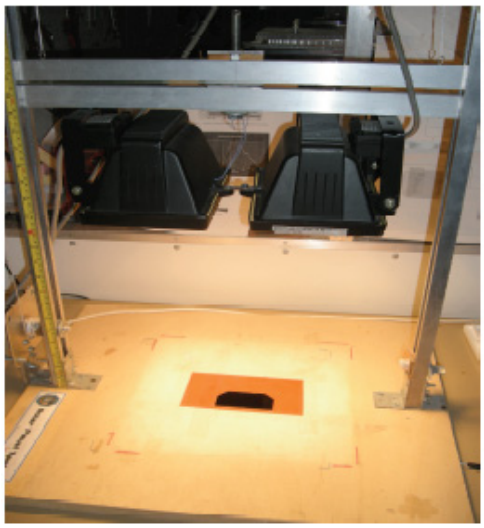

Fig. III-27. Solar cells characterization at GAUSS Laboratory

III.2.7 Edusat ADCS

III.2.7.1 ADCS requirements and design drivers

The following requirements have been considered:

- Allow satellite stabilization after in-orbit injection

- Allow satellite oscillation damping during nominal operations (about 10° accuracy)
- No manoeuvrability required

The main design drivers adopted in the EduSAT attitude determination and control system are:

- easy to realize
- low cost
- low power consumption

III.2.7.2 ADCS baseline design

EduSAT attitude control system is based upon a passive magnetic attitude stabilization system because it is easy to realize and low cost. Moreover it does not require power consumption and software development. The weakness is the accurate design of damping system needed.

This method exploits a permanent magnet to provide a restoring torque and permeable rods for oscillation damping. Onboard permanent magnet dipole is on the order of 1 Am^2 and this sizing has been assessed by estimating worst-case disturbance torques (see following table).

Disturbance	Gravity Gradient	Solar radiation	Magnetic field	Aerodynamic	Worst case
Value (N·m)	$4{,}7 \cdot 10^{-8}$	$2{,}8 \cdot 10^{-8}$	$9{,}8 \cdot 10^{-7}$	$7{,}6 \cdot 10^{-7}$	$1{,}8 \cdot 10^{-6}$

Fig. III-28. Worst case disturbance torques estimate for EduSAT (Ref. 34).

Permeable rods manufactured using Mumetal have been selected for EduSAT, on the basis of reference literature and previous UNISAT experience.

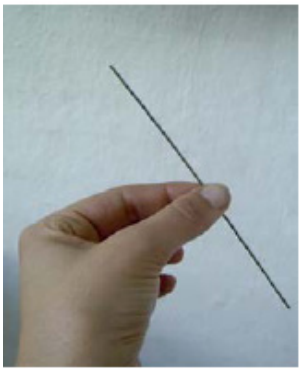

Fig. III-29. Permeable hysteresis rod manufactured in Mumetal (Ref. 34).

These rods have been manufactured using commercial soft magnetic material (Mumetal) with density 8700 kg/m3 and chemical composition in weight %: 77%Ni, 4.4%Cu, 2.67%Mo, 0.29%Mn and Fe balance. Permeable rods 20 cm-long have been selected to be boarded on EduSAT; the rod volume is 0,2 cm^3.

The attitude determination system is based on the UNISAT3 previous experience. The TFM 100S triaxial magnetometer (BILLINGSLEY AEROSPACE & DEFENSE) is responsible for the determination of the Earth magnetic field direction.

Moreover three photovoltaic panels acts as a sun sensors, detecting the sun pointing position.

Fig. III-30. TFM 100S magnetometer

Radiation Tolerance:	> 300 kRADs (with 1.59 mm cover) > 100 kRADs (with 0.79 mm cover) Option
Axial Alignment:	Orthogonality better than ± 1° ; ± 0.5° special; calibration data provided to ± 0.1°
Input Voltage:	+ 15 to + 45 VDC + 45 to + 125 VDC Option
Input Current:	20 mA at 28 V
Isolation:	between power and signal ground > 200 MΩ at 500 VDC
Field Measurement Range:	± 100 μT
Accuracy:	± 0.5% of full scale
Linearity:	0.015% of full scale
Sensitivity:	100 μV / nT
Scale Factor Temperature Shift:	.0075% full scale / °C
Output Ripple:	3 mV peak to peak @ 2nd harmonic
Analog Output @ Zero Field:	± 0.025V
Zero Shift with Temperature:	≤ 1.0 nT /°C
Susceptibility to Perming:	± 25 nT shift with ± 5 Gauss applied
Output Impedance:	332 Ω ± 5%
Frequency Response:	- 3 dB @ > 150 Hz
E M I:	CEO1, CEO3, REO2, CS01, CSO2, CSO6, RSO1, RSO2, RS03
Random Vibration:	20G RMS (20 Hz to 2 KHz)
Shock:	>230 G
Temperature Range:	- 40° to +85 °C
Weight:	200 grams (1.59 mm cover) 166 grams (0.79 mm cover) Option
Size:	3.66 cm x 3.58 cm x 15.44 cm
Connector:	NON-MAGNETIC 9 PIN "D" TYPE

Fig. III-31. TFM 100S magnetometer specifications

III.2.8 Edusat OBDH

III.2.8.1 OBDH requirements and design drivers

The On Board Data handling (OBDH) subsystem shall provide the capability to perform the following onboard functions:

- *ADCS*. Interface the ADCS sensors (Solar panels acting as suns sensor, magnetometer) during all mission phases.
- *Telecommands*. Include the telecommands handler that demodulates, decodes, validates, distributes and executes ground commands.
- *Telemetry*. Acquire telemetry data for transmission to ground
- *Payload.* Support autonomous functions for payload data management
- *Power control*. Monitor the battery status (mainly the charge/discharge current and voltage) and the solar arrays status.
- *On-board time*. Provide On-board Time reference generation and distribution to assure synchronisation among different subsystems.
- *On-Board storage*. Provide on-board data storage capability to temporarily store all telemetry data.

III.2.8.2 OBDH baseline design

The OBDH subsystem architecture is shown in Fig. III-32, highlighting the two μprocessor (for redundancy reason), one master and one slave, but both able to handle all the satellite subsystems.

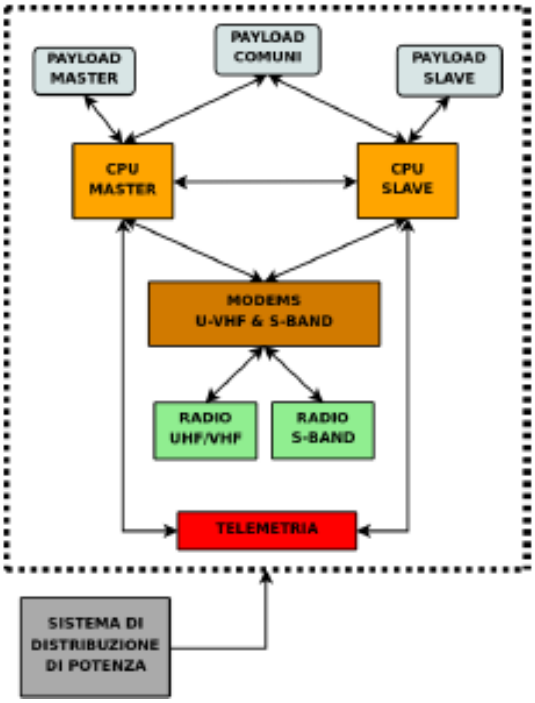

Fig. III-32. EduSAT OBDH architecture

The OBDH main characteristics satisfy all the other subsystems requirements and provides 16 MByte Static RAM, 16 MByte Flash Memory and 256 Kbytes PROM. The voltage needed is 3.3 V and the operative temperature is -10°C to +60°C.

Moreover it is important to emphasize that there are not electrical connections between launcher and satellite; during ascending phase satellite is turned off and at the separation it is switched on.

III.2.9 EduSAT Telecommunication system

III.2.9.1 Telecommunications requirements and design drivers

EduSAT telecommunication system requirement are given as follow:

- Provide telemetry, telecommand and P/L data links with Ground Stations
- Preferring use of COTS components with high TRL and ITAR-free components.

III.2.9.2 Telecommunications assumptions and trade-off

EduSAT communication system, is based on UNISAT satellites communication system previous experience; it will use data transmission in VHF

band (145 MHz) for up link and in UHF band (436 MHz) for down link. Bit rate is 9600 bps for these channels.

III.2.9.3 Telecommunications baseline design

If required EduSAT communication system is able to use UHF and VHF channels in both uplink and downlink. Moreover payload data transmission can use a buck-up channel in S band (2.2-2.4 GHz) with a bit rate of 400Kbps.

The radios characteristics are here summarized (see also Fig. III-33):

- *UHF transceiver*: Downlink transmitter frequency 436.800 MHz, power 2W. Uplink receiver frequencies: 436.800 MHz.
- *VHF transceiver*: Downlink transmitter frequency 145.85 MHz, power 2W. Uplink receiver frequency: 145.85 MHz.
- *S-band transmitter*: Downlink transmitter frequency 2.3 GHz, power 2W.

Fig. III-33. UHF, VHF transceiver and S-Band transmitter.

In the following figures the EduSAT uplink budget in both UHF and VHF modes. The signal to noise ratio and the margin are calculated exploiting SPIV ground stations features, the receiver antenna gain and the slant range as input parameters. Moreover the receiver noise figure and the cable, pointing and polarization losses are considered. In UHF band the EduSAT received power is $1{,}73^{-11}$ W while in VHF band the EduSAT received power is $8{,}73^{-11}$ W.

EduSat UHF UpLink Budget w/ SPIV					
Input Frequency in MHz	436,80				
Input B sys (KHz)	32				
Input Power of Transmitter (W)	75,000		or	48,751	dBm
Input Trans. Ant. Gain (dB)	16,15		or	4,12E+01	
Input Rec. Ant. Gain (dB)	0		or	1,00E+00	
Input Rx Noise Figure	3	dB			
Input Req. S/N Ratio for FM	12	dB			
Input Slant Range	730	km			
Input Other Losses (Cable, Pointing, ...)	5	dB			
FSPL	5,6024E-15				
	-142,5162556	dB			
Noise Calc.					
Calc. Noise Temp (293 K ref.)	291,6118583	K			
Top (assumes 20 K sky)	311,6118583	K			
Noise Output Power	1,37608E-16	W			
	-128,6135696	dBm			
Power Received	1,73E-11	W			
	-7,76E+01	dBm			
Wavelength (meters)	0,686813187	m		lam squared	0,471712354
SNR	**50,998**	**dB**			
Margin	**33,998**	**dB**			

Fig. III-34. EduSAT UHF uplink budget with SPIV ground station.

EduSat VHF UpLink Budget w/ SPIV				
Input Frequency in MHz	145,85			
Input B sys (KHz)	20			
Input Power of Transmitter (W)	75		or	48,751
Input Trans. Ant. Gain (dB)	13,65		or	2,32E+01
Input Rec. Ant. Gain (dB)	1,5		or	1,41E+00
Input Rx Noise Figure	3	dB		
Input Req. S/N Ratio for FM	12	dB		
Input Slant Range	730	km		
Input Other Losses (Cable, Pointing, Polarization, etc.)	8	dB		
FSPL	5,02489E-14			
	-132,9887316	dB		
Noise Calc.				
Calc. Noise Temp (293 K ref.)	291,6118583	K		
Top (assumes 20 K sky)	311,6118583	K		
Noise Output power	8,60049E-17	W		
Noise Output power	-130,6547694	dBm		
Received Power	8,73E-11			
	-7,06E+01			
Actual Rec Power needed	-118,6547694	dBm		
--->This is (watts)	1,36E-15			
Wavelength (meters)	2,056907782			lam squared
SNR	**53,567**	**dB**		
Margin	**33,567**	**dB**		

Fig. III-35. EduSAT VHF uplink budget with SPIV ground station.

III.2.10EduSAT Programmatics

EduSAT program schedule has been extensively described in II.2.2.2 paragraph, exploiting ESA ECSS standards.

III.2.11 EduSAT Risk analysis

EduSAT risk assessment and management has been extensively described in II.2.2.3 paragraph, exploiting ESA ECSS standards.

III.2.12 EduSAT GS&Ops (SPIV)

III.2.12.1 GS&Ops requirements and design drivers

Requirements

The EduSAT Ground Segment and Operations (GS&Ops) subsystem is named SPIV (San Pietro In Vincoli ground segment) and its requirements have been identified at the beginning of the EduSAT mission study, and are summarized as follow:

- *Functional requirements*
  - To provide and maintain the ground segment to space segment communication links.
  - To provide and maintain the ground to ground link, that is the link with external ground stations.
  - To provide the User interface.
- *Mission requirements:*
  - Satellite access according to LEO orbit condition
  - EduSAT expected operational life is 5 years (due to the UNISAT3 mission success).
- *Communication requirements:*

  The communication link features (radio frequencies used in uplink and downlink, and the relative data rates), modeling:
  - The ground antennas characteristics to fit the low power signal received.
  - The number of ground stations to be used.

Design Drivers

- Reuse of SPIV existing proven components.
- Improve UNISAT3 SPIV capabilities exploiting new radio amateur devices.
- Low cost solutions for new components and operations maintenance.

III.2.12.2 GS&Ops assumptions and trade-offs

The SPIV capabilities in UNISAT3 tracking and telemetry acquisition has been taken into account. In general microsatellites is characterized by low power (5-10 W) and in particular low power available for communication link (about 2 W).

The entire SPIV receiver system chain has been extensively tested during UNISAT previous missions and has been adopted as start up design for EduSAT mission ground segment.

On April 2010 the GAUSS laboratory (with the SPIV ground station) has been moved in the new location of the School of Aerospace Engineering. Due to the increase of the distance between the antennas and control centre, a trade-off has been carried out to evaluate the use of an additional preamplifier or a smaller attenuation coaxial cable. The more powerful coaxial cable solution has been chosen.

III.2.12.3 GS&Ops baseline design

SPIV architecture

The SPIV ground station of the EduSAT microsatellite is located in Rome (41°54′N, 12°29′E) and operated by GAUSS.

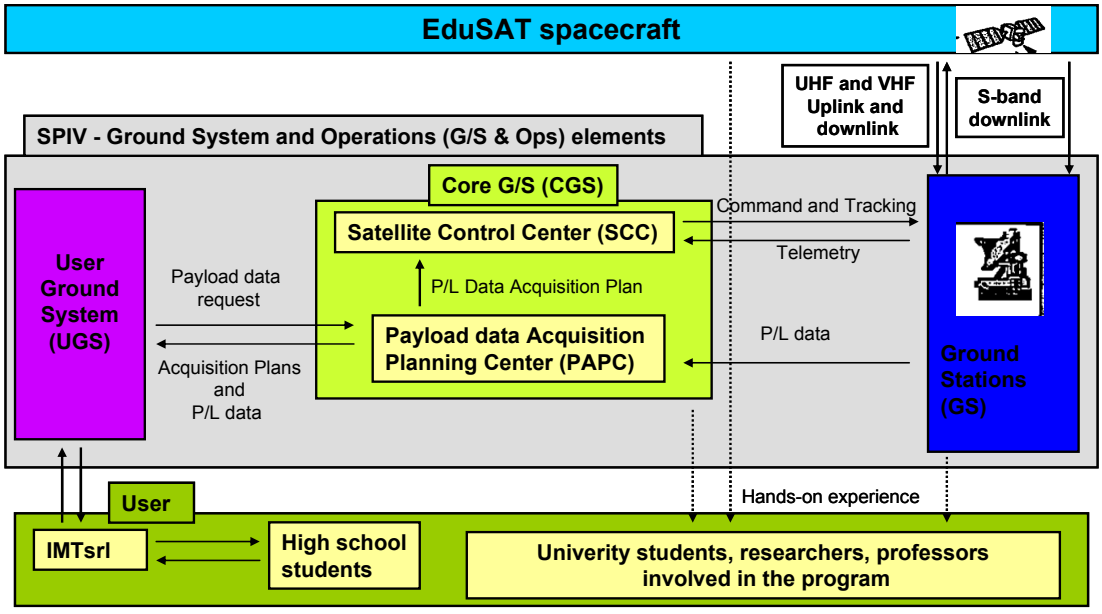

Fig. III-36. EduSAT SPIV-GS&Ops architecture.

Following the method adopted for SEO mission (described in II.5 paragraph), EduSAT GS&Ops subsystem has been divided in three elements. Each element has

been customized to match EduSAT mission requirements and the overall architecture is shown in Fig. III-36.

- *Ground Stations (GS)*: this element is responsible for the Space segment to Ground segment communication links (see dedicated chapter for more details).
- *User Ground Segment (UGS)*: it provides the interface with the IMTsrl sun sensor user. It allows IMTsrl to monitor the payload status and high school students (through IMTsrl) to follows the experiments results.
- *Core Ground Segment (CGS)*: it includes two subsystems. The Payload data Acquisition Planning Center (PAPC) and the Satellite Control Center (SCC). PAPC pre-processes the Payload data Requests received from UGS, sorting the requests taking into account the EduSAT satellite in-orbit status. The SCC is responsible for the EduSAT satellite Command and Tracking (through the UHF or VHF uplink) and for the EduSAT satellite Telemetry data acquisition (through the UHF, VHF or S-Band downlink).

It is important to emphasize that the main EduSAT program objective is the didactical purpose. For this reason the university students, researchers and professors involved in the program are users too.

Ground stations features

Both UHF and VHF antennas of the SPIV ground station are controlled by the same azimuth motor (AM) and elevation motor (EM) (left side Fig. III-37).

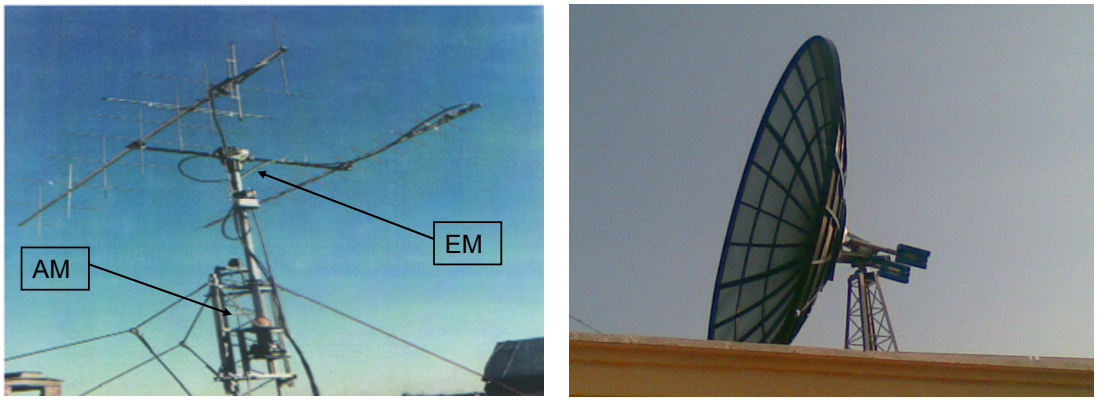

Fig. III-37. UHF and VHF Yagi antennas of the SPIV ground station.

The UHF antenna operate at 436.8 MHz (Free Space Wavelength = 686.8mm) . The element exposed length is 155mm while the element total length is 172mm. The beamwidth is 28-30 degree @ half power and the Gain = 14 dBdc.

The VHF antenna operate at 145.85 MHz (Free Space Wavelength = 2056mm). The element exposed length is 521mm while the element total length is 538mm. The Beamwidth is 40-43 degree @ half power and the Gain = 11.5 dBdc.

Both VHF and UHF elements are based upon 0.039" Dia Steel, plated with White-Bronze. The Radio Tx Power = 70 W.

The Yagi antenna is fully automatic and remotely controlled to track and control EduSAT satellite, and to download telemetry and payload data. The azimuth rate is 2°/sec while the elevation rate is 4°/sec thus allowing to track all LEO orbit satellites. The full-duplex coaxial cables allow both downlink and uplink communication in both channels, exploiting 2 transceivers and 2 receivers.

The S-Band antenna is a 3,6 meter diameter parabola (right side Fig. III-37), fully automatic and remotely controlled. The antenna Gain is 36.1008 dBi while the Effective Isotropically Radiated Power (EIRP) is 53.5826 dBW. The Beamwidth = 2.5362 degree @ half power.

Boarded on the antenna feeder, a low noise block (Keps 13pbc7-01) converts the 2220 MHz input signal in 145 MHz output signal, thus allowing:

- a low attenuation in the path from antenna to the SCC
- reuse of VHF preamplifier and receiver at the SCC

For this reason each frequency link satisfy the following functional diagram:

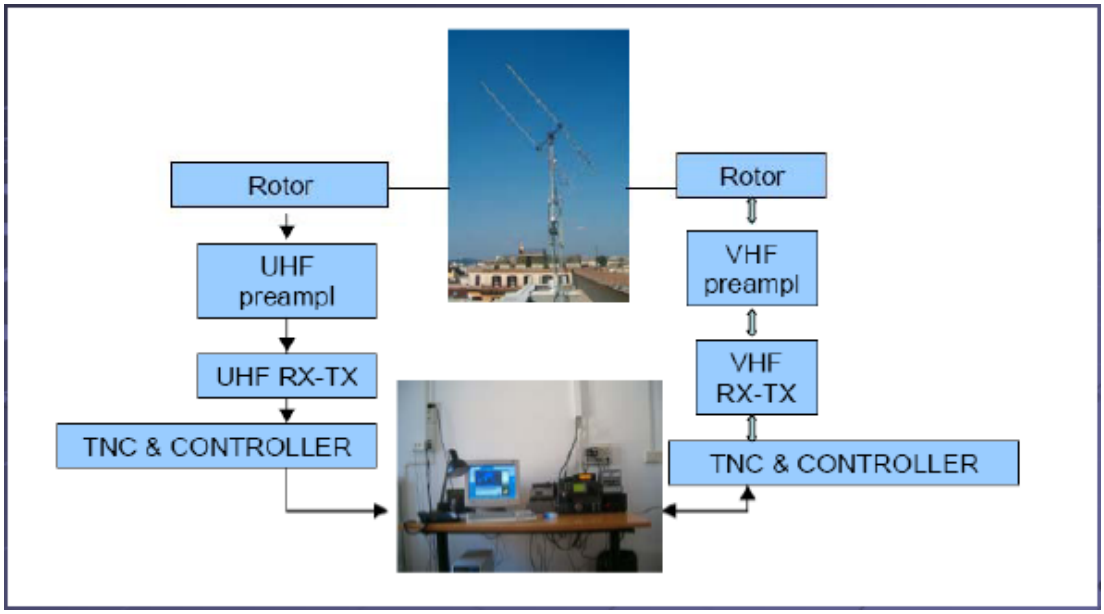

Fig. III-38. SPIV ground station functional diagram.

Satellite Control Centre hardware

The satellite control centre (SCC) is equipped with the following devices:

- YAESU FM transreceiver FT2800M, to ensure the nominal telecommands in VHF uplink.
- VHF/UHF transereceiver IC-910, to provide telemetry, tracking and payload data communication in both channel (also S-Band trough VHF channel).
- CT-17 communication interface. It is responsible for downlink doppler shift correction, exploiting satellite coordinates from tracking software
- Modem PacComm Spirit-2, the terminal node controller (TNC).
- 2 Elevation-Azimuth controllers for Yagi and parabola antennas

Satellite Control Centre software

Orbitron software is used for EduSAT Two Line Elements (TLE) propagation. It allows also to share satellite coordinates information with WiSP DDE and ARSWiN software. WiSP DDE provides doppler shift calculation, sending the results to the CT-17. ARSWiN is used to automatically sent command to the antennas motors.

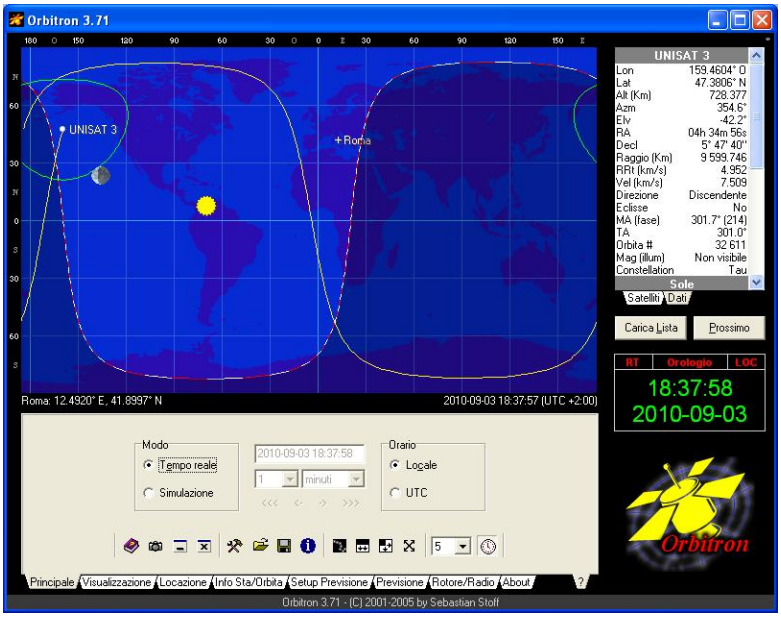

Fig. III-39. Orbitron

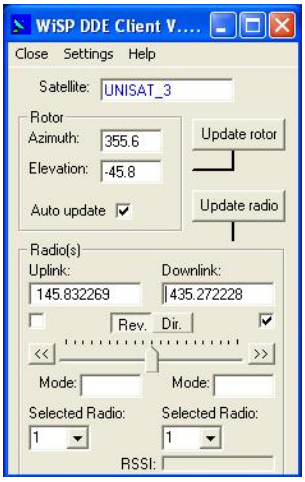

Fig. III-40. WiSP DDE Client

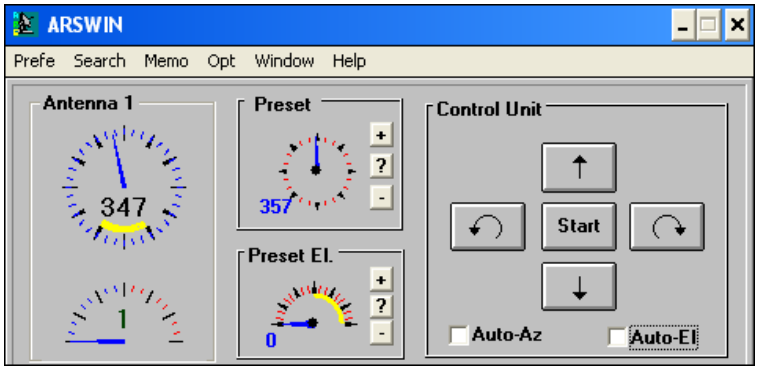

Fig. III-41. ARSWiN

SPIV modes

EDUSAT/ SPIV	**UPLINK**		**DOWNLINK**		
Frequencies	UHF 436.800 MHz	VHF 145.850 MHz	UHF 436.800 MHz	VHF 145.850 MHz	S 2.3 GHz
Data Rate	9600 bps	9600 bps	9600 bps	9600 bps	400 Kbps

Tab. III-9. SPIV modes.

The data rate available are 9600bps for the VHF and UHF, 400Kbps for the S-Band. Normal operation will occur via VHF uplink command and UHF telemetry download in real time.

Capitolo IV
Microsatellite optical payload for space debris monitoring

In the last twenty years the university-class microsatellites have seldom if ever boarded "relevant" payloads, focusing their efforts on a functional but "modest" spacecraft.

After the detailed analysis of the technologies nowadays adopted in the design of university-class microsatellites (one of the objective of this work), I agree with Mr. Michael Swartwout suggestion (Ref. 36): *try to board "real" payload to tackle research problems that are not addressed in industry.*

For this reasson I have designed a university microsatellite optical payload for space debris monitoring, following ESA ECSS mission phasing methods and exploiting ESA standard tools as ESA PROOF-2005.

Space debris are a concern for operative satellites and human missions. This problem, arisen in the last 25 years and enhanced in LEO orbit by recent space debris-creation events (ASAT-test in 2007, Iridium33-Cosmos2251 collision in 2009), requires specific strategies to know accurately the orbital debris environment, with the main intent of avoiding collisions between orbital debris and spacecrafts. Since nineties, the Group of Astrodynamics of the University "Sapienza" (GAUSS) of Rome has been involved in optical surveillance of space debris from SpaDE ground based observatory and in UNISAT microsatellite projects (four satellites have been launched from Baykonur cosmodrome in Kazakistan using the Dnepr space launch vehicle). As a member of GAUSS group, in 2008 I began the feasibility study

of an UNISAT mission with the aim to identify small LEO space debris with a LEO space based optical system, taking advantage of an observation above Earth's atmosphere. During the last two years, the mission configuration and the main satellite subsystems features has been selected. Recently I was able to coordinate a joint activity between GAUSS and the Department of Physics of the University "Sapienza" of Rome in order to develop the optical payload to be boarded in the next UNISAT 5 microsatellite. Moreover, due to the recent interest in the development of CUBESAT standard technologies, the proposed payload has been also designed for triple cubesat (3U) dimensions.

This chapter deals with the design of a university microsatellite formation flying for the in-situ space debris monitoring. First the mission feasibility study will be shown (phase 0-A). Than the payload design (phase B), analysing the best trade-off between low cost, low burden and high performance. Also a large FOV and high resolution trade-off will be considered to maximize the number of objects that can be detected and to increase the sensitivity to small debris (< 1 cm size). Moreover a low cost method for the payload manufacturing phase (phase C-D) will be proposed.

IV.1 Microsatellite remote sensing payloads

In the following pages will be shown different microsatellite optical payloads used for different remote sensing applications, most of them are developed for Earth observation missions.

IV.1.1 Earth observation application

Since Spot1 hit the market in the early 1980's the world has seen many commercial satellite remote sensing systems. Despite the hopes of the 90's the market for Space Imagery is not very prosperous. Main reason for this is the end user price. As long as an earth observation satellite costs about ten times more than a comparable reconnaissance plane most of the users will rely on aerial imagery (Ref. 37).

As a reaction to the aerial challenge there is a trend to use cost effective micro-satellite systems in mapping and High Resolution (HR) markets while the Super High Resolution (SHR) market is reserved for the big and expensive systems.

Until now Microsatellites are limited in their capabilities to achieve super high resolution. The problem is that doubling the Ground Sample Dimension (GSD) of a system means in most cases an 8-10 times bigger telescope (volume, mass). In Tab. IV-1 recent Earth Observation microsatellites missions are shown. Today most capable optical system based on a Microsatellite using solid telescope design is the British Topsat mission with a GSD of 2,5m.

Microsatellite	Mass at lunch [Kg]	GSD [m]	Launch date
DST	150	0,8	Not launched
Deimos 1	91	22	2009 July
RappidEye	150	6	2008 August
Topsat	150	2,5	2005 October
Nigeriasat 1	100	32	2003 September
AISat 1	90	32	2002 November
Tsinghua 1	49	39	2000 Jun
DLR TUBSat	50	6	1999 March

Tab. IV-1. Earth Observation microsatellites.

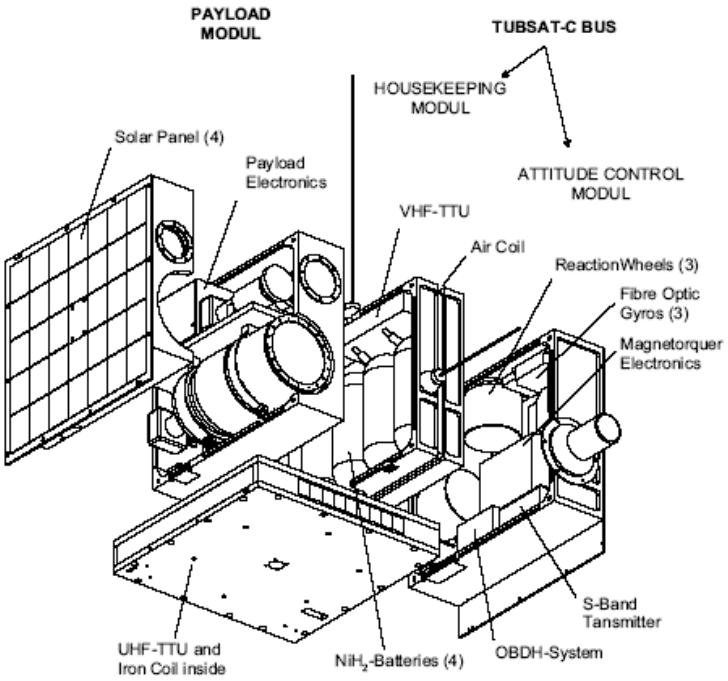

Fig. IV-1 Exploded view of the microsatellite DLR-TUBSAT

The smaller in orbit microsatellite boarding an optical payload is the DLR-TUBSAT telescope (f = 1m, f/# = 11).

The most challenging payloads have deployable mirrors but the technology is not mature and very costly. Telescopes with deployable structures and without collimation are easier to handle but have limited optical capabilities. Telescopes with deployable structures and collimation like those developed at the TU-Berlin are a good trade off solution (DST in Ref. 38). They maintain the capabilities of classical solid telescopes but for a much lower price. Today the DST is a 50cm diameter telescope, but they are studying the feasibility to board the scaled DST configuration in a 3U standard with a 6 m resolution capabilities (DST-8).

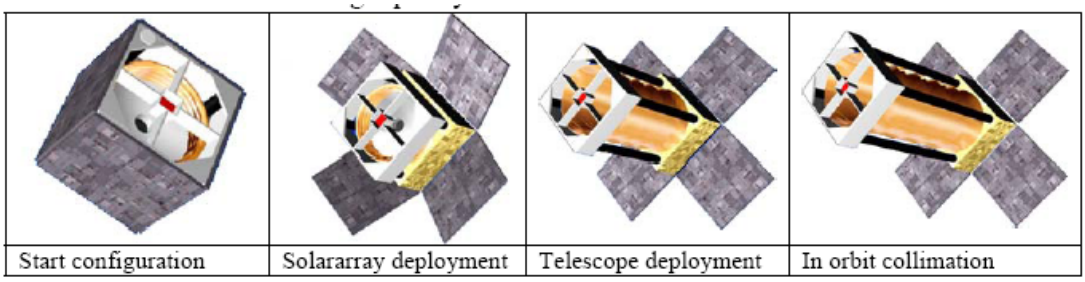

Fig. IV-2 DST in Orbit deployment simulation

It is also important to emphasize the RapidEye compact system. This is a Three Mirror Anastigmat (TMA) configuration (f/# = 4.3, D = 15cm) that allow 6.5 m resolution at 630 km altitude. The five RapidEye spacecrafts were launched in August 2008 and the Commissioning and Calibration phase of the has been successfully completed at the end of January 2009 (Ref. 39).

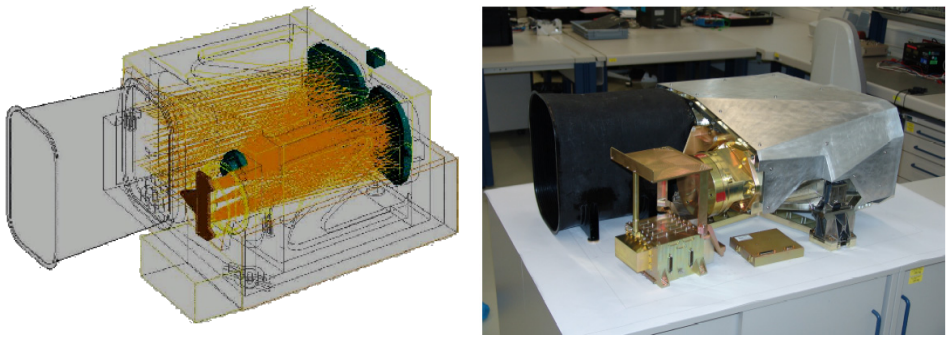

Fig. IV-3 RapidEye configuration

IV.1.2 Earth environment monitoring application

Sapphire (Fig. IV-4 and Ref. 40) will be a Canadian Forces space-based space surveillance sensor (program started in October 2007), forming one part of the Canadian Space Surveillance System. It will be a unique small satellite (approximately 150 kg) using a 15 cm aperture Three Mirror Anastigmat (TMA) telescope similar in design to the Space Based Visible sensor on the US MSX satellite (a 2700 kg satellite boarding different remote sensing instruments). The optical sensor will have a 1.4 degree field of view to observe man-made objects in deep space (6,000 – 40,000 km altitude). The satellite will be in a sun-synchronous, dawn-dusk orbit to maintain a relatively constant aspect with respect to the sun (its ground path on Earth always being close day/night terminator). The satellite's telescope will point away from the sun so it can observe objects with an aspect that provides the maximum amount of reflected sunlight (best possible phase angle).

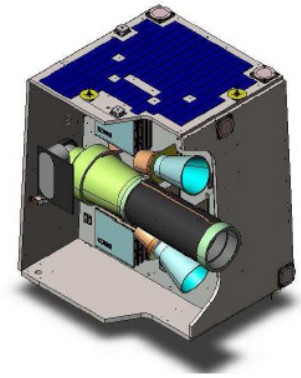

Fig. IV-4 Sapphire Satellite

The data collected will be processed by a ground-based system and the results will be used to update the U.S. Satellite Catalogue that is used by both NORAD and Canada to provide space situational awareness.

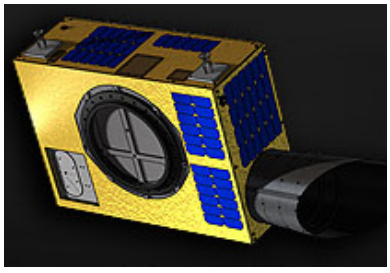

Fig. IV-5 NEOSSat

An other important project is the Near Earth Object Surveillance Satellite (NEOSSat, Ref. 41). It will systematically discover, track and determine orbits of near-Earth asteroids and comets, focusing on those in near-Sun orbits. The microsatellite mass is about 75 Kg, the available power approximately 35 Watts and the dimensions are 1 x 0.8 x 0.4 m. The payload Customized is a 15 cm aperture F/6 Maksutov telescope. The Filed of view is 0.85 deg and the CCD array 1k x 1k pixels (Pixel scale: 3 arcsec/pixel).

With the aim to monitor space debris, the European Space Agency and the Astronomical Institute of University of Bern presented at COSPAR 2010 the Space Based Optical (SBO) feasibility study, a LEO microsatellite for GEO orbit monitoring (see Fig. IV-6 and Ref. 42). The mission is based on a 800 km SSO orbit with sensor pointing orthogonal to the orbital plane.

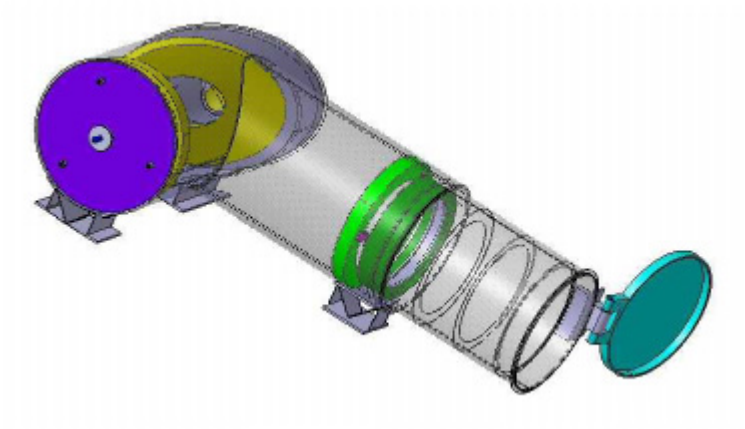

Fig. IV-6 SBO

Again the advantages are the low phase angles, the slight seasonal variations. The optical system selected is a 20cm diameter telescope (f/# = 2) with a wild field of view (FOV = 6°x6°). The detection capabilities is a dimension of objects in GEO <1m. Moreover the SSO orbit guarantees low angular velocities (optimal exposure time selected is 1-2 s) and high coverage of GEO population (see Fig. IV-7).

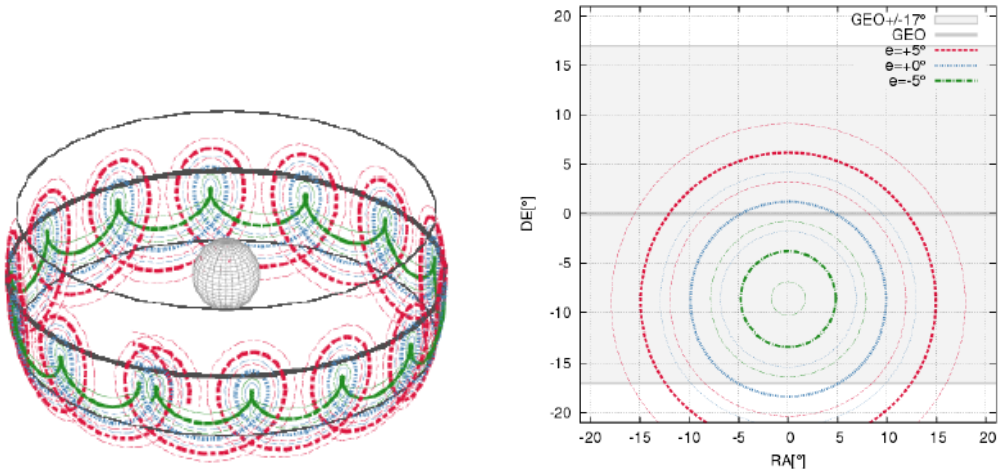

Fig. IV-7 GEO orbit coverage (Ref. 42)

IV.2 Space Debris measurement methods.

Before studying the possibility to use an optical payload to monitor space debris, let us consider the state of the art in the space debris measurements, showing the experience gained as member of GAUSS group during the participation in the design and manufacturing of the first Italian space debris observatory.

IV.2.1 Systems for space debris observation

Ground-based optical telescopes and radar can be used for the detection and orbit determination of space debris. The differences between the detection capability of these two systems is basically due to the fact that the power of the signal received by an optical system is proportional to $1/(d^2)$ (where d is the distance from the orbiting object) whereas for a radar it is proportionally to $1/(d^4)$.

For this reason radars are mainly used for the surveillance of LEO objects, whereas optical systems allow detecting more distant objects. With a ground-based radar system it is possible to detect LEO objects with size down to 1 centimeter; these objects cannot be seen with a ground-based optical system. On the other hand, optical systems have several advantages with respect to radars, such as the possibility of monitoring GEO regions, as well as the capability of identifying the shape and the attitude of an orbiting object. Another important feature of optical systems is the possibility to compare different images from distinct observation sites, thus allowing an improved orbital determination. In situ space debris monitoring systems are based

on impact sensors and on the analysis of surfaces returned from space, but these methods do not allow preventing the possible collisions.

Otherwise in situ measuring of space debris can been exploited using a microsatellite equipped with an optical system or radar based system. This last system is not suitable for university microsatellite due to the large amount of required power.

For these reasons this work has been focused on the use of optical systems for in-situ debris detection. First a detailed comparison study between ground based systems and orbiting systems will be presented (also presenting the Italian ground facilities for space debris measurements). Then the mission analysis and the payload design and manufacturing phases will be shown.

IV.2.1.1 The Italian ground facilities for space debris measurements

ASI Space Debris program exploits optic and radar observations, featuring three research lines:

- Optical observations down to 40 centimeters object dimension in GEO. Different orbit regimes monitoring capabilities with both a 30 cm and a 50 cm telescopes;
- Centimeter and sub-centimeter debris detection in LEO by means of bi-static radar facilities;
- observation of down to sub-millimeter particles in reentry phase by means of a multi-static radar system.

The following sections describes the facilities and the first results achieved with the First Italian Space optical observatory.

IV.2.1.2 The SpaDe optical observatory

Since a few years, GAUSS group has started space debris optical observations in GEO (Ref.43and 44) and Low Earth Orbit (LEO) (Ref. 45). The observation campaigns were carried out exploiting the facilities of the Associazione Astronomica Frusinate (Frosinone Astronomical Society) which operates the Campo Catino and the Collepardo observatories. Moreover, a joint campaign from

Collepardo Automatic Telescope and Observatori Astronòmic de Mallorca (Spain) was performed (Ref. 46).

As a member of GAUSS team, in 2006 I have been involved in the design and development, under ASI contract, of the first Italian optical observatory completely dedicated to space debris detection (called SpaDe, SPAce DEbris; see Ref. 47). The SpaDe peculiar requirement is the transportability; this was a driver for all the design choices. For this project two optical tubes have been procured: The first one is a Baker-Schmidt with a diameter of 300 mm and a focal ratio of f/2.8 (Fig. IV-8). It is a classical Baker-Schmidt configuration with a spherical primary mirror, an hyperbolic secondary mirror and a correction lens that removes the aberrations of the mirror as coma and astigmatism. The second optical tube of the SpaDe observatory (RILA500) is under construction and will be available in November 2010. It is a 500 mm diameter Newtonian configuration, with a focal ratio of f/3.6. At the standard Newtonian configuration (parabolic primary mirror) coma correction lens have been added to correct coma aberration (Fig. IV-9). For this reason chromatic distortion appear in the multi spot diagram shown in Fig. IV-10.

Fig. IV-8. 30 cm Baker-Schmidt optical tube (Ref. 47).

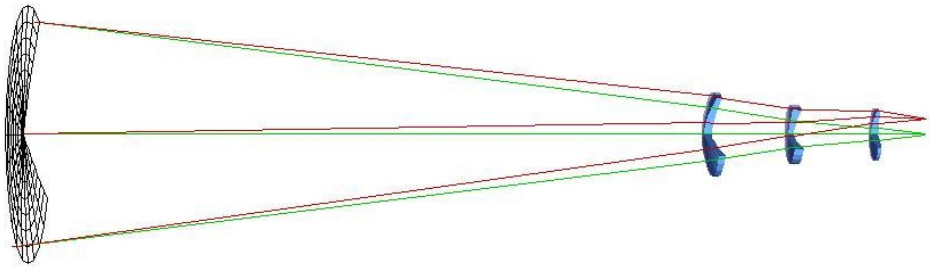

Fig. IV-9. 50 cm Newtonian configuration.

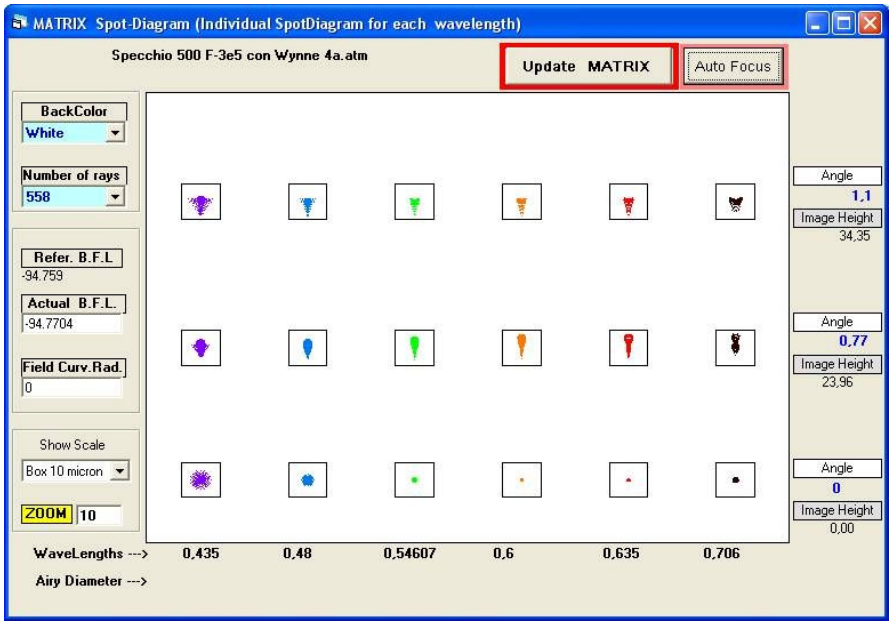

Fig. IV-10 RILA500 multi spot diagram.

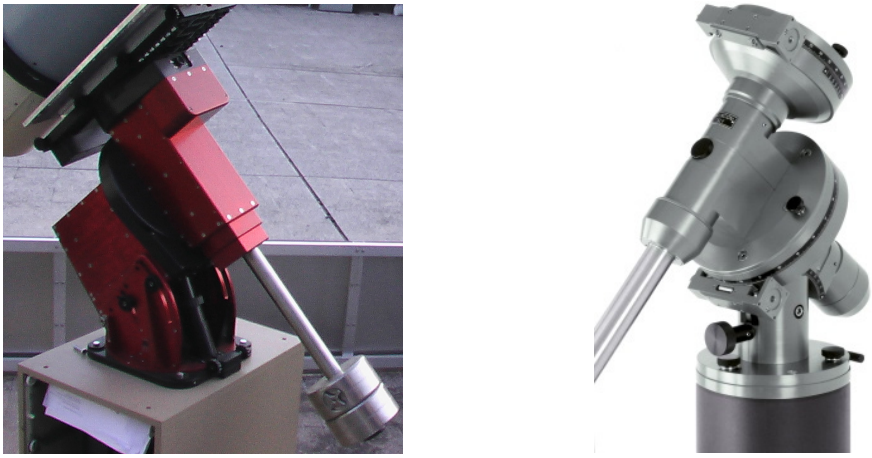

Fig. IV-11. Paramount GT 1100 ME and Bellincioni GAMMA mounts (Ref. 47).

For space debris optical observation campaigns a tracking system is required. For this reason a Paramount GT 1100 ME commercial mount has been chosen (Fig. IV-11) for the 30cm telescope. This mount is capable to support up to 45 Kg and to rotate with a maximum angular velocity of 5 deg/s in right ascension and 7 deg/s in declination. For the 50cm telescope a bellincioni GAMMA mount has been selected. This is a hand made equatorial mount (Fig. IV-11), produced by a small Italian enterprise. Its accuracy is better than any other same class commercial mounts. It can sustain up to 130 Kg within an arm of one meter; it has a tracking speed of 5 deg/s on both axes and it can be interfaced with a work station.

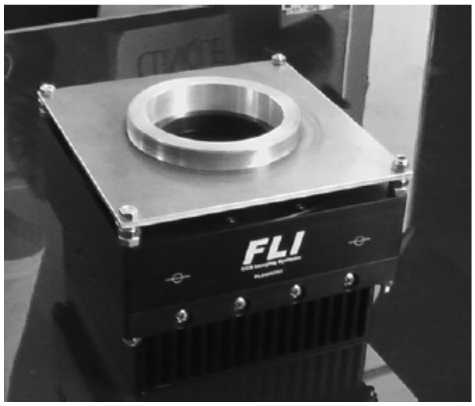

Fig. IV-12. FLI Proline CCD with the adapter (Ref. 47).

Number of Pixels	4096(H) x 4096(V)
Pixel Size	9 μm (H) x 9 μm (V)
Chip Size	38.6 mm(H) x 37.76 mm(V)
Quantum Efficiency (@ 500 nm)	60%

Tab. IV-2. SpaDE CCD parameters (Ref. 47).

SpaDe observatory has been equipped with a FLI Proline 16803 CCD camera, with a Kodak Kaf 16803 sensor. This is a commercial off-the-shelf CCD camera; its main features are summarized in Tab. IV-2. This CCD has a downloading speed of 12 Megapixels per second.

In Fig. IV-12 the FLI Proline, with the Baker-Schimdt adapter is shown. This CCD permits to achieve a field of view of about 2.6 deg for the Baker-Schmidt and about 1 deg for the Newtonian telescope.

The semi-transportability requirement resulted in the design and manufacture a new kind of dome, easily transportable, even by car . The structure is based on four quadrangular arcs which rotate around a central axis (see Fig. IV-13) by means of an electrical motor (remotely controlled). It has a Poly/450/pvc coverage. The main characteristics of this dome are modularity and lightness, both essential to comply with the transportability requirement; the structure can be actually disassembled in small modules.

Fig. IV-13. Dome design and in closed configuration (Ref. 47).

The observatory was initially assembled at University of Rome, in order to perform hardware and software tests. Since 2007, SpaDe observatory is located in Collepardo, nearby the "Collepardo Automatic Telescope" of the "Associazione Astronomica Frusinate" amateur astronomy society. Tab. IV-3 reports geodetic position and seeing (full width at half maximum, FWHM) of the site. Fig. IV-14 shows the Collepardo horizon. Fig. IV-15 depicts the observatory control scheme; all SpaDe functions can be operated by means of a laptop PC, which, in turn, can be remotely controlled through an internet connection, thus providing the observatory with complete remote control.

Site:	Collepardo, Italy
Latitude [deg – North/South]:	41°45'54'' N
Longitude[deg – East/West]:	13°22'29'' E
Altitude [m]:	576
Seeing (FWHM) [arcsec]:	8.48

Tab. IV-3. Collepardo site features (Ref. 47).

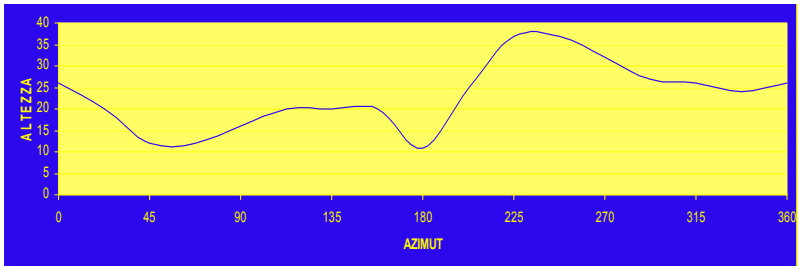

Fig. IV-14. Collepardo horizon (Ref. 47).

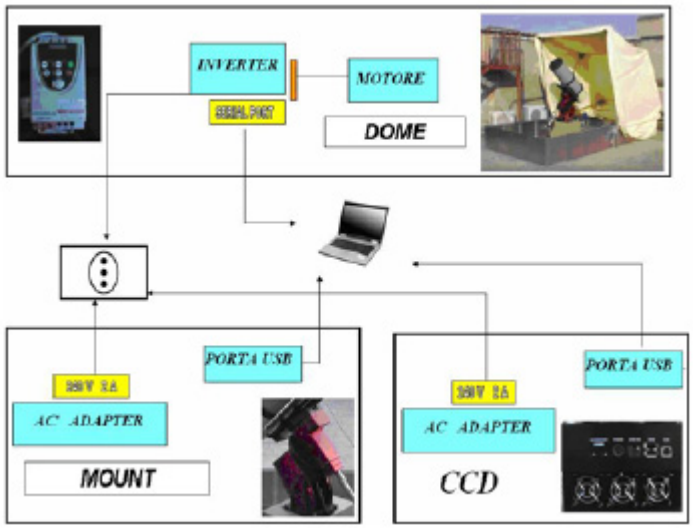

Fig. IV-15. SpaDe observatory connections (Ref. 47).

Recently Italian Space Agency proposed to improve the GAUSS SpaDE observation capability installing a new observatory in cooperation with the Keldysh Institute of Applied Mathematics (KIAM) of Russian Academy of Sciences (RAS) of Moscow. In the summer of 2009 GAUSS group cooperated with Russian researchers to install it in Collepardo. FIRST, First Italian Russian Space debris Telescope, was also included in the ISON network (International Scientific Optical Network) for the near-Earth space surveillance of the KIAM of Moscow. The FIRST observatory is based on a 22 cm telescope and a 4K x 4K pixels CCD. The field of view is about 4 by 4 degree. The mount is an equatorial EQ6 able to support 25 kg of weight, with a tracking velocity greater than 3°/sec. The shutter is controlled by a GPS board, in order to achieve a very precise timing. Two computers are used: one is dedicated to the robotic mount and CCD control, whereas the second one is dedicated to the image analysis. The software for the observatory control and image analysis were developed by researchers of the KIAM.

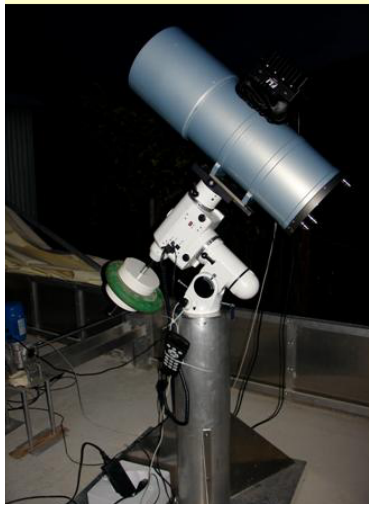

Fig. IV-16. FIRST: First Italian Russian Space debris Telescope.

The SpaDE 30cm telescope and the CAT 25 cm telescope have been used as ASI instruments during the 2008 IADC coordinated campaigns for GEO orbit monitoring (IADC Action Item AI23.4).

Aperture [mm]	FOV [°]	
300	2.6	ASI
250	0.73	ASI
250	1.86	CNES
1040	2	CNSA
1000	0.66	ESA
350	1.26	JAXA
610	1.3	NASA
410	0.33	NASA
220	2.8	ROS
640	1	ROS
2600	0.14	ROS

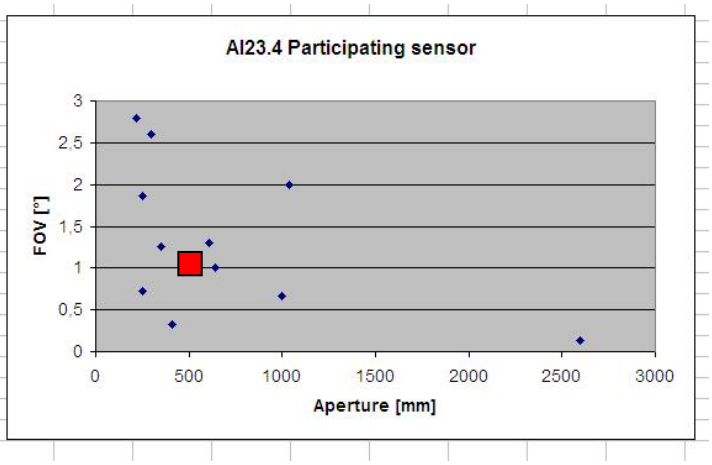

Fig. IV-17. Optical systems involved in the 2008 IADC coordinated campaigns for GEO orbit monitoring (IADC Action Item AI23.4).

In Fig. IV-17 are shown the optical systems involved in these campaigns. The square shaped point shows the RILA500 telescope that will be available at SpaDE observatory in November. This telescope will clearly increase the Italian observation capabilities in the field of space debris optical monitoring.

IV.2.1.3 High Earth Orbit monitoring campaigns

In this section are presented the results relevant to the high Earth orbit (HEO) monitoring campaigns that I have performed from February to June 2008 (IADC AI23.4) and presented at 5th European Conference on Space Debris (Ref. 48). All the results are reported, including those achieved with the Collepardo Automatic Telescope (CAT). This allowed also to assess a rough comparison of the performances of SpaDe with respect to a telescope which was widely used by GAUSS in the optical campaigns of the previous years. In Tab. IV-4 the main features of the two optical systems (SpaDe and CAT) are summarized. We remark that the two telescopes were co-located in Collepardo, Italy.

	SpaDe	CAT
Optical tube:	Baker-Schmidt	Baker-Schmidt
Diameter [m]:	0.300	0.250
CCD size [pixels]	4K x 4K	512 x 512
Field of view (FOV) [degrees]:	2.6° x 2.6°	0.74° x 0.74°
Pixel scale [arcs/pixel]:	2.2	5.16
Tracking [sidereal only or any rate]:	Any rate	Any rate

Tab. IV-4. Main features of the SpaDe and CAT optical systems (Ref. 48).

Tab. IV-4 shows the results of the HEO orbit monitoring campaigns carried out in the framework of the IADC Action Item (AI) 23.4. All the orbiting objects were automatically detected and identified with the software that I developed in the framework of the ASI Space Debris Project (Ref. 49); this software is capable to automatically process all the images of an observation campaign. Images were taken with three different observation strategies as hereafter detailed. All the images were taken during new moon periods. Each row of the table reports the data referring to a single observation night. The table columns report the following information:

• Column 1

- the date (dd-mm-yyyy) of the observation campaign;
- the Universal Time Coordinated (UTC) at the beginning and at the end of the images sequence.

• Column 2

information about the observation site and the optical system used. It is also shown the ratio between the total number of frames achieved and the total time spent during the night of observation.

• Column 3

the number of pixels in the CCD image (depending on the binning used). It is important to point out that some observation campaigns have been carried out with two different binning settings, in order to verify and test the optimal image acquisition configuration in the "seeing" conditions of Collepardo observation site.

• Column 4

the ratio between usable frames and the total number of frames achieved during the observation campaign. A typical example of useless frame is one heavily affected by bad weather conditions.

• Column 5

the number of frames taken with the three different observation strategies used:

- STM - Sidereal tracking mode: the pointing is fixed with respect to the inertial reference frame.
- OTM1 - Object tracking mode 1: during the exposure time the mount is fixed with respect to the Earth, while it is moved back to the same inertial coordinates before taking a new image. With this method the GEO objects are point-shaped.
- OTM2 - Object tracking mode 2: the mount is fixed with respect to the Earth. This method allows the same GEO object tracking during the whole observation session.

• Column 6

the detected orbital objects are classified as it follows:

- CTs - Correlated Targets: orbital objects correlated with NASA's "Geosynchronous Catalog Report".
- USCTs - UnSuccessfully Correlated Targets: orbital objects not correlated with the "NASA Geosynchronous Catalog".

- OF-USCT – One Frame UnSuccessfully Correlated Targets: orbital objects not correlated with the "NASA Geosynchronous Catalog" and detected in one image only.

• Column 7

- USs - UnSeen: orbital objects in the "NASA Geosynchronous Catalog" that should have been in the frames but actually not detected in the images.

The CAT telescope participation in the IADC joint campaign provided the possibility to compare images of the same orbital region, with the same sky illumination conditions, taken with different optical systems. The SpaDe larger FOV allows to monitoring a larger orbit region and to collect a larger number of images of the same object (resulting in better results in the orbital determination of the detected debris).

The software developed by GAUSS is able to automatically process all the images of an observation campaign regardless for the observation strategy (STM, OTM1 and OTM2), allowing to detect and identify the orbiting objects in each frame.

It is also important to point out that most of the SpaDe observation campaigns have been carried out with a 2x binning, in order to obtain a CCD size of 2K x 2K pixels and a pixel scale of 4.4 arcseconds. This is the best accuracy achievable taking into account the seeing of Collepardo site. Moreover the image size decreases (32 Mbyte for a 4K x 4K CCD size and 8 Mbyte for a 2K x 2K CCD size), allowing a faster image processing procedure.

N° of frames	**2793**
Nights of observation	**15**
Total time [hours]	**53.31**

Tab. IV-5. Performances during the GEO Orbit measures carried out by ASI-GAUSS group from February 2008 to June 2008 (Ref. 48).

Tab. IV-5, Tab. IV-6 and Fig. IV-18 show the results of the HEO monitoring campaigns carried out in the framework of the IADC AI 23.4, from February to June 2008. 2793 frames have been achieved in 15 nights of observation (53.31 hours of effective observation time). In these campaigns, 305 orbiting objects (184 CTs, 88

USCTs and 33 OF-USCTs) were automatically identified while 12 objects resulted unseen.

OBSERVATION DAY AND TIME	TELESCOPE (N° FRAMES / OBSERVATION TIME)	IMAGE PIXELS	USABLE FRAMES / TOT. N° OF FRAMES	OBSERVATION STRATEGY	DETECTED OBJECTS				US
					CT	USCT	OF-USCT	TOT	
11-02-2008 21:57:59 22:27:01	SpaDe (103 fr. / 0,5 h)	1365x1365	103/103	STM (103 fr.)	0	1	0	1	0
				OTM1 (no fr.)	/	/	/	/	/
08-03-2008 21:11:53 00:05:04	CAT (361 fr. / 2,87 h)	512x512	300/361	STM (300 fr.)	4	2	1	7	0
				OTM1 (no fr.)	/	/	/	/	/
09-03-2008 00:18:23 03:32:00	SpaDe (500 fr. / 3,23 h)	2kx2k	420/500	STM (420 fr.)	6	3	1	10	0
				OTM1 (no fr.)	/	/	/	/	/
09-03-2008 00:21:57 02:52:23	CAT (340 fr. / 2,52 h)	512x512	340/340	STM (340 fr.)	4	4	1	9	0
				OTM1 (no fr.)	/	/	/	/	/
04-04-2008 20:09:00 20:28:00	SpaDe (9 fr./ 0,32 h)	4kx4k	0/9	STM (no fr.)	/	/	/	/	/
				OTM1 (no fr.)	/	/	/	/	/
05-04-2008 21:03:20 02:59:00	SpaDe (246 fr. / 5,93 h)	4kx4k	226/246	STM (70 fr.)	4	1	0	5	0
				OTM1 (156 fr.)	6	7	0	13	0
01-05-2008 19:38:00 02:30:00	SpaDe (333 fr. / 6,87 h)	4kx4k	132/132	STM (42 fr.)	13	0	0	13	0
				OTM1 (90 fr.)	26	3	2	31	1
		2kx2k	201/201	STM (68 fr.)	31	3	3	37	0
				OTM1 (133 fr.)	38	9	5	52	0
02-05-2008 19:30:00 01:01:00	SpaDe (289 fr. / 5,5 h)	2kx2k	132/289	STM (68 fr.)	16	2	1	19	0
				OTM1+OTM2 (38 fr.)+(26 fr.)	8	4	1	13	0
03-05-2008 19:30:00 02:30:00	SpaDe (321 fr. / 7 h)	4kx4k	82/89	STM (33 fr.)	1	1	1	3	1
				OTM1 (49 fr.)	1	4	1	6	0
		2kx2k	232/232	STM (93 fr.)	6	8	1	15	2
				OTM1 (139 fr.)	4	8	2	14	2
06-05-2008 23:01:00 02:30:00	SpaDe (173 fr. / 3,5 h)	2kx2k	142/173	STM (56 fr.)	0	5	0	5	0
				OTM1 (86 fr.)	4	4	3	11	0
07-05-2008 19:31:00 02:30:00	SpaDe (335 fr. / 7 h)	2kx2k	244/335	STM (147 fr.)	6	5	0	11	1
				OTM1 (97 fr.)	5	9	3	17	0
30-05-2008 20:01:00 21:14:00	SpaDe (76 fr. / 1,22 h)	4kx4k	76/76	STM (no fr.)	/	/	/	/	/
				OTM1 (76 fr.)	1	1	3	5	3
01-06-2008 22:52:00 00:59:00	SpaDe (105 fr. / 2,12h)	4kx4k	105/105	STM (no fr.)	/	/	/	/	/
				OTM1 (105 fr.)	0	3	3	6	2
03-06-2008 20:53:00 23:23:00	SpaDe (108 fr. / 2,5 h)	2kx2k	0/108	STM (no fr.)	/	/	/	/	/
				OTM1 (no fr.)	/	/	/	/	/
04-06-2008 20:34:00 22:48:00	SpaDe (113 fr. / 2,23 h)	2kx2k	58/113	STM (no fr.)	/	/	/	/	/
				OTM1 (58 fr.)	0	1	1	2	0

Tab. IV-6. Results of the GEO Orbit measures carried out by ASI-GAUSS group from February 2008 to June 2008 (Ref. 48).

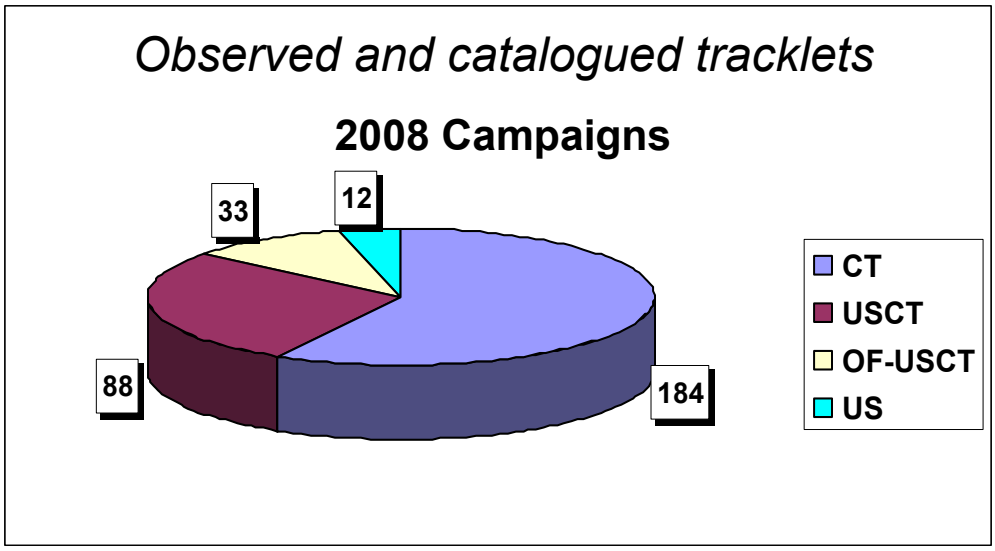

Fig. IV-18. Detected And unseen object in the HEO monitoring campaigns, February - June 2008 (Ref. 48).

Bad weather conditions affected most of the IADC 2008 observation campaigns. There were only a few nights with good weather condition: the 01-05-2008 session, carried out in both STM and OTM1 observation strategies, is an example of a good weather condition observation campaign, with 133 orbital objects detected (108 CTs, 15 USCTs and 10 OF-USCTs) and 1 unseen.

In the 02-05-2008 observation session all the three observation strategy (STM, OTM1, OTM2) were used in order the compare the different results. Moreover this night of observation was the first test of the OTM2 automatic image processing procedure.

The ratio between the total number of frames and the usable frames achieved during the 2008 IADC campaign (Table 4) is 2793/3412 (619 frames have been badly affected by adverse weather condition), with a total time spent of 53.31 hours.

Fig. IV-19 shows the position of the identified objects with respect to the propagated positions of the objects in NASA's "Geosynchronous Catalog Report". The coordinate system used is the equatorial celestial frame, centred in Collepardo observation site. It is important to emphasize that the ratio between USCTs and CTs increases moving away from -6° declination, (which is the declination of the geostationary ring with respect to Collepardo).

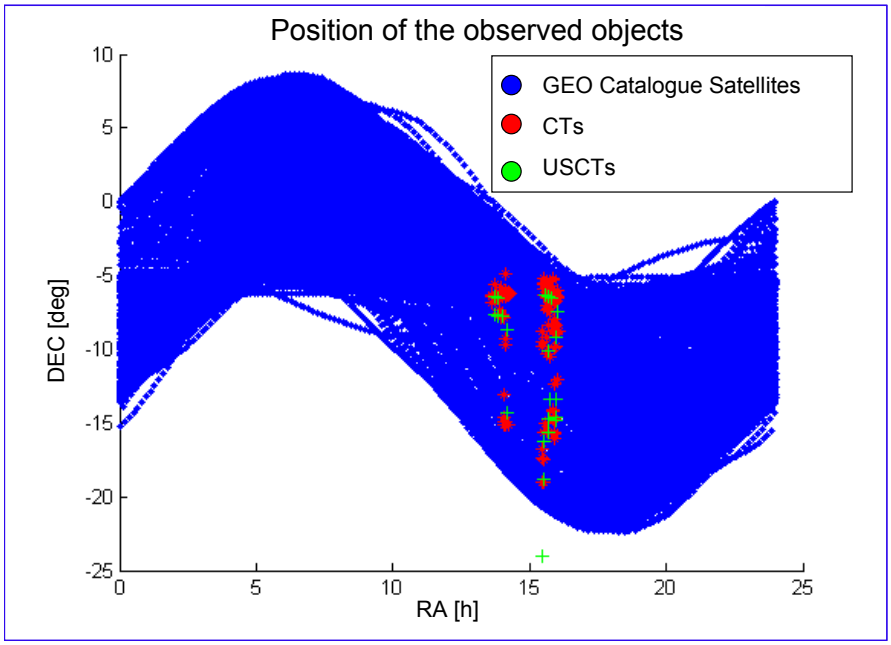

Fig. IV-19. Position of the detected objects and of the geosynchronous objects in the Collepardo-centred celestial reference frame (Ref. 48).

Fig. IV-20 shows the phase angle of the 184 CTs detected (a phase angle close to zero degrees represents the best illumination condition).

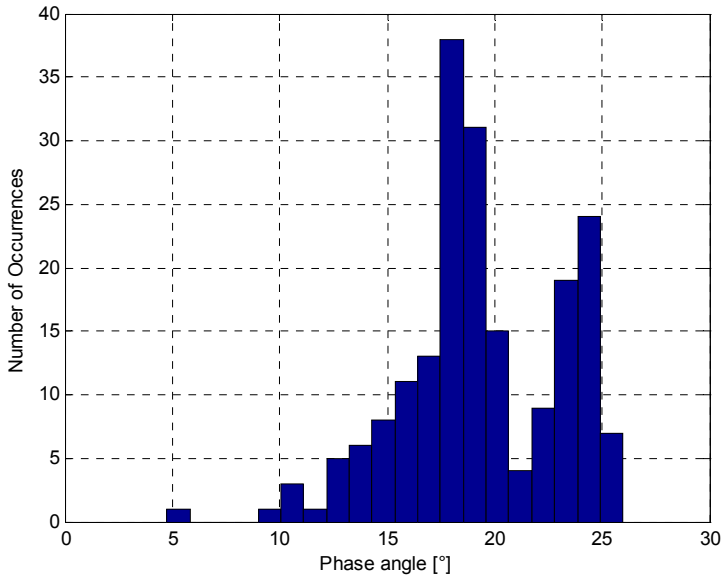

Fig. IV-20. Phase angle of the 184 CTs (Ref. 48).

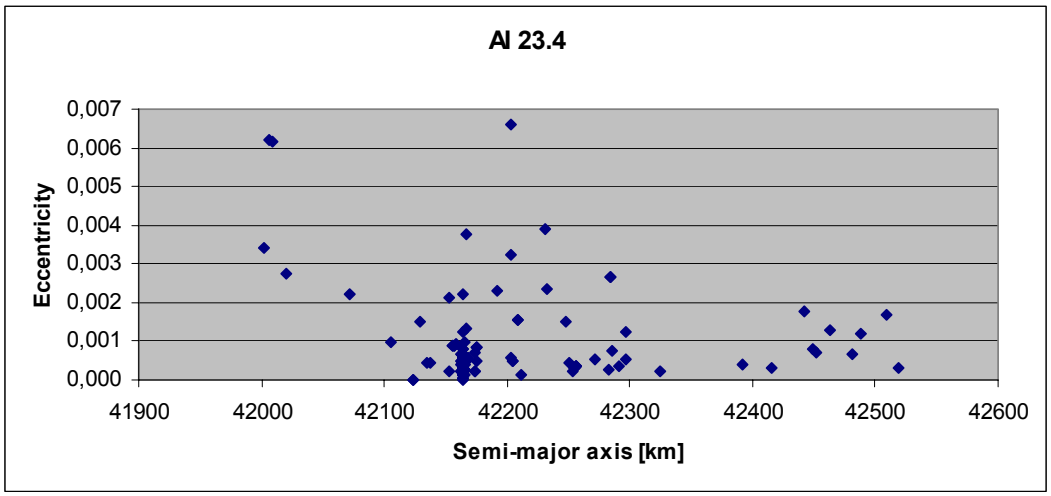

Fig. IV-21. Eccentricity vs. semi-major axis of the 184 CTs (Ref. 48).

In Fig. IV-21 and Fig. IV-22 are shown the eccentricity vs. semi-major axis and the inclination vs. the Right Ascension of Ascending Node (RAAN). It is important to emphasize the J2 and lunisolar precession effect in Fig. IV-22, where are clearly visible the uncontrolled GEO objects inclination values.

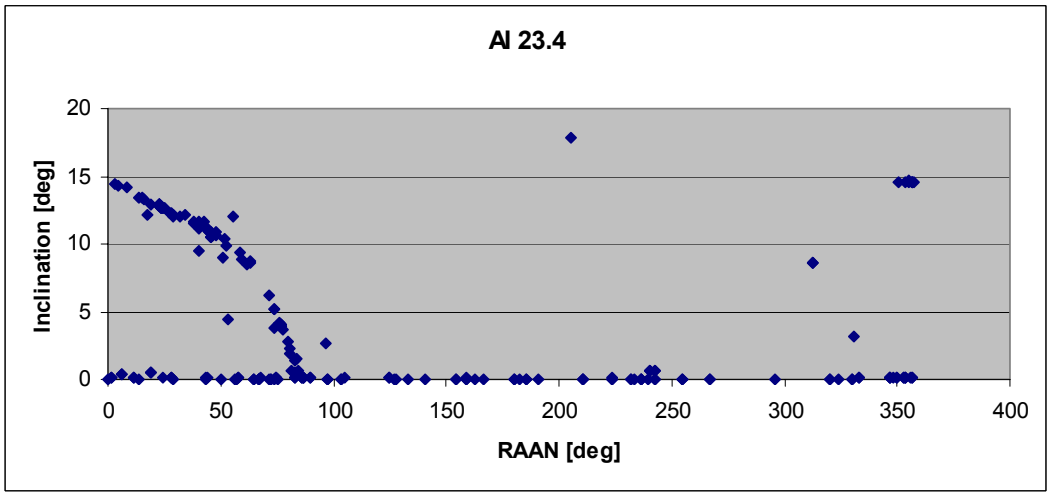

Fig. IV-22. Inclination vs. RAAN of the 184 CTs (Ref. 48).

IV.2.1.4 Low Earth Orbit monitoring campaigns

Although optical observation are mainly used to obtain statistic measurements of HEO objects, ground telescopes could be also used to track LEO objects. The SpaDE 30 cm telescope is also able to track Low Earth Orbit (LEO) objects. In particular in this section the International Space Station (ISS) test

campaign and the Iridium 33 and Cosmos 2251 impact debris observation campaign. These campaigns results have been already presented in Ref. 48.

ISS campaign

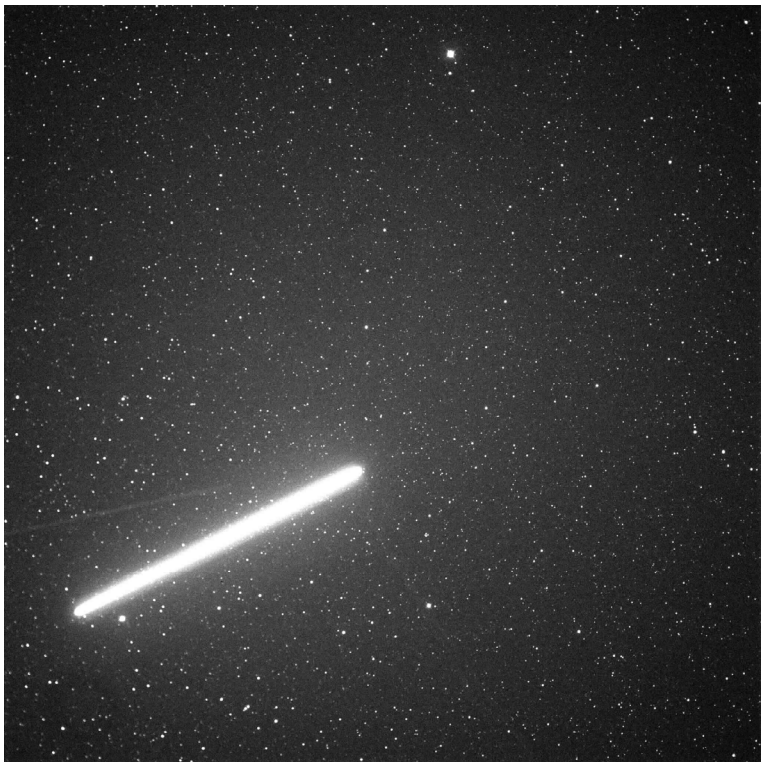

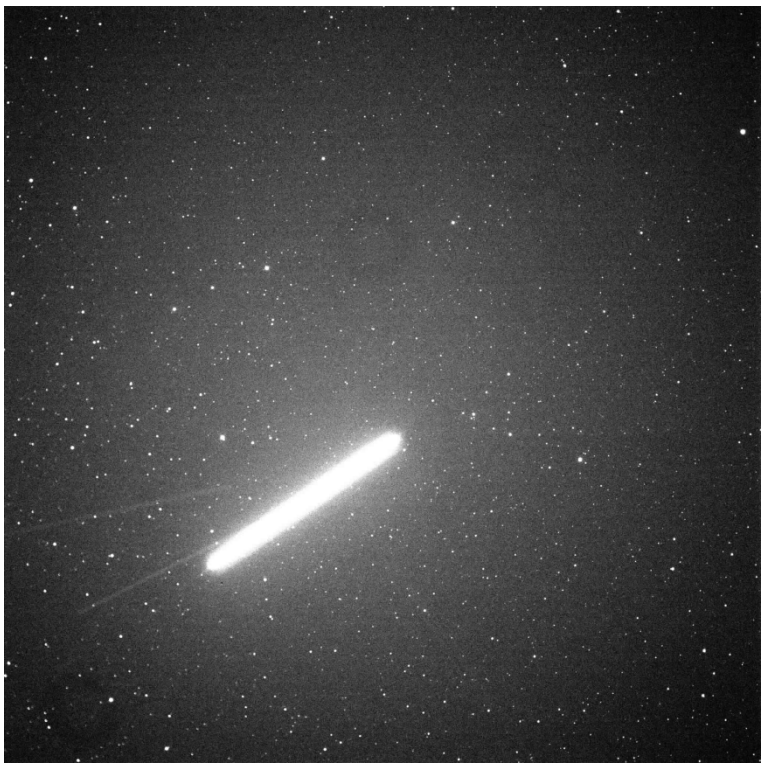

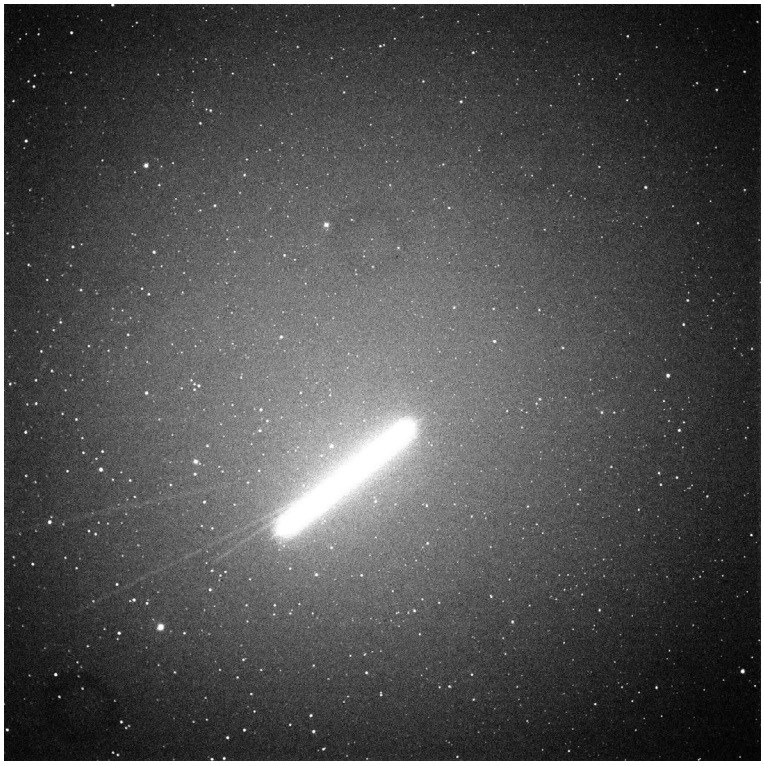

Fig. IV-23. ISS19 July 2008 sequence. Exposure time 2 seconds .2Kx2K image. Sidereal tracking mode. Visual magnitude: -1, -0.5, -0.2 (Ref. 48).

Fig. IV-24. ISS 21st July 2008 image. Exposure time 0.01 seconds .4Kx4K image. Sidereal tracking mode. Visual magnitude: +0.5 (Ref. 48).

Iridium 33 and Cosmos 2251

OBSERVATION DATE	TRACKLETS IDENTIFIED
08-03-2009	4
09-03-2009	5
12-03-2009	2
17-03-2009	3
TOT	14

Tab. IV-7. GAUSS observation campaigns of the Iridium 33 vs. Cosmos 2251 impact event (February 2009) (Ref. 48).

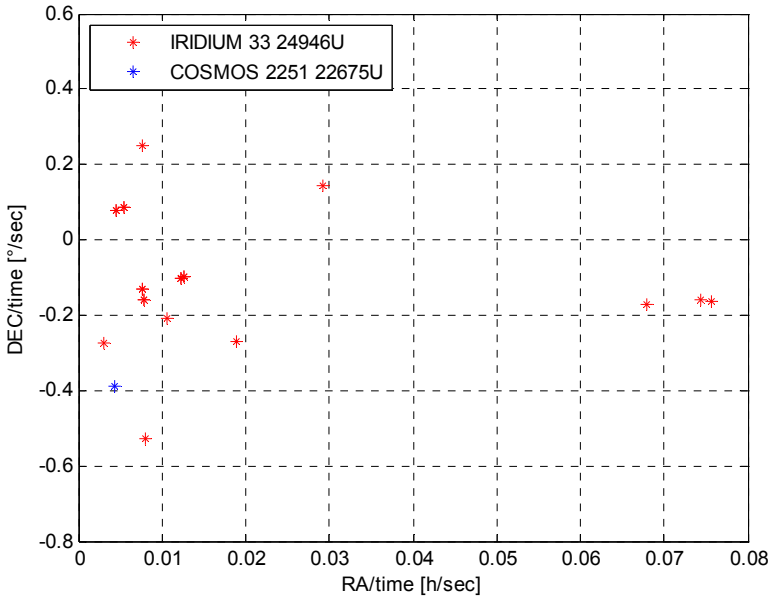

Fig. IV-25. Angular rates of the Iridium 33 vs. Cosmos 2251 impact debris detected (Ref. 48).

As shown in Fig. IV-25, the Iridium 33 vs. Cosmos 2251 impact debris detected have a very high angular rates. To be able to observe this kind of orbiting objects confirms the SpaDE tracking capabilities.

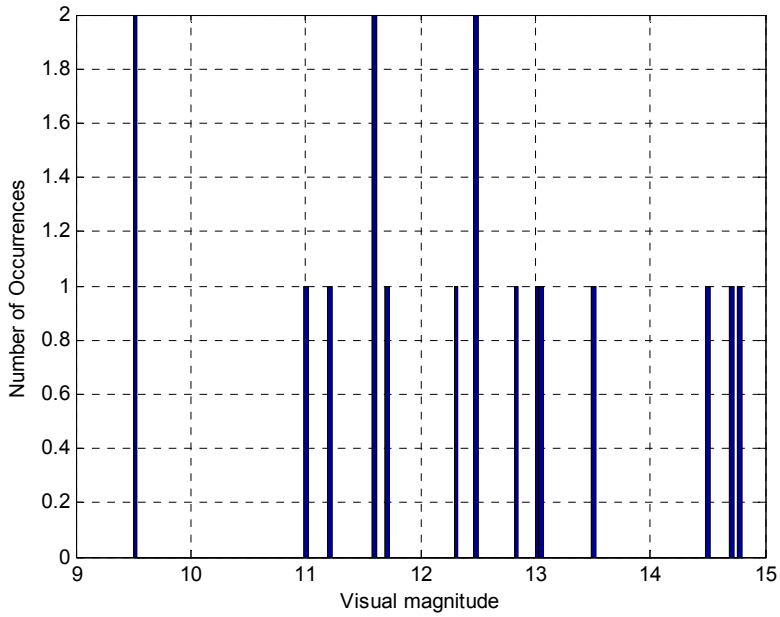

Fig. IV-26. Visual magnitude of the Iridium 33 vs. Cosmos 2251 debris detected (Ref. 48).

As depicted in Fig. IV-26, the visual magnitude values of the Iridium 33 vs. Cosmos 2251 debris detected spread from 9.5 to 14.8. This result means that the observed objects have different size or shape (15 is the limit magnitude for the 30 cm SpaDE telescope).

In the following pictures will be shown the images obtained. In particular Fig. IV-29 shows how the SpaDE 30 cm telescope can detect objects that have visual magnitude close to the limit value.

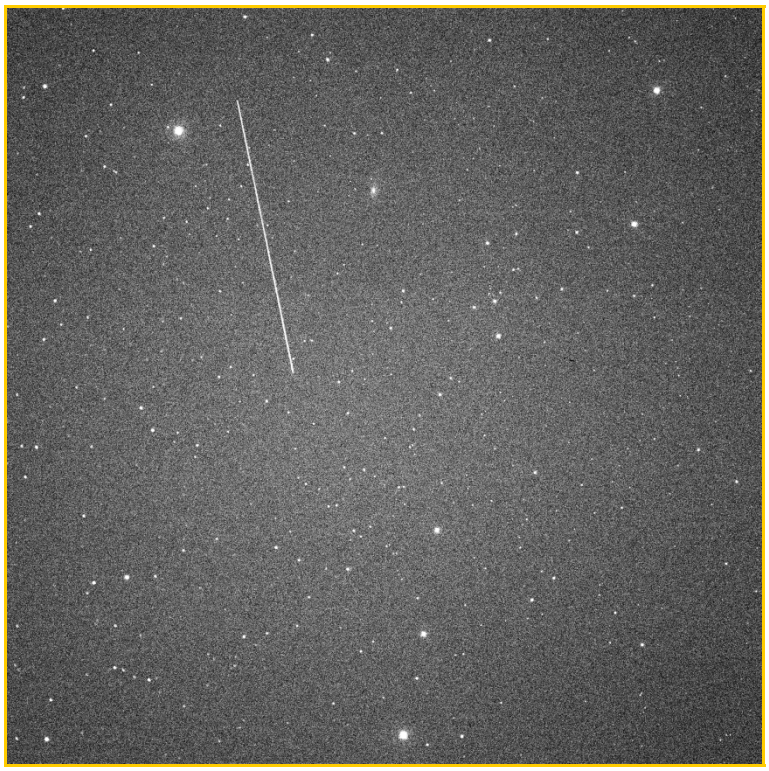

Fig. IV-27. Iridium 33 vs. Cosmos 2251 impact debris detected during the 09/03/2009 campaign (Ref. 48).

UTC = 18:45:12
RA = 11h 25m 43s
DEC = +43d 22m 30s
EXPOSURE TIME = 2 sec
VISUAL MAGNITUDE = + 12,3
BINNING = 2X2

Fig. IV-28. Details of Fig. IV-27 image.

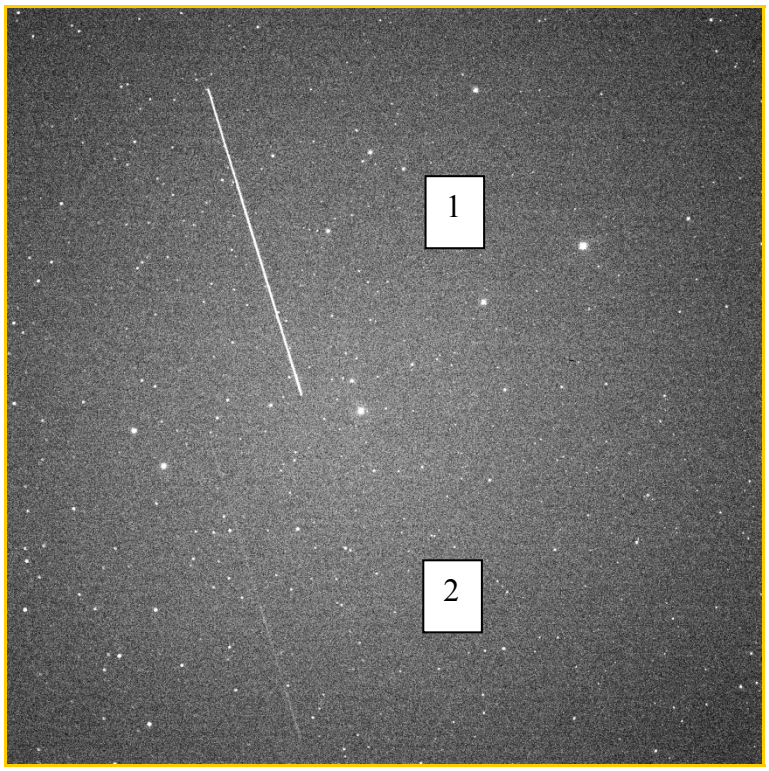

Fig. IV-29. Iridium 33 vs. Cosmos 2251 impact debris detected during the 09/03/2009 campaign (Ref. 48).

UTC = 18:23:03
RA = 09h 41m 49s
DEC = +35d 04m 14s
EXPOSURE TIME = 2 sec
VISUAL MAGNITUDE 1 = + 11
VISUAL MAGNITUDE 2 = + 14,8
BINNING = 2X2

Fig. IV-30. Details of Fig. IV-29 image.

IV.3 Phase 0-A. The mission feasibility study

Since nineties, GAUSS has started the UNISAT program with the aim of designing, manufacturing and launching educational microsatellites, completely built and operated in orbit by students of the School of Aerospace Engineering (Ref. 50). In the framework of this program four satellites have already been launched, and a fifth satellite (UNISAT5) is nowadays under construction.

In this chapter, the feasibility of a UNISAT microsatellites formation flying boarding an optical payload capable to detect space debris above the Earth's atmosphere is analyzed, using the results presented in Ref. 51.

The concept is to use optical devices to make observation and orbit determination with the use of a formation of two or more microsatellites (depending on the error constraints) taking pictures of the same area from different locations and making a reconstruction of the position of the object using angular measurements. These are obtained through a comparison of the images taken from multiple points of observation by the satellites.

IV.3.1 Mission architecture trade-off

Two different options have been considered, analysing the feasibility of a LEO formation flight mission in order to detect space debris:

- OPTION1 - The detection of objects along MEO orbits.
- OPTION2 - The detection of objects along LEO orbits.

IV.3.1.1 SSO formation flying to monitor MEO debris.

This OPTION1 feasibility study has been analysed in dept in Ref. 51. A great surveillance of MEO orbits is needed in order to avoid collisions between debris and navigation satellites (GPS, Glonass and Galileo constellations). In the MEO region there are about 60 000 objects larger than 1 cm that are possibly crossing the orbits of the navigation constellations (Ref. 52 and 53).

The formation selected is characterized by three microsatellites (weight approximately 100 kg) positioned in the same sun-synchronous dawn/dusk orbit, 120 degrees apart (Fig. IV-31). Each satellite boards optics and sensors sensible to infrared or visible radiation.

The observation strategy adopted permits to discriminate the objects in MEO from the stars. The orbital determination has been carried out taking advantage of two methods: the first one consists of taking different pictures in order to estimate the position at distinct instants of time; the second one involves capturing a single picture from each satellite, with a higher shutter time so that the position and velocity can be estimated analysing the trail of the object’s stripe in the picture. In this framework the onboard automatic image processing has a great importance, and for

this reason a lot of efforts have been dedicated to this argument. The attitude control designed for the satellites is based on the use of pulsed plasma thrusters. The control is designed using analytical formulas for simplified model of the system, and then tuned using complete simulation, considering all the effects, made in simulink.

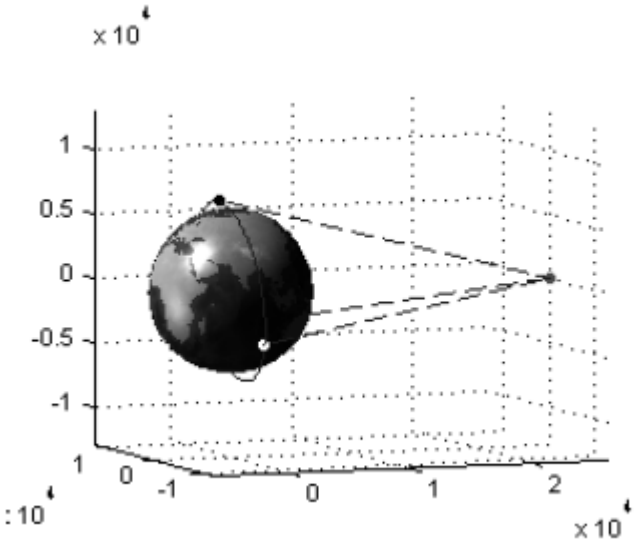

Fig. IV-31: LEO microsatellite formation for MEO region onitoring (Ref. 51).

IV.3.1.2 SSO formation flying to monitor LEO debris.

Also OPTION2 feasibility study has been analysed in dept in Ref. 54.

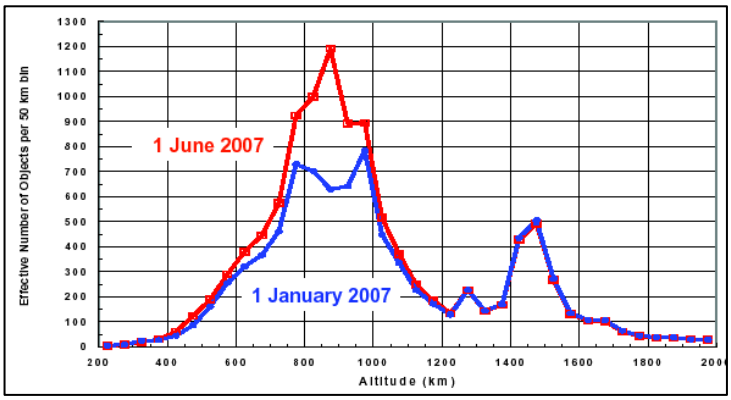

Fig. IV-32. Chinese ASAT-test results (Ref. 54).

Space debris problem, arisen in the last 25 years, has been enhanced in LEO orbit by recent space debris-creation events (ASAT-test of 2007, Iridium33-Cosmos2251 collision of 2009). In Fig. IV-32 the results of the Chinese ASAT-test.

The objective of this mission is to monitor the higher density orbit (results of this event) at about 900 km altitude, allowing in orbit objects detection and orbit determination.

In particular a possible configuration for a satellite's formation dedicated to in situ space debris detection has been studied. A statistical analysis of the number of possible debris detection has been presented showing the possible result achievable by the mission. Strategies for formation maintenance and for debris tracking have been also presented showing the way and the costs for the mission accomplishment.

Talking about the realization of a software able to automatically process the in-orbit images sequence, a lot of simulations has been carried out in order to test the algorithms in different acquisition modes.

IV.3.2 In-situ observation advantages

This paragraph deals with the possibility to carry out an optical surveillance of space objects by using mirosatellites equipped with an optical payload, analyzing in dept the improvement of the performances with respect to a ground based system (Ref. 55).

IV.3.2.1 Ground based optical systems and orbiting systems characteristics

The Earth's atmosphere hinders the monitoring of space debris environment. Clouds and pollution depend on the observation site; however, several undesired effects due to atmosphere remain even when the observations are performed from the best available site (as, for instance, from 4200 meters of altitude, in Mauna Kea, HI) (Ref. 57). Basically, the Earth's atmosphere filters selectively distinct electromagnetic wavelengths and this circumstance implies the existence of two specific narrow-band transparency windows available to optical and radiofrequency devices.

Atmospheric effects in the optical band

- SEEING: the scattering effect caused by the passage of light through turbulent atmosphere.

- SKY GLOW: the atmosphere, even in the best Earth's observation site, glows due to atomic processes in the air. This light emitted by the sky, called sky glow, is a severe problem when observing faint objects, because the sky glow photons make extra noise which degrades the accuracy of measurements.
- ATMOSPHERIC EXTINCTION: the atmosphere absorbs and scatters some fraction of the light at all optical wavelengths. This causes objects to be dimmer than they would be without the atmosphere.
- ATMOSPHERIC REFRACTION: except when looking at the zenith, the atmosphere acts as a weak prism, spreading out light in a small spectrum along the line pointing to the zenith.

When compared to an identical telescope placed outside the atmosphere, these phenomena badly affect the observation campaigns. Seeing causes the lost of much of the detail that powerful (large) telescopes are able to provide. Seeing and sky glow severely limit the accuracy of the optical measurements regarding faint objects.

Moreover, also additional random disturbs can severely compromise the observations from the Earth, such as wind (which shakes the telescopes, degrading the image quality) or clouds (that interferes with light). Even high humidity (especially in presence of dust and pollution) severely affects the performance attainable by telescopes, due to the possible degradation of optical surfaces and rust metal parts.

Seeing and angular resolution

Stars and orbiting objects can be considered a point like source. However, even if the telescope is located outside the atmosphere, focusing a point source into a point image is impossible. The light can be viewed as a wave, and waves that come from different parts of the telescope mirror interfere with each other. In the image the result is a "bulls eye" pattern, termed "Airy disk" .

The angular size of the Airy disk pattern on the sky only depends on the diameter (D) of the primary mirror or lens and is independent of its focal length. The linear size (in the focal plane) of the Airy disk in the image plane is determined by the angular size (related to D) and the image scale (related to the focal length) (Ref. 58).

The angular radius of the first dark ring radius (named the Dawes limit or the diffraction limit) is given by:

$$\Theta = 1.22 \cdot \frac{\lambda}{D} \ (\text{rad}) ;$$

where λ is the wavelength of the radiation.

As aforementioned, the Earth's atmosphere spreads the light coming from a point source (seeing). The angular extension of the quasi-Gaussian profile associated to the seeing PSF (Point Spread Function) is determined by the atmosphere characteristics, and not by the telescope. In the best observation sites, seeing turns out to be responsible of a light scattering of 1 arcsec (measured at a level equal to half of the maximum, FWHM (Full Width at Half Maximum).However, these sites are hardly available for university purposes and funds.

In our University/ASI observatory GAUSS-SpaDE (Space DEbris) located in Collepardo (Fr), Italy, at 555 meters of altitude, seeing is responsible of a light scattering of about 8 arcsec . In Fig. 1 illustrates the Dawes limit angles as a function of the wavelength λ for different diameters D. The GAUSS-SpaDE CCD is a FLI PROLINE 16803, with a quantum efficiency peak of 60% at 550nm. For example, boarding this CCD on a university microsatellite (equipped with a 20 cm diameter telescope) an angular resolution 16 times better than the ground-based one can be achieved. As shown in the plot of Fig. IV-33, if λ = 0.5 micron and D = 20 cm, θ = 0.5 arcsec.

For this reason, outside the atmosphere the angular resolution limit is lower than the ground-based one, with the exception of very small telescopes (D<15cm), which have Airy patterns comparable to the seeing of the better ground observation sites (with regard to angular extension).

However, compared with the SpaDE observation site, also a 10 cm space based telescope improves 8 time the resolution limit. At the same time the weight and dimension are minimized.

The ideal resolution and field of view

Pixels with sizes of about 1/3 or 1/2 the resolution limit represent the best solution to balance field of view and resolution. With a 2048x2048 pixels CCD (pixel size of 5,8 micron), an optical system Field of View (FOV) set to 0.7° and a focal length of 1 meter (f/ = 10, D=10 cm), the angular dimension of the pixel FOV

turns out to be equal to 1.2 arcsec, equal to the resolution limit. The 20 cm telescope gives a pixel size of 1/2 the resolution limit but produces a larger burden for UNISAT5 microsatellite.

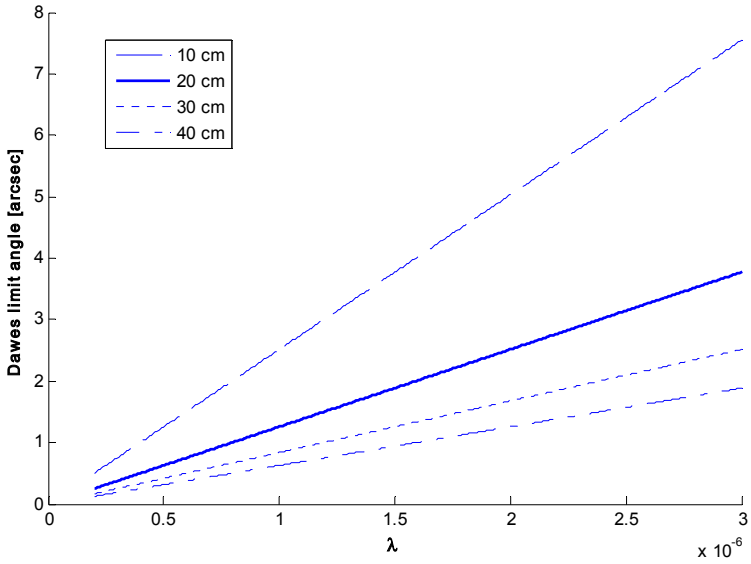

Fig. IV-33. Dawes limit angle (arcseconds) vs wavelength lambda for different telescope diameters (Ref. 55).

Atmospheric extinction

The atmosphere absorbs and scatters some fraction of the light at all optical wavelengths. This causes objects to be dimmer than they would be without the atmosphere. Astronomers call this phenomenon atmospheric extinction.

If this effect is taken into account, for a ground-based telescope the transmitted power is partially absorbed, and this circumstance implies that also the size of detectable debris reduces.

For this reason it is necessary to compare the transmitted power vs. debris dimensions for the two different systems with reference to different diameters. The method used has been proposed in Ref. 56. The sun light reflects on the object surface and it's detected by optical system. Assuming spherical object and diffuse reflection, the received power P depend on the telescope aperture D, the phase angle (sinα), the solar constant Q, the observed object diameter d, and it's inversely proportional to the distance R between the object and the telescope:

$$P = \frac{0.6 \cdot 1/24 \left(Q \cdot D^2 \cdot d^2 \left(\sin(\alpha) + (\pi - \alpha) \cdot \cos(\alpha) \right) \right)}{R^2}$$

The SpaDE CCD (Charge Coupled Device) with a peak quantum efficiency of 60% (in the range of commercial off the shelf CCD) has been considered in order to calculate the power noise threshold. Moreover a fixed phase angle value ($\alpha = 30°$) has been considered. In Fig. IV-34 it is possible to see that in the MEO case study we don't have a very important difference but in the LEO case study (Fig. IV-35) the difference is clearly visible.

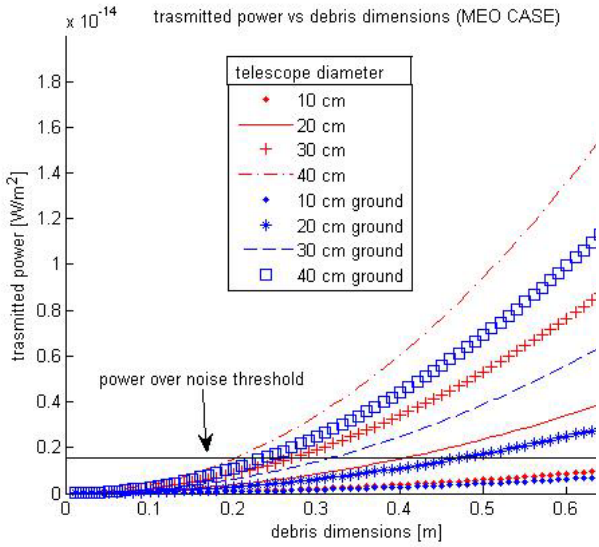

Fig. IV-34. Absorbed power vs. debris dimensions for different telescope diameters (MEO case) (Ref. 55).

In LEO case the difference between the two systems is not only due to the atmospheric extinction but mainly at the distance with the optical system. As matter of fact considering a LEO formation flight at 700 Km to detect objects with an altitude of 800 Km we have a real advantage respect ground-based telescopes. Considering the MEO case, using microsatellites in a sun-synchronous dawn/dusk orbit, we don't have a significant difference on received power but we can have others advantages which are illustrate in the following paragraphs. Another significant advantages in orbiting observations is the possibility to use thermal infrared which is absorbed by atmosphere.

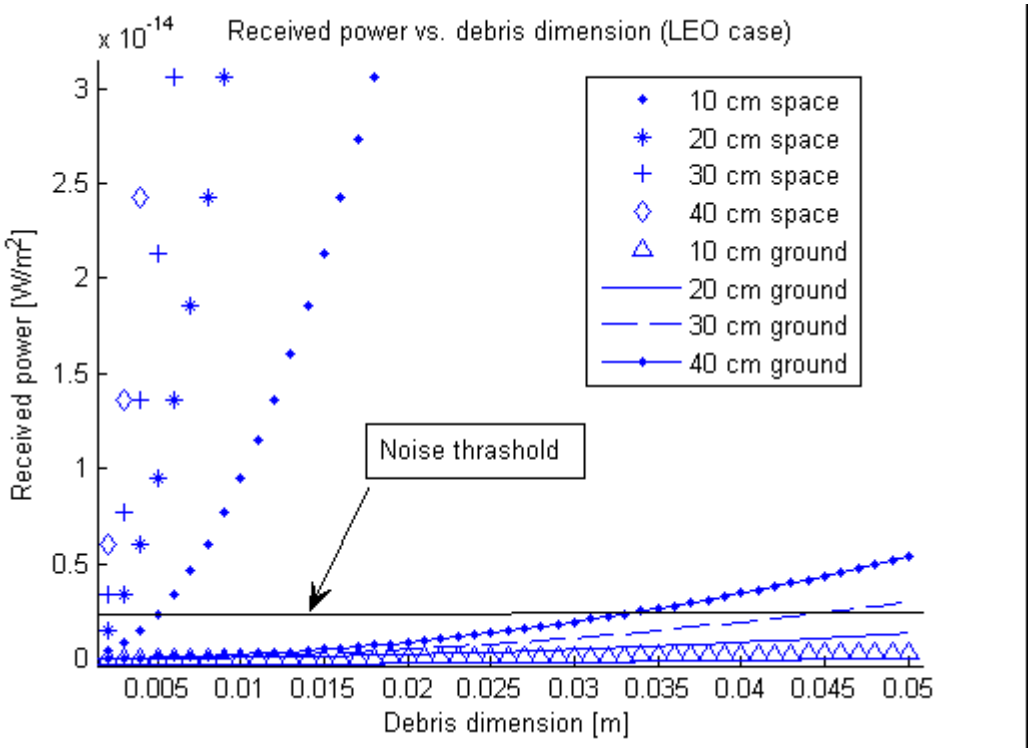

Fig. IV-35. absorbed power vs. debris dimensions for different telescope diameters (LEO case) (Ref. 55).

Phase angle and baseline

An important difference between ground-based and orbiting optical systems is debris lighting condition. With a ground-based system it is impossible to observe orbiting objects in LEO with low phase angle because the objects are eclipsed by Earth. So it is possible to carry out observations only at dawn or at dusk with phase angle close to 90° (Ref. 56). Conversely, this circumstance does not occur if the observations are performed from orbiting telescopes, because different configurations (i.e. different mutual positions between the sensor and the observed object) can be encountered, thus allowing the use of different observation strategies

An accurate orbit determination requires the collection of observational data from a number of distinct locations. For this reason, joint space debris observational campaigns from different sites on the Earth's surface have been carried out. However, the baseline of these campaigns is limited.

Conversely, orbiting systems make possible the use of different baselines, which allow a more accurate orbit determination. In particular, in the MEO study case (Ref. 51) the baseline has been fixed close to 14.000 km.

IV.3.2.2 Space based telescope vs. ground based telescope

Optical System Features	Ground Based	Space Based
Diameter [m]	0.3	0.1
FOV [deg]	2.6	0.7
Number of pixels per row	2048	2048
Pixel size (width of square pixel) [µm]	18.0	5.8
Scale (pixel FOV) [arcsec/pixel]	4.4	1.2582
FWHM (full width at half max.) [pix]	2.0	2.0
Integration time [s]	2.0	0.01

Tab. IV-8. Optical system features of the ground based telescope and the space based telescope (Ref. 55).

This paragraph shows the differences between a 10 cm space based telescope and the SpaDE 30 cm ground based telescope, exploiting a 24 hours ESA-PROOF2005 statistic simulation (as suggested in ECSS –E – Space environment, Ref. 8). In order to test these differences it has been chosen to monitoring LEO objects in the range from 700 km to 1600 km.

The space telescope is placed in a 700 km dawn-dusk Sun Synchronous Orbit (SSO) in order to obtain an orbit node line orthogonal to the sun light direction. The launch date of the simulation is the 21 of December 2008. For this reason the telescope will point 90° of azimuth in order to obtain a phase angle close to zero during the whole orbital revolution. Also an elevation of 0° permits to detect orbiting objects in the selected range.

The Spade ground telescope is placed in Collepardo site (latitude 41.765°, longitude 13.368° and altitude 555 m). In Tab. IV-8 are shown the main features of the two optical systems.

In the following figures the results of 24 hours ESA-PROOF2005 (ECSS-E-ST-10-04C) statistic simulation are shown.

Fig. IV-36 plots the number of crossing objects vs. range of the ground based telescope and the space based telescope. Due to the larger FOV, more objects cross the ground based sensor. In both case the crossing objects size is in a range from 0,01 m to 10 m (Fig. IV-37 - left side).

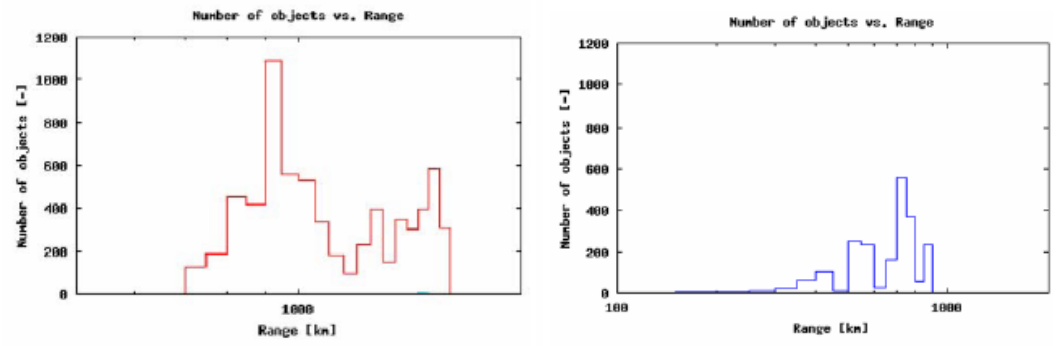

Fig. IV-36. Number of crossing objects vs. range (24 hours ESA-PROOF2005 statistic simulation) of the ground based telescope (left side) and the space based telescope (right side) (Ref. 55).

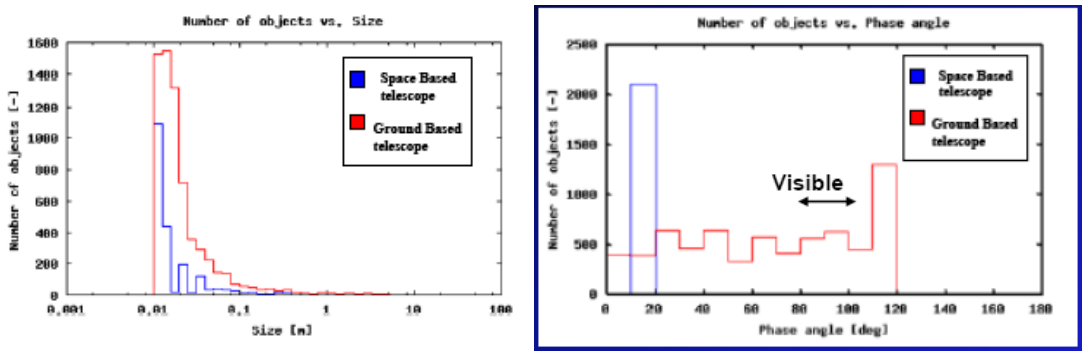

Fig. IV-37. Left side: Number of crossing objects vs. Size (24 hours ESA-PROOF2005 statistic simulation) of the ground based telescope and the space based telescope. Right side: Number of crossing objects vs Phase angle (24 hours ESA-PROOF2005 statistic simulation) of the ground based telescope and the space based telescope (Ref. 55).

It is important to emphasize that with this mission configuration the orbiting telescope monitors LEO region with an optimal illumination condition (phase angle between 10° to 20° is due to the Earth inclination and orbit inclination).

In ground case the phase angle change during the day (only in dawn and dusk it is possible to observe with a good illumination condition) (see right side of Fig. IV-37).

The left side of Fig. IV-38 shows the number of crossing objects vs. inclination: Most of these are LEO satellites and debris with semi major axes in the range 7000 and 8000 km and inclination between 60° to 100°.

Another important result is plotted in the right side of Fig. IV-38. The space based FOV is crossed by faster objects than ground based one. In fact due to high SSO orbit velocity, the relative velocity between space sensor and target increases.

So the short exposure time selected (0,01 seconds, see Tab. IV-8) improve the space telescope performance and allows to detect objects with 1 deg/s relative angular velocity. With this observation strategies these targets will be about 30 pixels trace shaped in the image. To process this kind of data a software for the on board images analysis has been already developed by GAUSS (Ref. 51 and 54).

The integration time comes from a trade off: more distance objects have a lower relative angular velocity and so an higher exposure time is needed.

In ground case the 2 seconds integration time allows to observe a 0,5 deg/s angular velocity target like a 400 pixels trailing trace in the image. The algorithms developed by GAUSS in order to process SpaDE data achieved in different observation strategy will permits to analyse these frames (Ref. 49).

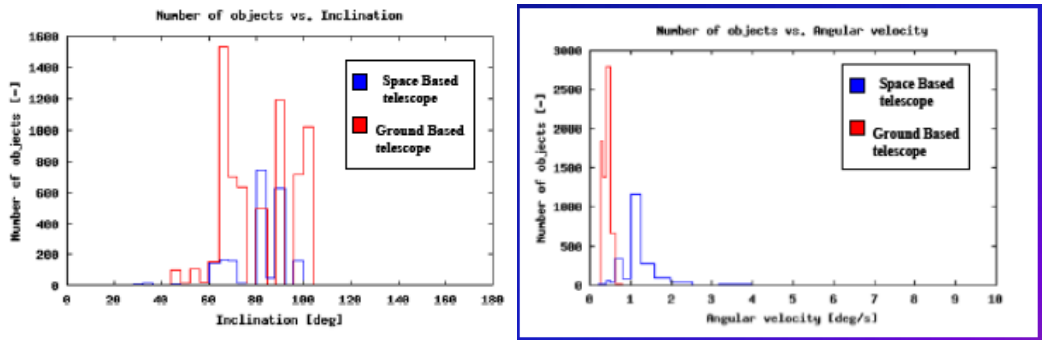

Fig. IV-38. Left side: Number of crossing objects vs. Inclination (24 hours ESA-PROOF2005 statistic simulation) of the ground based telescope and the space based telescope. Right side: Number of crossing objects vs. Angular velocity (24 hours ESA-PROOF2005 statistic simulation) of the ground based telescope and the space based telescope (Ref. 55).

In conclusion of this section, the in-situ observation advantages have been investigated . With a LEO orbiting optical system it is possible to have a better resolution and to observe smaller objects (LEO objects) in better illumination condition. For this reason GAUSS plans to board a optical payload on a university microsatellite formation flying (2 UNISAT class satellites) to carry on space debris observations.

IV.3.3 The selected mission

Recently I have been able to coordinate a joint activity between GAUSS and the Department of Physics of the University "Sapienza" of Rome. The results of this

cooperation is the development of the optical payload to be boarded in the next UNISAT 5 microsatellite (Ref. 59). Moreover, due to the recent interest in the development of CUBESAT standard technologies, the proposed payload has been also designed for triple cubesat (3U) dimension.

IV.3.3.1Mission objective

Due to the recent interest in the LEO orbit monitoring (as a conseguence of ASAT-test of 2007) and the real advantages of a LEO microsatellite formation flying observing LEO debris (see section IV.3.2), the mission objective selected is OPTION2: to monitor the higher density orbit (results of this event) at about 900 km altitude, allowing in orbit objects detection and orbit determination.

IV.3.3.2 Mission configuration

A two satellites in a LEO formation flying boarding the same optical system as been selected to allow the detection and orbit determination of space debris at 900 km altitude (on the basis of the 2008 GAUSS study in Ref. 54). During the last two years, the mission configuration and the main satellite subsystems features has been also selected. The main mission configuration features are shown:

- Orbit altitude H = 800 km
- Dawn-dusk Sun Synchronous Orbit and sun light telescope pointing in order to obtain a phase angle close to zero during the whole orbital period.
- Two satellites close in the orbit (d = 100km) with the same Local Time at Ascending Node (LTAN = 6.00).
- Observation range W = 100 – 200 km

In Fig. IV-39 the formation flying draft is shown.

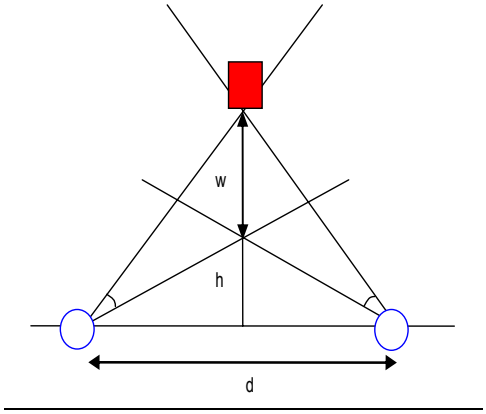

Fig. IV-39. The microsatellite formation flying draft. The square shaped figure is the orbiting object. The two point shaped figures are the microsatellites (Ref. 59).

IV.3.3.3 Observation strategy

Two different observation modes have been selected:

A. Survey mode. Both telescopes track the same celestial coordinates.
B. Urgent mode or Object Tracking mode. Both telescopes track a special interest object.

Automatic image processing software will process image exploiting the on-board computer. In survey mode, only the objects parameters (astronomical and image coordinates, magnitude value, UTC image time and the 19KB 1 bit processed image) will be sent to the GAUSS SPIV Ground Station, to avoid large scientific data downlink (see communication link design in following pages).

In urgent mode, when the space telescope follows an high interest object, the raw data will be formatted with a lossless compression method and sent to the SPIV Groung Station.

IV.4 Phase B. Optical P/L design.

In this paragraph will be shown the optical payload design phase taking into account the microsatellite constraints and the small debris detection objective (Ref. 59).

IV.4.1 Optical P/L design - Microsatellite constraints

IV.4.1.1 Optical P/L design - Burden, mass and power constraint

In order to board the optical payload a 3U Cubesat bus has been considered. This particular kind of bus can allow to have two different possibilities for the launch:

- board the payload inside Unisat5 satellite
- launch separately the 3U satellite.

The typical dimension for a 3U Cubesat are 30cm x 10cm x 10cm. The weight available to board the payload and all other subsystems components is about 3 Kg.

Different solutions has been analyzed to board the payload inside the 3U Cubesat. The configuration choose is shown in Fig. IV-40.

A cube of 10x10x10cm is used to board the battery package, the radios, the On Board Computer the ADCS, in order to have a 2U Cubesat available for the optical payload.

All the structure has been designed using ERGAL - aluminium 7075. This kind of material can be used to manufacture mirrors and can be used also for the main structure. Using the same material it is possible to minimize the thermal stress during the in orbit phase and avoid not only structural problems but also image quality degradation.

The primary mirror and the secondary mirror are directly fixed to the main structure in order to minimize the weight and the burden. In particular the dimension of the primary mirror match perfectly with the 3U structure and it is possible to fix this directly on the structure only using 4 screws.

The weight of the primary mirror is about 200 gr and of the secondary is about 10 gr. The secondary mirror is fixed using 3 rods at 120 degree one each other. The total weight of the telescope is about 400 gr. The CCD Camera is (500 gr.) fixed on a plate that separate also the optical system to the other subsystems.

The power system has been realized using Lithium batteries and triple junction solar cells. A dedicated Battery Charge Regulator Board for the power

system is installed on the bottom of the satellite. The mean power available for the 3U cubesat is 3 W.

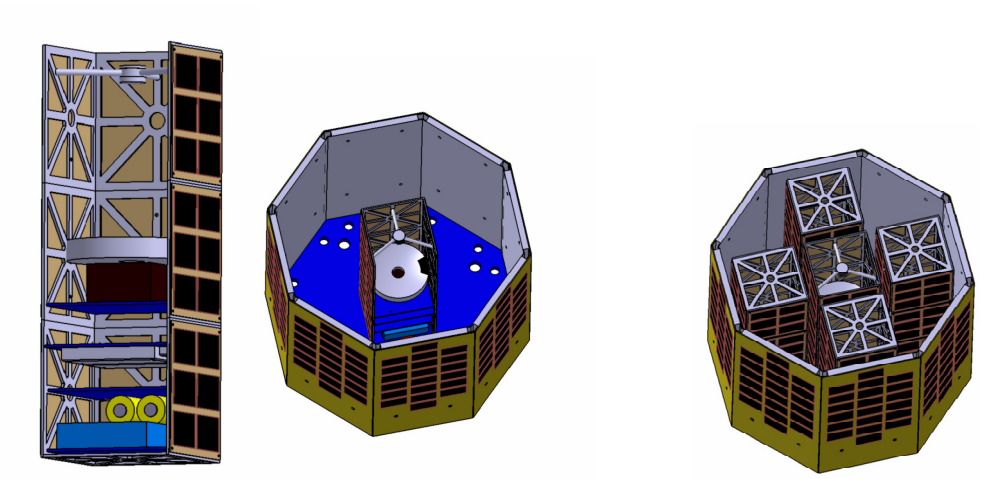

Fig. IV-40. P/L burden in the 3U Cubesat and 3U Cubesat burden in UNISAT5 (Ref. 59).

The 3U cubesat described can be boarded inside Unisat5 microsatellite. Unisat5 is fifth satellite designed and manufactured by students and researchers of GAUSS group. This satellite (UNISAT4 like) has an octagonal prism shape. Each side is 15 cm X 31 cm.

The idea is to board inside the Unisat5 different payload hosted in cubesat slot (Fig. IV-40). The central part of the satellite will be host the optical payload.
In order to reduce structural stress during the launch phase, the optical axis overlap the z axis of the satellite that is also the rocket trust axis.

IV.4.1.2 Optical P/L design - Communication, Data handling and ground station constraints

The scientific data downlink is allowed exploiting the UHF, VHF and S-Band on-board radio and GAUSS SPIV ground station. The downlink data-rates for the different bands (VHF, UHF and S) are shown in the Tab. IV-9 and are 9600bps for the VHF and UHF, 400Kbps for the S-Band. Normal TT&C operation will occur via VHF uplink command and UHF telemetry download in real time.

The Telemetry communication downlink is based on a 436,8 MHz downlink @ 9600 bps and a 145,83 MHz uplink @ 9600 bps, exploiting SPIV Yagi antennas.

The P/L data downlink will be performed exploiting SPIV S-band 3.8 meter parabola.

	UHF	VHF	S - Band
Mode	Telemetry	Telemetry	P/L data
Downlink Frequencies	436.8 MHz	145.850 MHz	2.3 GHz
Data Rate	9600 bps	9600 bps	400 Kbps

Tab. IV-9. Communication downlink capabilities (Ref. 59).

The raw image is a 2Kx2K 16 bit image (8 MB image shown in Tab. IV-10). Exploiting the GAUSS image processing software (Ref. 49, 51 and 54) it is possible to on-board process the images. After the object detection and identification steps, the result image is a 1 bit (19 KB size) image. However in the object tracking mode observation strategy, the raw image have to be sent to the ground station and a compression method is needed.

The Command and Data Handling (C&DH) subsystem will be used to manage all forms of data on the spacecraft, including both commands and telemetry. The spacecraft time will be used to initiate stored commands or scientific data in the Solid State Recorder (SSR). The SSR is the primary location to store instrument data onboard the spacecraft.

	Image size [MB]	Data tx. Time [sec]	% Pass. [%]
Raw Image	8,1990	163,9800	34,1625
Binning 2x2	2,0498	40,9960	8,5408
Binning 4x4	0,5124	10,2480	2,1350
JPEG-LS 3.81:1	2,1520	43,0400	8,9667
Post Procesing Image (1 bit)	0,019	0,3800	0,0792

Tab. IV-10. Image size with different image compression methods. Data downlink time and passage percentage (average passage 8 min) for each image size (Ref. 59).

There are two partitions in the SSR. One for raw data storage and one for processed data storage. Once the data is in the raw data storage partition in the SSR, it will be edited and formatted by the flight computer with a lossless compression method (method used in Ref. 60).

Two standard compression schemes have been considered (Ref. 61) to achieve state of the art performance: JPEG-LS (ISO/IEC 14495-1) and JPEG 2000

(ISO/IEC CD15444-1). Both JPEG-LS and JPEG 2000 performs equally well (3.81:1). JPEG-LS has been selected, because is simple, easy to implement, consumes less memory, and is faster than JPEG 2000 (though JPEG 2000 supports losses and progressive transmission).

The image size with different image compression method are shown in Tab. IV-10. There are also shown the data downlink time and the passage percentage (average passage 8 minutes) for each image size.

IV.4.2 Optical P/L design - Requirements and design drivers

For the P/L design phase, the following requirements and design drivers have been taken into account:

- Optical system burden (including CCD): 10x10x20 cm box.
- Telescope diameter D <= 10cm.
- Optical system optimization for visible spectrum. The wavelength design value is λ = 550 nm.
- Large Field Of View (FOV).
- Image pixels number Npixel <= 2Kx2K to avoid large image size (see communication link constraint).
- In axis optics to match the 3U burden.
- In axis two mirror optical system to allow low cost, manufacturing phase simplicity, high thermal and structural stress strength during the launch and the in orbit phase.
- Optimal image resolution condition.

IV.4.3 Optical system configurations trade-off

Pixel scale value equal to the Full Width at Half Maximum (FWHM) have been considered, sampling the Airy Disk with 2 pixels. Pixel scale < FWHM (sampling the Airy Disk with more than 2 pixels) are not considered in order to satisfy large FOV and limited image pixels number requirements. However, to obtain a larger FOV with the limited pixel number, a shorter focal length study case will be analysed. In this case a 3° FOV as been selected (the larger IADC FOV value) taking

into account the losses in sensitivity and object coordinates determination. In this solution the resolution will decrease 4 time the longer configuration one (Pixel scale > FWHM). The possibility to defocus the image will be also take into account to optimize positioning precision and sensitivity. In Fig. IV-41 the object position determination error in Pixel scale = 2*FWHM case and in the Pixel scale = 6*FWHM case.

Considering the trade-off analysis, the long focal length study case allows as to obtain the optimal resolution condition. The short configuration study case allows as to track faster objects or to increase exposure time.

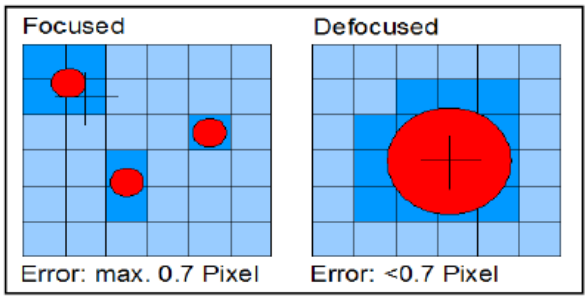

Fig. IV-41. Position evaluation error (Ref. 62).

IV.4.3.1 Long focal length study case

In order to satisfy the optimal resolution requirements, first the Airy Disk semi angle has been calculated: $\theta = 1.3840$ arcseconds. Then sampling the Airy Disk with 2 pixels the pixel FOV results 1.3840 arcsec and the FOV = 0.7874° (Number of pixel = 2048).

Starting from the selected image pixels number and with the aim to select the pixel size, Fig. IV-42 shows the sensor size with respect to different pixel size. The points in the curve highlight Commercial Off-the-Shelf (COTS) CCD pixel size (5.8µm, 9 µm, 15 µm and 24 µm).

Due to the P/L burden requirement, the sensor size threshold is 20 mm (the square shaped flag for the sensor size allowed and circle shaped flag for the sensor size not allowed). This results is the same for the long and the short optical configuration.

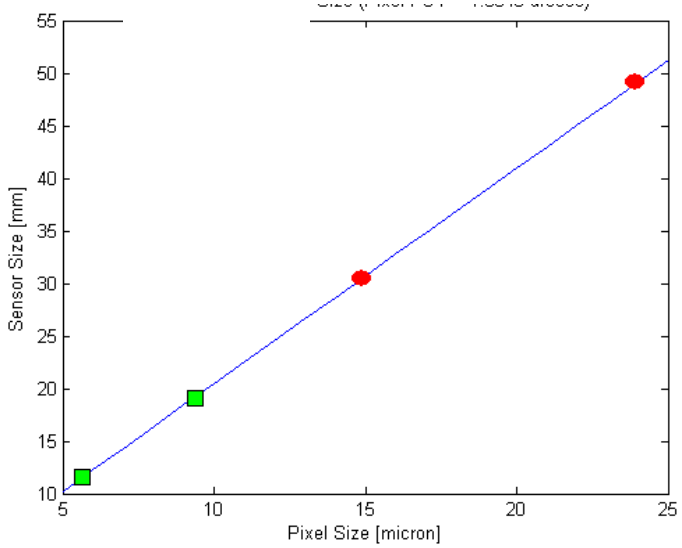

Fig. IV-42. SensorSize vs. PixelSize (Ref. 59).

Talking about the long optical configuration, to identify the focal length value, in Fig. IV-43 is shown the Focal Length vs. Pixel Size trend. Large focal lengths in compact optical configurations produce large off-axis aberrations, because of the small secondary mirror curvature radius and the increasing ratio between primary mirror and secondary mirror focal lengths (see Ref. 58). Moreover we have small luminosity for large f/#. So increasing the focal length means an increasing of the f/# and consequently a reduction of the luminosity.

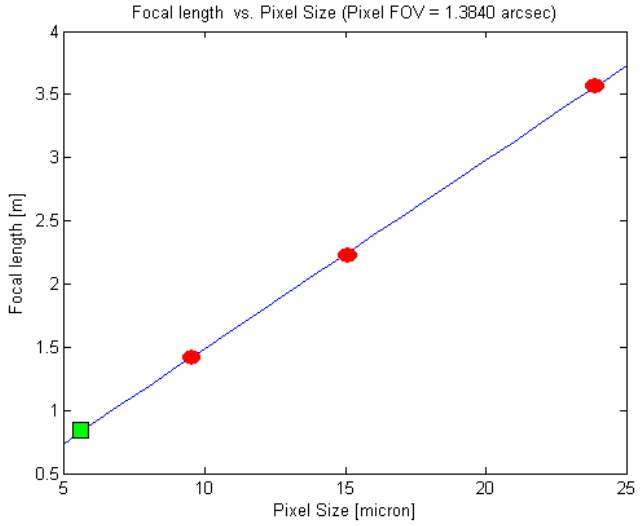

Fig. IV-43. Focal Length vs. Pixel Size. Long focal length configuration (Ref. 59).

For these reasons (sensor size and focal length evaluation) in the long configuration study case the selected pixel size is 5.8μm.

IV.4.3.2 Short configuration study case

The FOV selected is 3° and the pixels number is 2048 (2Kx2K image), obtaining a pixel FOV = 5.2734 arcsec. Fig. IV-44 shows the Focal Length vs. Pixel Size trend in the short focal length configuration case.

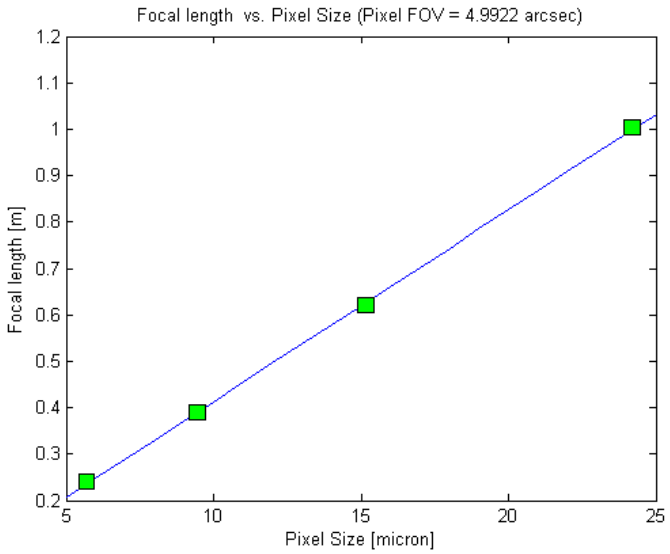

Fig. IV-44. Focal Length vs. Pixel Size. Short focal length optical configuration (Ref. 59).

If Pixel Size = 5,8 micron, Focal Length = 0.2215 m and f/# = 2.215. In the case of Pixel Size = 9 micron, Focal Length = 0.3438 m and f/# = 3.438. The 9 micron short focal length configuration has been selected to minimize off-axis aberration with respect to the 5.8 micron pixel size.

IV.4.3.3 Optical system optimization

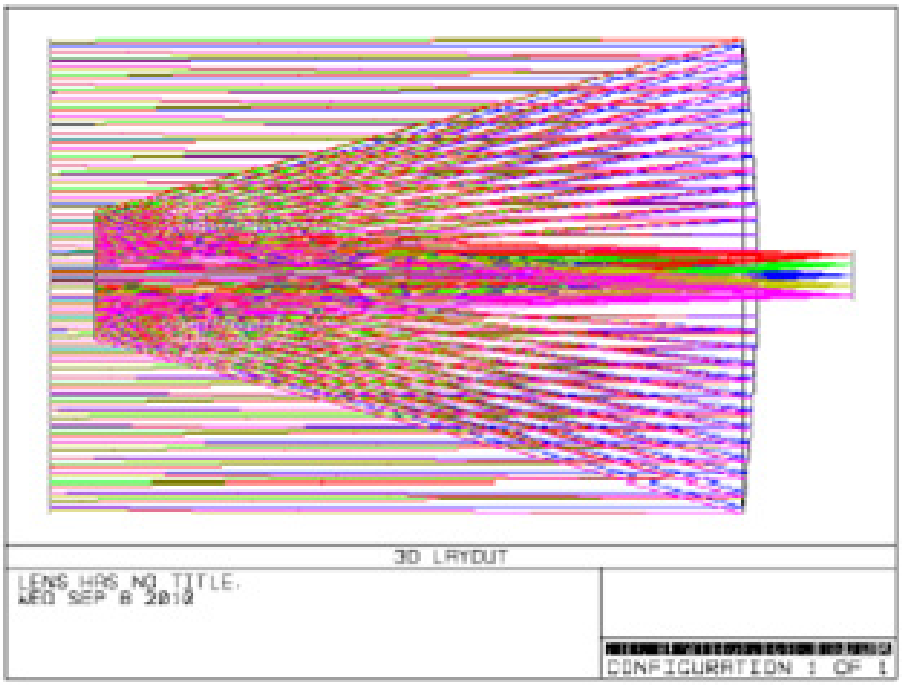

Fig. IV-45. 3D layout. Long optical configuration (Ref. 59).

The 3D layout and the spot diagram of the long configuration is shown in Fig. IV-45 and Fig. IV-46, exploiting ZEMAX dedicated software. The optical configuration has been optimized exploiting the ZEMAX optimization tool and the Ritchey-Chrétien solution has been selected. In the optimization procedures, the design values referred to the mission and satellite requirements have been fixed (primary mirror diameter, sensor size, the distance between the two mirrors and the distance between the secondary mirror and the focal plane).

In particular in Fig. IV-46 the 5 fields spot diagram (0°, +/- 0.2°, +/- 0.4°) are shown and the image at focal plane is compared with the Airy Disk dimension.

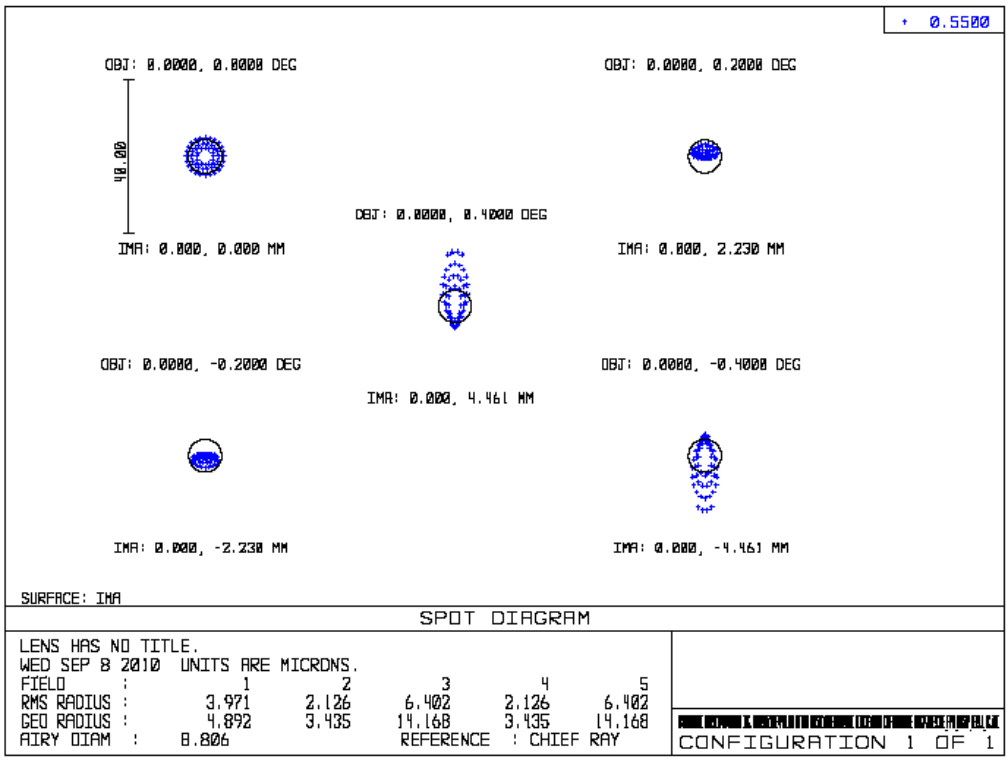

Fig. IV-46. Spot diagram. Long optical configuration (Ref. 59).

The main optical features of the optimized long focal length configuration are summarized as follows:

- Ritchey-Chrétien solution
- FOV = 0.8°
- Pixel size = 5.8 micron (2kx2k image)
- Primary mirror diameter D1 = 94mm
- Secondary Mirror Diameter D2 = 26mm
- Entrance Pupil Diameter D_{ep} = 94mm
- Image Diameter D_{imm} = 10mm
- d12 = 140mm
- d2,imm = 160mm
- feff = 0.6 m
- Pixel FOV (with 2k x 2k image) = 1.3840 arcsec
- Pixel resolution (@ 100km) = 0.671m

and the f/# could be calculated as follow:

$$f/\# = \frac{f_{eff}}{D_{ep}} = 6.4$$

Talking about the short configuration case, in terms of performance requirements, the two mirror reflecting telescope cannot be optimized for a 3° FOV with the short focal length, and the result are large off-axis aberrations. A better solution can be found by using commercial objectives or catadioptric systems. This choice, however, raises structural questions: thermal, barometrical and structural tests have to be dealt with, in order to check if the instrument is suitable for orbit conditions.

IV.4.3.4 Optical system focusing

As discussed in Ref. 57 and shown in Fig. IV-47, the smaller your focal ratio, the shorter the zone of critical focus is. For the purposes of focusing, a small focal ratio is f/5 or lower; a large focal ratio is greater than f/8. Scopes with a short focal ratio will be more challenging to focus, and scopes with long focal ratios will be a little more forgiving.

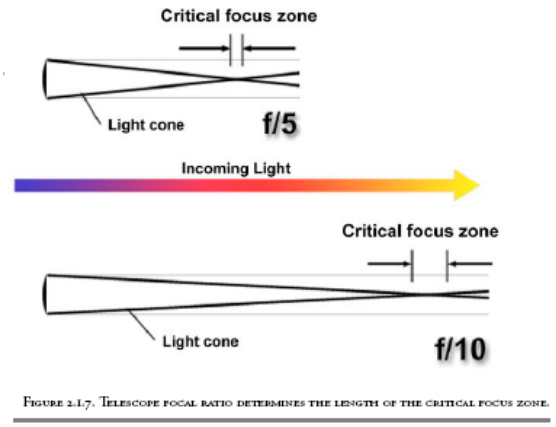

Fig. IV-47. Critical focus zone for different f/# optical systems.

The equation below computes the size of the critical focus zone (CFZ) in microns for a "perfect" optical system that is perfectly collimated:

$$CFZ = f/\#^2 \times 2.2$$

where f/# is the focal ratio.

Than CFZ for both short optical configuration (CFZ1) and long optical configuration (CFZ2) have been calculated:

CFZ1 = 26.0037 microns

CFZ2 = 122.1711 microns

So large focal length configuration allows also an higher focusing tolerance.

Moreover, in order to analyse in dept the focusing problem, we have to take into account the possible imaging differences between the various detected objects. The study deals with the defocus effect occurred observing objects located at different distances. In order to minimize the complexity of the discussed optical payload, we need to fix the focal plane in the optical configuration. With simple calculations we can quantify the defocus by starting from the spherical mirror equation:

$$\frac{1}{q} = \frac{1}{p} + \frac{1}{f} = \frac{f+p}{fp}$$

The quantity we want to estimate is the difference between the image position on the optical axe q and the focal distance f. By expressing the defocus in terms of the object distance p, we have

$$\delta = q - f = \frac{f^2}{f+p}$$

The plot in Fig. IV-48 shows the defocus versus the object distance, for the two different optical configuration discussed. In particular the red points refer to the small FOV case and a sensor of 2048 pixels, the light blue points represent the same case but consider a sensor of 4096 pixels, while the dark blue points refer to the larger FOV case, with a sensor dimension of 2048 pixels.

It is clear that the defocus vanishes at large object distances: for distances up to 100 km, the defocus is lower than 1micron. However, this estimation have to be accounted for when we are dealing with object distances ranging between 10 and 100 km.

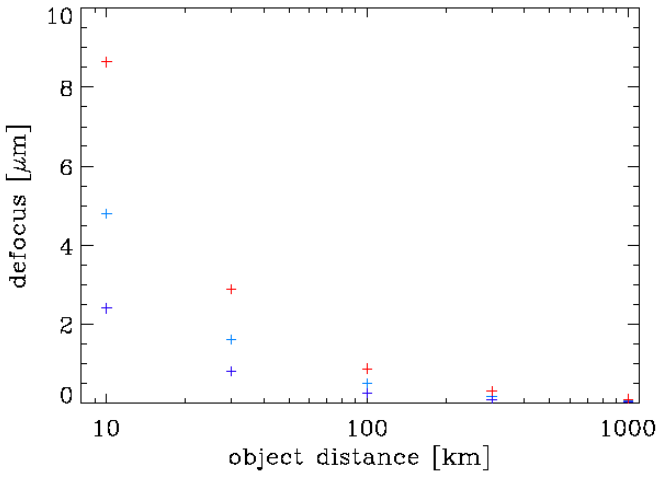

Fig. IV-48. Defocus effect vs. object distance (Ref. 59).

IV.4.4 On board image processing

In 2006, in the framework of the realization of the First Italian Observatory fully dedicated to space debris monitoring (Ref. 49), a software for the automatic image processing has been designed, developed and tested by GAUSS. It consist of four main procedures (Fig. IV-49):

A. Noise reducing.
B. Star background removing.
C. Objects detection
D. Objects identification procedure.

GAUSS usually adopt different observation strategy: Sidereal Tracking mode (STM) allows to observe star point shaped and orbiting object trace shaped. Object Tracking Modes (OTM1 and OTM2) allows to observe Geostationary Earth Orbit (GEO) objects point shaped.

In 2008, GAUSS was able also to test the algorithm with the observation strategies proposed in the case of an orbiting telescopes, changing the Star background removing steps (Ref. 51 and 54).

In particular, when we use the object tracking mode observation strategy and we are tracking an high interest object, it is also possible to select different exposure time belonged to different satellite-object relative angular velocity.

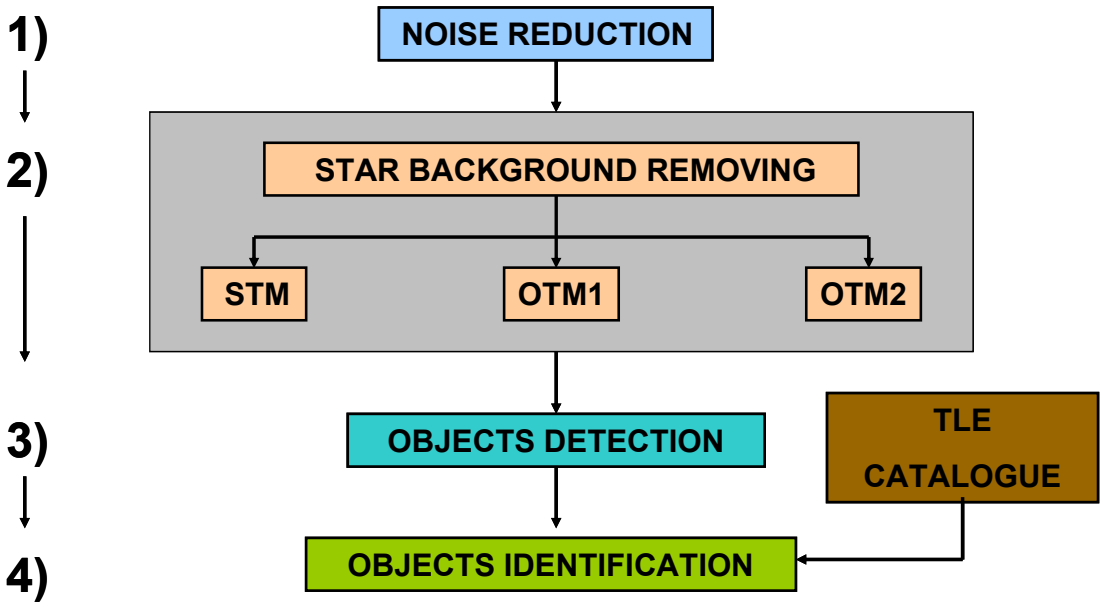

Fig. IV-49. On board image processing architecture (Ref. 59).

Following the results in Fig. IV-38 (right side) the worst case relative angular velocity is $\omega_1 = 2$ °/sec. In this case the optimal exposure time is 0.02 seconds to obtain a 104 pixels trace. In this observation mode the stars results point shaped and the image star background removing procedure is STM like (Ref. 49).

On the contrary, if the object have lower relative angular velocity, we can increase exposure time to obtain a comparable object length (see Tab. IV-11). In particular, in the best case, when the object relative velocity is 0,5 °/sec, the optimal exposure time is 0.1 seconds

Pixel FOV [arcsec]	ω [°/sec]	EXPTIME [sec]	Object length [pixels]
1,384	2	0,02	104,0462
1,384	0,5	0,1	130,0578
5,2734	2	0,02	27,3069
5,2734	0,5	0,1	34,1335

Tab. IV-11. Exposure time and relative object length in both optical configuration selected, considering faster object case and slower (Ref. 59).

IV.5 Phase C-D. Optical P/L manufacturing

In this chapter a low cost manufacturing and test technique is proposed. With this method the microsatellite optical payload construction is possible exploiting university facilities and founds.

IV.5.5 Optical P/L manufacturing

The trade-off of cost minimization, required by the optical payload project discussed in this chapter, can be achieved by reducing at first the manufacturing procedures.

Facilities available at the Department of Physics of the University "Sapienza" of Rome will be used to machine the mirrors.

However optical surfaces require further treatment to reduce surface roughness, due to the processing mill, in order to be optimal for the purpose of the mission. It is then performed by treating the mirror surface with abrasive paste containing granules of different size. In particular we employ four different pasta with grains size of 15μm, 9 μm, 3 μm and 1 μm.

The mirror requires a preliminary cleaning, consisting in immersing it in an ultrasonic bath of alcohol, drying it with compressed air and subsequently by applying the abrasive pasta, from the 15μm up to the one 1μm (in descending order of size of granulation). Between treatments with two different pasta we repeated the cleaning operation of the mirror to remove debris from the surface of the dough barely used. The entire process of an optical surface, i.e. the application of all the abrasive paste up to the 1μm, was done by hand and required a time of about an hour (the mechanical mirror treatment is usually employed to large surfaces).

As the mirrors were processed, we acquire the intensity profile of a laser reflection (for each processing degree we take data in five different places) to check the goodness of treatment. It is important to note that the application of a paste with the granulation of a certain size is useless if the treatment with pasta of large granulation has not been successful, i.e. to eliminate the roughness on spatial scales corresponding to the size of that granulation. In this case it is necessary to repeat the application of that dough. The roughness data presented here are related to final machining of mirrors.

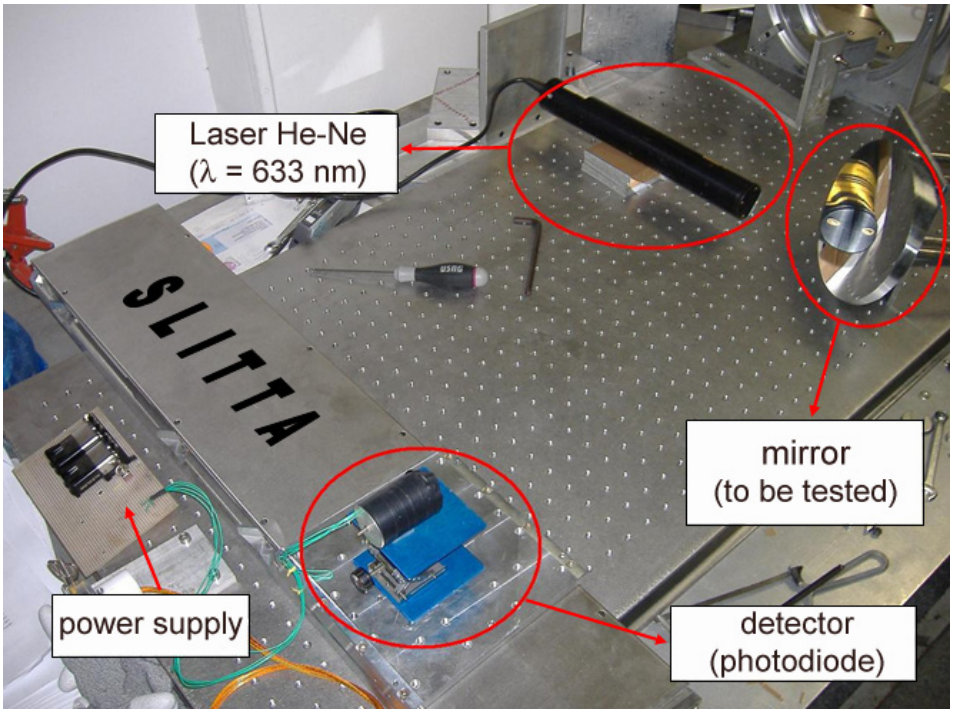

Fig. IV-50. Optical desk in the test configuration (Ref. 59).

Measurements are based on the optical method, which consists in studying the intensity of reflected light from the mirror as a function of displacement of the photodiode from the centre (Fig. IV-50), i.e. the position corresponding to maximum intensity. We used an He-Ne laser with wavelength of 633nm.

The mirror was positioned so that the incidence and reflection angles of the laser beam were equal to 45 degrees. The photodiode, located on a step motor controlled by a software (Labview), scan the intensity of reflected laser moving, along the *x* direction, at a speed of 1 mm/s, making a total distance of 80 mm. The distance between the mirror and photodiode was d = 795 ± 5 mm.

The photodiode, connected to a 18 Volt cc power supply was connected to an analog to digital converter interfaced to software that allows a direct check of the intensity received on the diode as a function of time.

For data analysis we used the discussion presented in Ref. 63. There are two classes of roughness surface:

A - periodic roughness, due to signs of the machine that produces the typical diffraction pattern;

B - random roughness (one-dimensional and two-dimensional), which leads to a light diffusion, defining the continuous component of the diffraction pattern.

In this work we only estimated the random roughness, since it is the type of roughness that characterizes most relevant areas of the mirrors after working with abrasive paste. The parameter that allows to estimate this type of roughness is given by:

$$\mathrm{TIS} = (2k\sigma_1)^2 = 4\sqrt{2}k^3 \int W(\xi)\cos\xi d\xi \quad \ldots..[1]$$

$$\mathrm{W}(\xi) = \frac{k^{-3}}{\sqrt{2}} \frac{R(45°)}{Q(\xi)} \frac{(1+\tan\xi)^{-1}}{\cos\xi\cos 2\xi} \frac{I_s(\xi)}{I_r} \frac{1}{\Delta l}$$

where the term "TIS" stands for "total integrated scatter". The quantity *W(ξ)* is a function of the deviation of surface profile from its mean, and for this reason it is a measure of surface roughness. We consider $\xi = arctan(x/d)$. The other quantities in the relations are:

$$\mathrm{k} = 2\pi/\lambda ,$$

where λ is the radiation wavelength,

$$\Delta\mathrm{l} = 2\sqrt{\mathrm{A}}/\sqrt{\pi}d ,$$

where *A* is the detector area, *R(θ)* is the intensity reflection coefficient and *Q* depends on the material. I_s and I_r represent respectively the diffuse intensity and the maximum intensity (which corresponds to $\xi = 0°$).

The intensity profiles obtained are normalized to maximum intensity and centred so that the maximum intensity corresponds to the central position of the step motor. In this way we are able to compare the different spectra with each other. Inverting equation [1] we then obtained roughness σ_l (see Tab. IV-12).

	Raw	$15\mu m$	$9\mu m$	$3\mu m$	$1\mu m$
#1	7.82 ± 0.73	5.32 ± 0.54	3.95 ± 0.18	0.485 ± 0.062	0.115 ± 0.015
#2	7.55 ± 0.77	5.43 ± 0.59	3.24 ± 0.13	0.454 ± 0.066	0.121 ± 0.017
#3	7.12 ± 0.71	5.39 ± 0.51	3.12 ± 0.15	0.419 ± 0.063	0.118 ± 0.013
#4	6.94 ± 0.75	5.32 ± 0.49	2.81 ± 0.13	0.393 ± 0.060	0.108 ± 0.011
#5	7.03 ± 0.70	5.35 ± 0.47	3.01 ± 0.11	0.401 ± 0.059	0.102 ± 0.010

Tab. IV-12. Roughness (σ_l) in microns for the five test measurements. The values of the first row refer to the paste granulation. The five measurements taken in different positions on the mirror (Ref. 59).

It is clear that the average roughness decreases from the 15 μm to 1 μm working. We present graphs for different diffuse intensity processing and before processing.

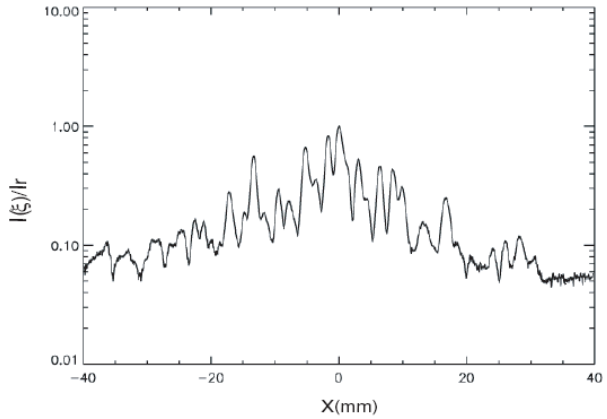

Fig. IV-51. Spectrum of the light reflected from raw mirror. The peaks correspond to the typical diffraction pattern due to the periodic roughness (Ref. 59).

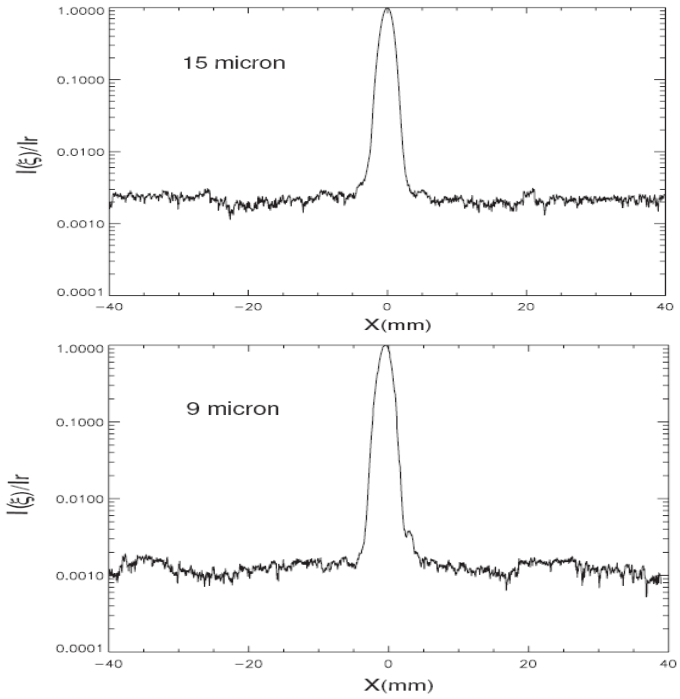

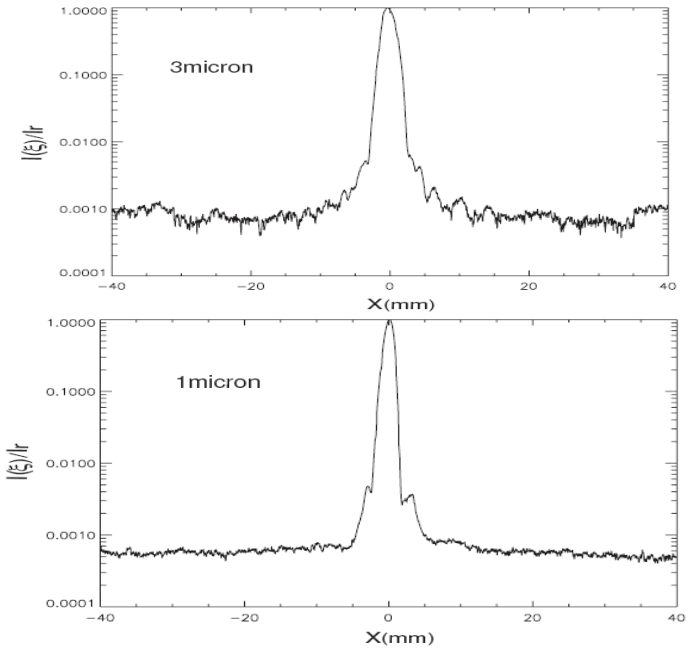

Fig. IV-52. Spectrum of the light reflected from the mirror after the different steps of the roughness reduction procedure. The continuous pattern is caused by the random roughness (Ref. 59).

As it is evident from the graphs, the spectrum of the raw mirror has many peaks due to diffraction. This is due significantly to the presence of the periodic component of roughness, eliminated with abrasive paste. Moreover, the figures show that between the various processes, the diffusion of light becomes less relevant, as can be seen from the greater light intensity with respect to the intensity of continuous. This was precisely due to the decrease of roughness, confirmed also by the average values of the parameter σ_I in Tab. IV-12.

Capitolo V
Conclusions

University microsatellite projects are an excellent way to educate and motivate students in all aspect of spacecraft engineering.

ESA standards give useful instruments to faster approach space systems design problems. This work have demonstrated the applicability of ESA standards to EduSAT mission. These standard have been applied, providing important support during the mission management and the satellite technologies development.

Due to the unexpected on-orbit success rate, university microsatellite programs have to see in close feature an increasing trend of real payload and not "modest" missions design. For this reason a very cost/effective payload for next UNISAT-class microsatellites have been proposed.

Review of Key Results

This thesis provides the following results and conclusions:

1. **ESA standards are applicable on university-class microsatellites**

   ESA standards are widely used in worldwide projects. For this reason they have to be considered and implemented in a university space program. The ESA ECSS standards applicability on EduSAT microsatellites program has been extensively demonstrated. In particular the ESA ECSS-M standards belonged to the Management branch are mandatory because provide excellent mission planning and phasing instruments. They also provide valuable risk assessment and management methods. The ESA ECSS-E belonged to the Engineering branch

have to be considered as reference document where it is possible to find useful suggestion for all space systems designers.

Through the SEO mission experience, the ESA CDF method has been analysed. This method provides a collaborative, co-operative, collective and simultaneous engineering working environment approach that overcome the communication gaps between the designers, and must be implemented in university-class microsatellites projects. CDF gives the opportunity to carry out pre-Phase A study in few week (usually 8 days), estimating also the mission costs. Moreover the CDF data archiving and sharing system is a reliable method to fast approach new missions design.

2. The ESA ECSS MDD has been used to describe EduSAT design technologies and methods

The technologies and methods used to design, manufacture, launch and operate in orbit EduSAT microsatellite have been shown in this thesis, exploiting the ESA ECSS Mission Description Document form.

3. A cost/effective microsatellite optical payload for space debris monitoring has been designed

It has been realized that the last twenty years have seen university-class microsatellites that seldom if ever have boarded "relevant" payloads, focusing their efforts on a functional but "modest" spacecraft. The suggestion for future university-class microsatellites is: *try to board "real" payload to tackle research problems that are not addressed in industry*. For this reason a university microsatellite optical payload for space debris monitoring has been designed, following ESA ECSS mission phasing methods and exploiting ESA standard tools as ESA PROOF-2005. The optical payload for space debris monitoring has been identified as a cost/effective payload for next UNISAT-class microsatellites. In particular the design phase has been shown, starting from the conceptual design (Phase 0-A) to the design definition (Phase B), and taking into account university microsatellite constraints. Moreover a low cost payload manufacturing and testing method has been identified for the phase C/D.

Capitolo VI
Appendix I - University microsatellites classification

Since the advent of modern technologies, microsatellites have been largely enrolled in space industry and research application because they offer an opportunity for countries with a modest research budget and little or no experience in space technology, to enter the field of spacecraft development and launch.

Moreover, low mass spacecraft results in a mission cost affordable by research institutes. For this reason the past twenty years have seen the increasing trend in university microsatellites design.

University-class spacecraft

As described in Ref. 36, "University-class missions are those students-build satellites where student training plays at least as important a role as the orbiting mission". Up to 31 December 2006, 60 "university-class" spacecrafts have been launched, and only 16 failed prematurely, highlighting an unexpected on-orbit success rate.

Objectives of a university-class mission

The objectives of a university-class mission are:

- Train students in the design, integration and operation of spacecraft, by giving students direct control over the process of the program.
- Develop cost effective platform for conducting space science missions.

- Demonstrate the feasibility of utilizing micro/nano commercially-off-the-shelf (COTS) parts to construct a reliable, short mission micro-satellite.

Design guidelines and suggestions

In the study mentioned in Ref. 36, an interesting analysis of university-class satellite characteristics is presented, underlining five main design guidelines:

- ***Small spacecrafts***. Launch cost is proportional to satellite mass (about 40 Keuro per kilo). Moreover a smaller spacecraft improves mission reliability: fewer parts and fewer interface reduce complexity, and smaller frame increase natural frequencies thus fitting launcher requirements for flight safety.
- ***Common interface***. Trough the use of common interface costs can significantly decrease and reliability significantly increase (i.e. the P-POD launcher for CubeSats).
- ***Very short duration mission***. Choosing a mission that can be accomplished in short duration (months and not years), from the design to the launch and operation, has two benefits: use of low cost/mass and Commercial Off-the-Shelf (COTS) components, that lead to an high-risk spacecrafts but have extensively demonstrated in-orbit survival in the short period (i.e. the Stanford University QuakeSat, launched on June 30th, 2003 and "Sapienza" University UNISAT3 launched in July2004); fit with university students lifetime.
- ***Large operational margin***. These are student-build spacecrafts, and for this reason design and fabrication errors may exist. It is important to mitigate the effects of these errors by building spacecraft with significant margin in mass, power, computation, pointing and communications. So it is recommendable to avoid mission that require state-of-the art performance (i.e. not in attempting to perform 3-axis, arcminute-level pointing control on a 10 kg spacecraft).
- ***Rigorous system-level functional and environmental testing***. Vacuum and thermal cycles testing identify discrepancies between manufacturer specifications and real behavior of key components. For this reason it is

necessary to plan an extensive test campaign (especially in power and communications subsystems). This is also an important instrument from educational point of view, because students may understand and solve design process errors.

Important suggestions that came from the statistical results investigated in the research work aforementioned are:

- Pay more attention in power and communication design than in structural or thermal design, especially at the level of system integration and functional testing.
- Try to attempt "real", relevant payloads, to tackle research problems that are not being addressed in industry.

Small satellite classification

An important study have been conducted in recent years to understand what exactly is a small satellite, and the sub-classification that characterize this branch of spacecrafts (Ref. 37). Confusion of small satellite definitions is clearly visible in Table 1.

ESA:	Small	350 kg – 700 kg
	Mini	80 kg – 350 kg
	Micro	50 kg – 80 kg
EADS Astrium:	miniXL	1000 kg – 1300 kg
	Mini	400 kg – 700 kg
	Micro	100 kg – 200 kg
CNES:	Mini	500 kg + P/L (Proteus)
	Micro	120 kg + P/L (Myriade)

Table 1. Confusion of small satellite definitions (Ref. 37).

To end this confusion, International Academy of Astronautics (IAA) proposed a simplified definition depicted in Table 2.

• mini satellites	< 1000 kg
• micro satellites	< 100 kg
• nano satellites	< 10 kg
• pico satellites	< 1 kg

Table 2. Small Satellite definition of IAA (Ref. 37).

However Figure 1 gives additional features which are essential when discussing small satellite characteristics like cost and response time.

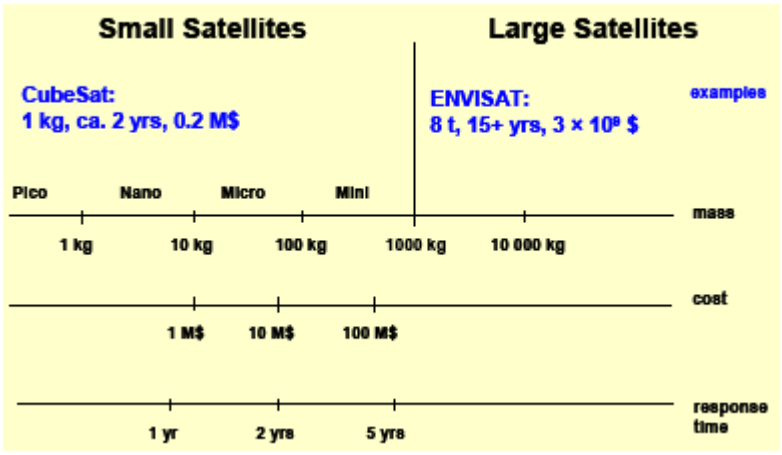

Figure 1. Some features of small satellites (Ref. 37).

References

1. "Satellite Didattico EduSAT", Contract ASI N. 1/051/07/0, December 2007.
2. ECSS-S Description, implementation and general requirement, ECSS-S-ST-00C(31July2008), http://www.ecss.nl/
3. "Project planning and implementation", ECSS-M-ST-10C Rev. 1 - 6 March 2009), http://www.ecss.nl/
4. Cost and schedule management, ECSS-M-ST-60C (31 July 2008), http://www.ecss.nl/
5. Risk management, ECSS-M-00-03A, http://www.ecss.nl/
6. Photovoltaic assemblies and components, ECSS-E-ST-20-08C (31July2008), http://www.ecss.nl/
7. ECSS-Q-70-01B Draft 1 (16 April 2008), http://www.ecss.nl/
8. Space environment, ECSS-E-ST-10-04C, http://www.ecss.nl/
9. Oswald, M., Stabroth, S., Wiedemann, C., Klinkrad, H., Vörsmann, P, MASTER-2005 - The Debris Risk Assessment Tool for the Space Industry, paper AIAA-2006-7219, AIAA Space 2006 Conference, San Jose, CA, USA, 2006.
10. Hernandez de la Torre C., F. P. Caballero, N. Sanchez Ortiz, H. Sdunnus, H. Klinkrad, "DISCOS Database and Web Interface, Proceedings of the Third European Conference on Space Debris, ESOC, Darmstadt, ESA SP-473, 19-21 March 2001.
11. Marconi A., Istituto Superiore di Sanità, Ann. Ist. Super Sanità publication, 2003.
12. FAA AC431-35-1
13. REXUS/BEXUS BUGS - Student Experiment Documentation (SED). Type: CDR, ID: RXBX-09-08-05 SED_BUGSTEAM_vers_5. M. Battagliere, J. Piattoni, C. Capelletti, F. Paolillo, E. Paolini, M. Meschini.
14. http://www.esa.int/esaMI/CDF/
15. *First Studies of ASI Concurrent Engineering Facility (CEF)*, SECESA 2010 13-15 October 2010, M. L. Battagliere, G. Casonato, M. Crisconio, C. Del

Vecchio, E. Duca, C. Facchinetti , F. Paolillo, R. C. Pellegrini, S. Pirrotta, M. Porfilio, C. Portelli, M. Salatti, G. Valentini.

16. ASI CEF Study Report, SEO (SYSTEM FOR EARTH OBSERVATION), July 2010, performed in the ESTEC Concurrent Design Facility (CDF), M. Bandecchi, C. Portelli, G. Valentini, G. Casonato, C. Del Vecchio Blanco, S. Pirrotta, S. Rabbia, G. Belvedere, R. Carmine Pellegrini, M. Crisconio, F. Paolillo, M. Battagliere, C. Facchinetti, M. Porfilio, M. Salatti.
17. Space Mission Analysis and Design 3rd ed - W. Larson, J. Wertz (Kluwer, 1999)
18. ESA TRACKING STATIONS (ESTRACK) FACILITIES MANUAL (EFM)
19. F. Graziani, M. Ferrante, G. B. Palmerini, F. Santoni, P. Tortora, UNISAT Program, a University Tool for Spave Education, paper IAF-P.2.07, 51st International Astronautical Congress, 2-6 Oct 2000, Rio de Janeiro, Brasil.
20. F. Santoni, F. Piergentili, F. Bulgarelli, F. Graziani, "The UNISAT program: lessons learned and achieved results", 57th IAC, International Astronautical Congress 2006, Valencia, Spagna, Ottobre 2006, IAC-06-E1.1.10
21. F. Santoni, F. Piergentili, "Analysis of the UNISAT-3 Solar Arrays In-Orbit Performance", Journal of Spacecraft and Rockets, Vol. 45, No 1, Jan-Feb 2008.
22. F. Paolillo, L. Ridolfi, E. Pifferi, F. Guarducci, C. Cappelletti, S. Battistini, P. Teofilatto, F. Graziani, *Space Debris and close approaches to UNISAT 3 microsatellite*, 5th International Workshop and Advanced School "Spaceflight Dynamics and Control" University of Beira Interior, Covilhã, Portugal, March 17-19, 2010.
23. F. Graziani, M. L. Battagliere, F. Piergentili, F. Santoni, "*UNISAT-5, UNICubeSAT and EduSAT: three Italian projects in hands-on education"*, International Workshop on Small Satellites, New Missions and New Technologies, 5-7 June 2008, Istanbul, Turkey.
24. ECSS-E, System engineering general requirements, ECSS-E-ST-10C (6 March 2009), , http://www.ecss.nl/
25. PRIMO RAPPORTO DI AVANZAMENTO: RA1; VERSIONE: ASI_RA1_V1.0, 2 SETTEMBRE 2008

26. SECONDO RAPPORTO DI AVANZAMEMNTO; VERSIONE: ASI_RA1_V2.2, 15 MAGGIO 2009
27. F. Graziani, G. Pulcrano, M. L. Battagliere, F. Piergentili, F. Santoni, G. Mascetti, "*Design of a small educational satellite for the Italian high school students: the EduSAT project*", Paper IAA-B7-0504, 4-8 May 2009, Berlin, Germany.
28. F. Graziani, F. Santoni, F. Piergentili, M. L. Battagliere, F. Paolillo, G. Mascetti, G. Pulcrano, "*The EduSAT microsatellite*", XX Congresso Nazionale AIDAA, 29 Giugno-3 Luglio 2009, Milano (in press)
29. F. Graziani, G. Pulcrano, F. Santoni, M. Perelli, M. L. Battagliere, "*EduSAT: an Italian Space Agency Outreach Program*", Paper IAC-09-E.1.3, 60° International Astronautical Congress, 12- 16 Oct. 2009, Dajeon, Korea.
30. INTERFACE CONTROL DOCUMENT, DNEPR-2010 № 1 PROJECT.
31. F. Santoni, M. Zelli, "Passive magnetic attitude stabilization of the Unisat-4 microsatellite", 57th International Astronautical Congress, Valencia, Spain, 2-6th October 2006
32. F. Santoni, F. Piergentili, "Analysis of the UNISAT- 3 Solar Arrays In-Orbit Performance", Journal of Spacecraft and Rockets, Vol. 45, No 1, Jan-Feb 2008.
33. F. Santoni, F. Piergentili "Attitude Determination using solar panel and magnetometer data", paper IAC-05-C1.2.06, 56th International Astronautica Congress, Fukuoka, Japan, 17-21 Oct. 2005.
34. M. L. Battagliere, F. Santoni, M. Yu. Ovchinnikov, F. Graziani, "Hysteresis rods in the passive magnetic stabilization system for university micro and nanosatellites", paper IAC-08-C.1.8, 59th International Astronautical Congress, October 2008, Glascow, Scozia.
35. DNEPR user's guide, ISC Kosmotras.
36. Twenty (plus) years of university-class spacecrafts: A review of what was, an understanding of what is, and a look at what should be next; Michael Swartwout; SSC06-I-3, 20th Annual AIAA/USU Conference on Small Satellites, Utah, 2006.

37. POTENTIAL FOR ADVANCEMENTS IN REMOTE SENSING USING SMALL SATELLITES, R. Sandau1, K. Brieß2, 37° ISPRS congress, Beijing 2008.
38. Dobson Space Telescope – the future of Microsat Based observation, Tom Segert, Björn Danziger, Matthias Lieder, TU-Berlin, Institut für Luft und Raumfahrt.
39. D. Schulten, G. Tyc, J. Steyn, N. Hannaford, M. Oxfort, P. Widmer, "RapidEye - The first six months in orbit," IAA-B7-1501, Proceedings of the 7th IAA Symposium on Small Satellites for Earth Observation, May 4-8, 2009, Berlin, Germany
40. Sapphire: Canada's Answer to Space-Based Surveillance of Orbital Objects, Captain Paul Maskell, Mr. Lorne Oram, AMOS congress 2008.
41. http://www.neossat.ca/mission.html
42. Feasibility of performing space surveillance tasks with a proposed space-based optical architecture. Tim Flohrer, Holger Krag, Heiner Klinkrad, Thomas Schildknecht, 38th COSPAR Scientific Assembly, Bremen, Germany, 18-25 July 2010, PEDAS1-0003-10.
43. M. Porfilio, F. Piergentili, F. Graziani, "The 2002 Italian optical observations of the geosynchronous region", Space-flight Mechanics 2003, Advances in the Astronautical Sciences, Vol. 114, pp. 1237-1252, Univet, San Diego, USA, 2003, AAS paper n. AAS 03-186.
44. M. Porfilio, F. Piergentili, F. Graziani, "First optical space debris detection campaign in Italy", Advances in Space Research, Vol. 34, n. 5, pp. 921-926, 2004
45. F. Piergentili, M. Porfilio, F. Graziani, "Optical campaign for low Earth orbit satellites orbit determination", Proceed-ings of the Fourth European Confer-ence on Space Debris, ESA SP-587, pp. 689-692, ESA Publications Division, Noordwijk, The Netherlands, 2005.
46. M. Porfilio, F. Piergentili and F. Graziani, "Two-site orbit determination: The 2003 GEO observation campaign from Collepardo and Mallorca", Advances in Space Research, Vol. 38, n. 9, pp. 2084-2092, 2006.

47. F. Graziani, F. Piergentili, C. Cappelletti, L. Murrali, F. Paolillo, C. Marchiori, M. Porfilio, "The first Italian observatory for space debris observation", 58th International Astronautical Congress, Hyderabad 24-28 Settembre 2007, IAF paper IAC-07-A6.I.06.
48. Italian Activity in Space Debris Measurements, 5th European Conference on Space Debris, April 2009 Darmstadt (Piergentili F., Paolillo F., Cappelletti C., Cevolani G., Grassi G., Marti M., Pupillo G.,Trivellone G., Portelli C., Porfilio M., Graziani F.)
49. F. Paolillo, M. Porfilio, F. Piergentili, "First Italian space debris observatory: the image processing automation", 58th International Astronautical Congress, Hyderabad 24-28 September 2007, IAF paper IAC-07-A6.I.05.
50. F. Santoni, F. Piergentili., F. Graziani,"In orbit performances of the UNISAT-3 solar arrays", 57th International Astronautical Congress, Valencia, Spain, 2-6th October 2006.
51. Paolillo F., Guarducci F., Cappelletti C., Ridolfi L., Murrali L. *Microsatellites Formation Flying for optical space debris in orbit observation*, 59th International Astronautical Congress, 29th September – 3rd October 2008, Glasgow, Scotland, UK.
52. Bendisch, J., Bunte, K., Klinkrad, H., Krag, H., Martin, C., Sdunnus, H., Walker, R. Wegener, P., Wiedemannendisch, C., "The MASTER-2001 model" Advances in Space Research, Vol. 34, pp. 959-968, 2004.
53. Rossi, A., "The Earth Orbiting Space Debris", Serbian Astronomical Journal, n. 170, pp. 1- 12, 2005.
54. C. Cappelletti, F. Guarducci, F. Paolillo, L. Ridolfi, F. Graziani, M.L.Battagliere, F. Piergentili, F. Santoni, "Microsatellites Formation Flying for In-Situ Space Debris Detection", 5th International Workshop on constellations and formation flying, CRIMEA, Evpatoria, July 2-4, 2008.
55. University Microsatellites Equipped with an Optical System for Space Debris Monitoring, IAA-B7-0234P, 7th IAA Symposium on Small Satellites for Earth Observation, May 2009 Berlin (Cappelletti C., Paolillo F.), Small Satellite Missions for Earth Observazion, Spriger book publication, pp 223-233.

56. M. Porfilio, “Metodi per l’individuazione di detriti spaziali” PhD Thesis, Scuola di Ingegneria Aerospaziale, “Sapienza” University of Roma, 1999-2000
57. W. Romanishin, “An Introduction to Astronomical Photometry Using CCDs”, University of Oklahoma, October 22, 2006.
58. M. De Petris, “Dispense del Corso di Ottica Applicata”, University of Rome “Sapienza”, September 13, 2006.
59. F. Paolillo, A. Conte, C. Cappelletti, M. De Petris, *Mcrosatellite optical payload for in-situ space debris monitoring*, IAC-10.D1.6.1, 61st International Astronautical Congress, Prague, CZ.
60. The Mars Reconnaissance Orbiter Mission, M. D. (Dan) Johnston, James E. Graf, Richard W. Zurek, Howard J. Eisen, Benhan Jai, Jet Propulsion Laboratory, California Institute of Technology Pasadena, California, USA, Vol. 1-191].
61. Lossless Compression of Grayscale Medical Images - Effectiveness of Traditional and State of the Art Approaches David A. Clunie Quintiles Intelligent Imaging 521 Plymouth Road, Suite 115, Plymouth Meeting PA 19462.
62. Star Sensor Development Based On The TUBSAT Experience, M. Buhl, U. Renner, Technische Universität Berlin, Institut für Luft- und Raumfahrttechnik, Marchstraße 12, D-10587 Berlin, Germany.
63. E. L. Church, H. A. Jenkinson and J. M. Zavata, Optical Engineering, 1977

List of proceedings and publications produced during the PhD experience

13) REXUS/BEXUS BUGS - Student Experiment Documentation (SED). Type: CDR, ID: RXBX-09-08-05 SED_BUGSTEAM_vers_5. M. Battagliere, J. Piattoni, C. Capelletti, F. Paolillo, E. Paolini, M. Meschini.

15) First Studies of ASI Concurrent Engineering Facility (CEF), SECESA 2010 13-15 October 2010, M. L. Battagliere, G. Casonato, M. Crisconio, C. Del Vecchio, E. Duca, C. Facchinetti , F. Paolillo, R. C. Pellegrini, S. Pirrotta, M. Porfilio, C. Portelli, M. Salatti, G. Valentini.

16) ASI CEF Study Report, SEO (SYSTEM FOR EARTH OBSERVATION), July 2010, performed in the ESTEC Concurrent Design Facility (CDF), M. Bandecchi, C. Portelli, G. Valentini, G. Casonato, C. Del Vecchio Blanco, S. Pirrotta, S. Rabbia, G. Belvedere, R. Carmine Pellegrini, M. Crisconio, F. Paolillo, M. Battagliere, C. Facchinetti, M. Porfilio, M. Salatti.

22) F. Paolillo, L. Ridolfi, E. Pifferi, F. Guarducci, C. Cappelletti, S. Battistini, P. Teofilatto, F. Graziani, Space Debris and close approaches to UNISAT 3 microsatellite, 5th International Workshop and Advanced School “Spaceflight Dynamics and Control” University of Beira Interior, Covilhã, Portugal, March 17-19, 2010.

28) F. Graziani, F. Santoni, F. Piergentili, M. L. Battagliere, F. Paolillo, G. Mascetti, G. Pulcrano, “The EduSAT microsatellite”, XX Congresso Nazionale AIDAA, 29 Giugno-3 Luglio 2009, Milano (in press)

48) Italian Activity in Space Debris Measurements, 5th European Conference on Space Debris, April 2009 Darmstadt (Piergentili F., Paolillo F., Cappelletti C.,

Cevolani G., Grassi G., Marti M., Pupillo G.,Trivellone G., Portelli C., Porfilio M., Graziani F.)

51) Paolillo F., Guarducci F., Cappelletti C., Ridolfi L., Murrali L. Microsatellites Formation Flying for optical space debris in orbit observation, 59th International Astronautical Congress, 29th September – 3rd October 2008, Glasgow, Scotland, UK

54) C. Cappelletti, F. Guarducci, F. Paolillo, L. Ridolfi, F. Graziani, M.L.Battagliere, F. Piergentili, F. Santoni, "Microsatellites Formation Flying for In-Situ Space Debris Detection", 5th International Workshop on constellations and formation flying, CRIMEA, Evpatoria, July 2-4, 2008.

55) University Microsatellites Equipped with an Optical System for Space Debris Monitoring, IAA-B7-0234P, 7th IAA Symposium on Small Satellites for Earth Observation, May 2009 Berlin (Cappelletti C., Paolillo F.), Small Satellite Missions for Earth Observazion, Spriger book publication, pp 223-233.

59) F. Paolillo, A. Conte, C. Cappelletti, M. De Petris, Mcrosatellite optical payload for in-situ space debris monitoring, IAC-10.D1.6.1, 61st International Astronautical Congress, Prague, CZ